Applied Energy 231 (2018) 502–533

Contents lists available at ScienceDirect

Applied Energy

journal homepage: www.elsevier.com/locate/apenergy

A comprehensive review of carbon and hydrocarbon assisted water electrolysis for hydrogen production

HyungKuk Ju[a], Sukhvinder Badwal[b], Sarbjit Giddey[a,*]

[a] CSIRO Energy, Private Bag 10, Clayton South, Victoria 3169, Australia
[b] BADWAL Hydrogen Energy, PO Box 318, Endeavour Hills, Victoria 3802, Australia

HIGHLIGHTS

- Carbon/hydrocarbon assisted water electrolysis reviewed for clean hydrogen production.
- Reviewed different electrochemical technologies using carbon fuels under development.
- This technology has been progressed to different levels of maturity for different carbon sources.
- This route of hydrogen production can lower the electric input and CO_2 emissions from the carbon sources.

GRAPHICAL ABSTRACT

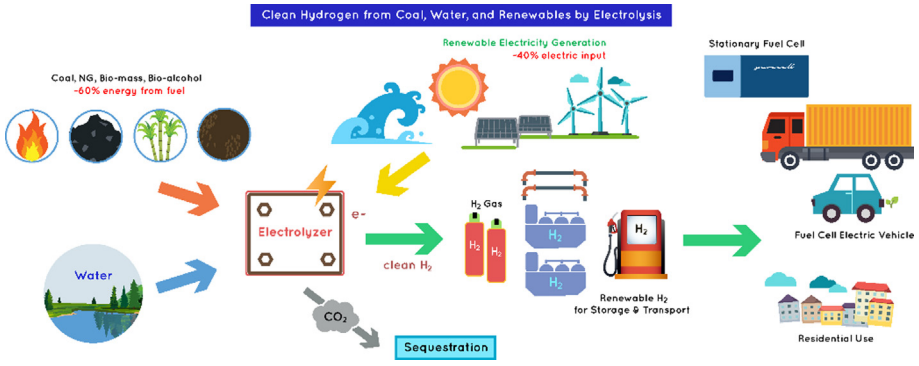

ARTICLE INFO

Keywords:
Electrolyser
Coal
Methanol
Ethanol
Natural gas
Alcohol

ABSTRACT

Hydrogen is mainly produced by natural gas reforming, which is a highly efficient process with low feedstock costs. However, the rising interest in clean technologies will increase the demand for hydrogen, meaning that other sources will need to be explored. Although coal is currently the major source of power generation, its demand appears to be declining due to the rise in electricity generated from renewable energy sources and the worldwide quest for low-emission power generation. Coal reserves worldwide are abundant, but new technologies would be needed to produce hydrogen from this feedstock. Coal gasification is one well-established technology for this purpose, but it is inefficient and produces high CO_2 emissions. An alternative technology that has been investigated over the past few decades is carbon assisted water electrolysis. The basic process is water/steam electrolysis, with part of the energy required for the electrolysis provided by the chemical energy of coal,

Abbreviations: ACFC, air-carbon fuel cell; AEM, anion exchange membranes; CAWE, carbon/coal assisted water electrolysis and carbon/hydrocarbon assisted water electrolysis; CHP, combined heat and power; COD, chemical oxygen demand; COR, carbon-water oxidation reaction; DCFC, direct carbon/coal fuel cells; DHA, 1,3-dihydroxyacetone; DMSO, dimethylsulphoxide; EAWE, ethanol assisted water electrolysis; FE, Faradaic efficiency or coulombic current efficiency; GC, gas chromatography; GDC, gadolinium-doped ceria; GDL, gas diffusion layer; HER, hydrogen evolution reaction; HHV, higher heating value, liquid water; HMF, hydroxymethylfurfural; HOR, hydrogen oxidation reaction; LHV, low heating value, steam water; LLNL, Lawrence Livermore National Laboratory; LMA, liquid metal anode; LSM, Sr-doped lanthanum manganite; MAWE, methanol assisted water electrolysis; MEA, membrane electrode assembly; NDIR, non-dispersive infrared detector; NG, natural gas; OCV, open circuit voltage; OER, oxygen evolution reaction; ORR, oxygen reduction reaction; PEM, proton conducting membrane and proton exchange membrane; PEMFC, polymer electrolyte membrane fuel cell; PSEM, proton-conducting solid electrolyte membrane; PTFE, polytetrafluoroethylene; SCAFC, steam-carbon-air fuel cell; SCFC, steam-carbon fuel cell; SMR, steam methane reforming; SOE, solid oxide electrolyte; SOEC, solid oxide electrolysis cell; SOFC, solid oxide fuel cell; SOM, small organic molecules; SPEEK, sulfonated polyetheretherketone; TOC, total organic carbon; WGS, water gas shift; YSZ, yttria stabilized zirconia

* Corresponding author.
E-mail address: Sarb.Giddey@csiro.au (S. Giddey).

https://doi.org/10.1016/j.apenergy.2018.09.125
Received 25 May 2018; Received in revised form 20 August 2018; Accepted 10 September 2018
Available online 21 September 2018

which reduces the overall electrical energy input. In addition to coal, the process can also use other carbon sources, such as biomass, alcohols or gaseous hydrocarbons. Several studies have investigated this electrochemical route of hydrogen production, employing different electrolytes in a wide temperature range (room temperature to 850 °C) under different process conditions. This paper presents a comprehensive review of carbon assisted water electrolysis, associated materials used and the challenges for the development of the technology at the commercial scale.

1. Introduction

Solutions for global energy challenges are being sought by moving towards eco-friendly technologies for a sustainable future. In an effort to reduce dependence on fossil fuel based energy sources, there has been substantial activity using renewable energy sources (e.g. solar, wind, hydro, ocean and geothermal). However, many such energy sources require substantial initial investment, and the cost of electricity generation can be high. Moreover, the intermittency of renewable energy sources and their dependence on environmental conditions places a strong emphasis on the need for cost-effective, large-scale storage solutions.

Hydrogen is an excellent energy storage medium, the use of which in fuel cells for stationary, transport and portable power applications offers several advantages. These include high efficiency, low greenhouse and pollutant (NOx, SOx, and particulates) emissions at the point of use, economies of scale (being modular in nature), and distributed and combined heat and power (CHP) generation. The majority of hydrogen produced at present (about 60 million tonnes per annum) is used for ammonia production, in oil refineries to generate a lighter oil fraction, and to a smaller extent in the chemical and pharmaceutical industries, space exploration and power generation. Most of this hydrogen is produced either by natural gas (NG) reforming with an efficiency of around 70–75%, or by coal gasification, which is about 45–65% efficient [1–5] and has high CO_2 emissions. Generally, these processes are suitable for large scale hydrogen production in central plants, which also offer a favourable cost structure. Only a small percentage of worldwide hydrogen production is via water electrolysis. Although suitable for distributed hydrogen production at demand centres, the process is very energy intensive, requiring 6–7 kWh electric input per m^3 of hydrogen produced (65–80 kWh kg^{-1} at 25 °C and 1 atm), and the capital cost and the cost of production are very high [6–8].

Coal is currently used to meet around 40% of total global electricity demand and is forecast to remain a major source for power generation for many more decades, due to its low cost and vast reserves [9]. However, due to the low efficiency of its conversion to electricity (typically 35–40%), it can contribute significantly to the CO_2 and other pollutant emissions. Although carbon capture and storage (CCS) technologies have the potential to reduce CO_2 emissions to the atmosphere, their large-scale deployment to capture even a small percentage of the 32 billion tons per annum of CO_2 generated globally and the further power generation efficiency losses resulting from this process means a range of solutions are required.

The electrochemical oxidation of solid carbon has been under investigation for many decades for power generation; for example, in direct carbon/coal fuel cells (DCFC) for efficient conversion of coal to low-emission electricity [10–16]. New electrochemical technologies are also currently under development that combine water electrolysis with the use of coal or hydrocarbon fuels to assist with the electrochemical reactions and reduce the overall energy consumption [17–21]. Thermodynamic and operational analysis of these systems suggest that about 60% of the energy required for water electrolysis can be provided by coal or other hydrocarbon (methanol, ethanol, NG) fuels in the form of chemical energy, thus substantially reducing the electric input [20–28]. Furthermore, if the process can be coupled with a renewable energy source, the intensity of CO_2 emissions can be significantly reduced and hydrogen can be generated at distributed or end-use sites as required by emerging power-generation technologies, such as fuel cells.

Carbon/hydrocarbon assisted co-electrolysis has the potential to offer a less energy-intensive and relatively clean method of using the chemical energy in various sources of carbon, such as low-rank coals, alcohols, methane, NG and even biomass, where pure CO_2 produced can be easily sequestered without the need for separation. In this article, we comprehensively review different low and high temperature electrochemical technologies currently under development, which use a range of electrode and electrolyte materials such as aqueous, polymer electrolyte membrane and solid oxide electrolyte (SOE) membrane cells. The review also covers:

- Various types of carbon sources (coal, methanol, ethanol, glycerol, ethylene glycol, cellulose, NG, methane and CO) used to assist the water electrolysis process
- The electrochemical reactions involved and electrode kinetic limitations
- Thermodynamic properties, such as free energy and enthalpy change of reactions and theoretical cell voltages required
- The energy input required for the electrolysis process with different types of carbon sources and under different process conditions

We also summarise and discuss the results obtained by various investigators in terms of cell designs, materials used, current densities obtained at given voltages, and electric energy savings in the electrolysis process. The review concludes with a discussion of the outlook for technical challenges and new opportunities in this field.

2. Fuel sources to assist with water electrolysis

The fuels that can be used to provide chemical energy to assist with the electrochemical splitting of water include coal (raw or processed to remove sulfur and ash impurities), carbon from biomass sources, methane, methanol, ethanol and some other organic materials, such as dimethyl ether (DME) and ethylene glycol. In terms of cost, coal or carbon from biomass are the most effective fuel sources available in large quantities, and costs increase for hydrocarbon fuels.

Carbon fuels can be used in both low and high temperature electrolysis systems. Methanol and ethanol are more suitable for low temperature (< 80 °C) electrolysis systems, while methane is more suited for high temperature electrolysis cells. Methane is a major constituent of NG (typically > 92%) and is available in reticulated form in most developing countries. Alcohols and carbon are easily transportable fuels; thus the water electrolysis process to generate hydrogen can be carried out at distributed or demand centres. Obviously, coupling of the electrolysis process with renewable energy for low temperature electrolytic processes would offer environmental benefits, with electricity input provided by solar photovoltaic or wind, for instance. Similarly, for high temperature electrolytic processes in addition to renewable energy waste thermal energy from industrial processes or solar thermal plants can offer further environmental sustainability.

Coal, despite being the most obvious and low-cost option to assist with water electrolysis, is composed of complex aromatic clusters with inorganic constituents containing a large range of species which varies significantly for different coals. Fig. 1 is an example of molecular model

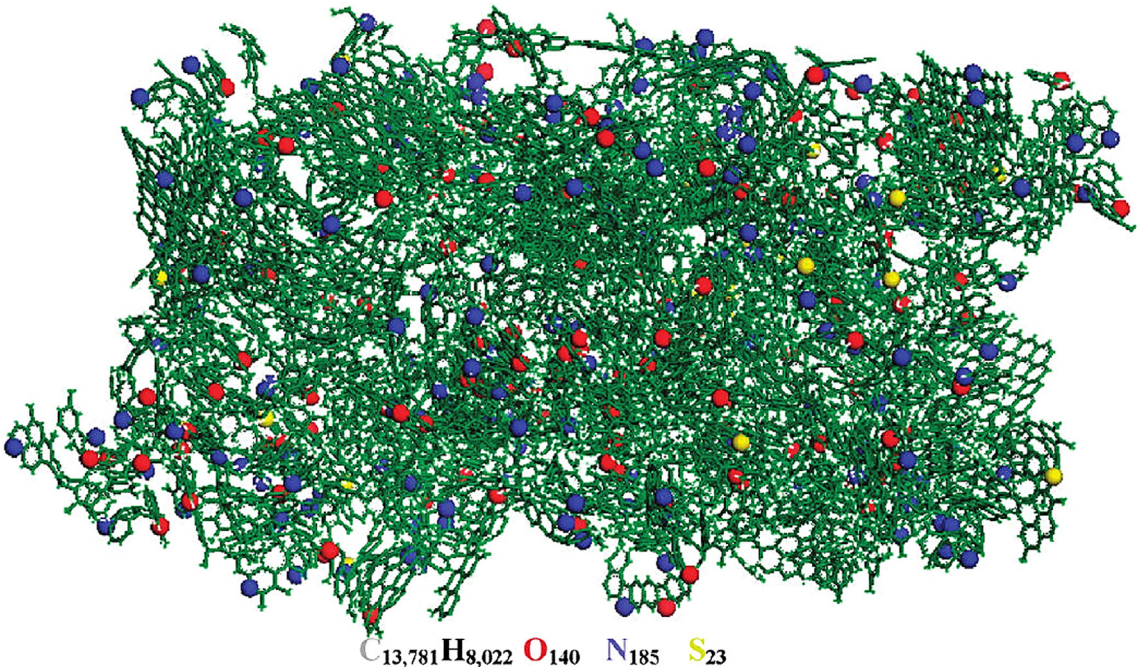

Fig. 1. Molecular representation of bituminous coal structure with heteroatoms simulated by Narkiewicz and Mathews. Figure reproduced with permission from [29].

of a bituminous coal structure containing highly functional, high molecular weight organic and inorganic matter [29]. The impurities in coal are important to support its utilisation in combustion and gasification processes, and for the long-term stability of electrochemical cells. Generally, the sulfur in coal is categorised as present both in inorganic (generally sulfides and sulfates) and organic forms, and pyrite is the major contaminant in coal. The removal of inorganic sulfur contamination can be carried out by well-established coal preparation techniques, but the removal of organic sulfur is still an issue [30–32].

The concept of solid carbon assisted water electrolysis (CAWE) in acidic media for hydrogen production was first proposed and investigated by Coughlin and Farooque from 1979 to 1982 [33–37] and involved a series of experiments in an electrochemical cell shown schematically in Fig. 2. The authors also used this technique to investigate sulfur removal from coal. They found that the mineral matter, other impurities and functional groups in coal can interfere with and influence electrochemical use of carbon both positively and negatively, and concluded that this requires careful investigation.

Another major source of carbon fuel is biomass. Carbon is produced by partial combustion (or pyrolysis) of a range of naturally occurring, fuel rich, carbonaceous biomass materials, such as forestry and agricultural residues, grasses, wood chips and wood shavings. The initial product obtained is then activated by chemical or a physical activation process to yield high surface area and porous carbon [38,39]. Due to different starting materials and activation processes used, the properties (e.g. pore size, volume and distribution, surface area) of activated carbon thus produced and to some degree, impurity levels can vary significantly. Activated carbons have substantial market for use as adsorbents to remove organic constituents from air and water, in industrial processes (e.g. treatment of gases, removal of trace metals, removal of volatile inorganic and organic compounds) and as a support for noble metal catalysts. They can also be used as a fuel in the carbon assisted electrolysis process to generate hydrogen [39].

Both ethanol and methanol can be produced using biomass. More than 85 billion litres of ethanol is produced annually worldwide, mainly through fermentation process from biomass sources such as sugarcane, corn, beetroot, switch grass and other food plant or forest residue. It is widely considered as a blended renewable fuel for transportation vehicles. The energy input to produce ethanol compared with its energy content varies significantly depending on the source and the process used for its production [40]; the energy balance is very favourable for sugarcane. About 90 billion litres of methanol is produced per annum for use in chemical production and as a transportation fuel. It is typically produced from syngas (a mixture of CO and H_2). Any fossil fuel (coal, NG) or biomass resource (wood, agriculture waste, forest residue) that can be converted to syngas via gasification, can be used as a feedstock for methanol synthesis. In a secondary process, syngas is converted to methanol via a catalytic process [41,42]. Although most

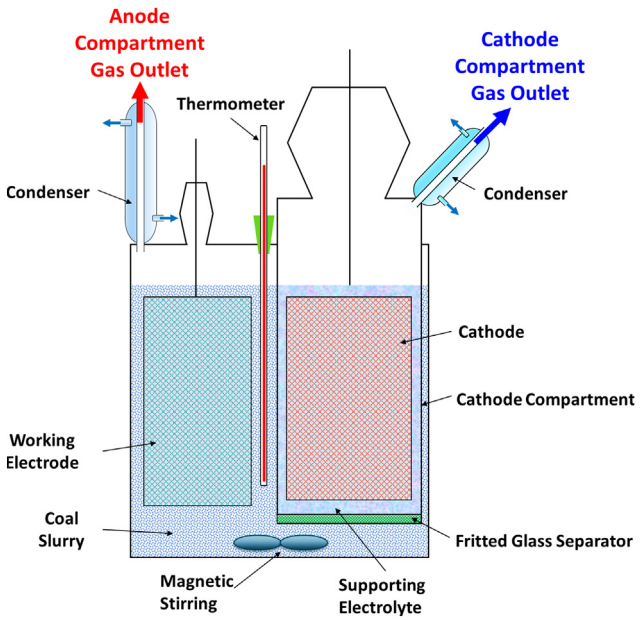

Fig. 2. Schematic drawing of the first electrochemical cell arrangement for hydrogen production from carbon/coal slurry in acid media [33]. Both anode and cathode compartments consist of a Pt gauge 52 mesh immersed in 3.7 M H_2SO_4 at 23 °C with respective areas of 96.5 and 158 cm^2. Figure redrawn from [33].

methanol is currently produced from steam reforming or partial oxidation of NG, bio-methanol can be produced from destructive pyrolysis of wood. Renewable methanol can also be produced from hydrogen, generated via electrolysis of water coupled to a renewable energy source (solar photovoltaics or wind), and the CO_2 captured from fossil fuel power plants or industrial processes [41].

Methanol and ethanol both have a high hydrogen content of ~13 wt % and are in liquid state at ambient temperatures. Therefore, both fuels are considered as good means of transporting large quantities of hydrogen for fuel cells [41]. The energy density of methanol is 6.20 kWh kg^{-1} (4.90 kWh L^{-1}) LHV compared with 8.0 kWh kg^{-1} (6.32 kWh L^{-1}) LHV for ethanol [40,43].

3. Fundamentals of conventional and carbon assisted water electrolysis

3.1. Basic principles

In the electrolysis process, water is decomposed into hydrogen and oxygen when an electrical current is passed through an electrolytic cell. Typically, the cell consists of an electrolyte, an anode and a cathode. A number of cells are connected in series (called an electrolyser) to produce quantities of gases. Different types of electrolysers can be distinguished based on the type of electrolyte used in the cell and the operating temperature regime. Fig. 3 shows a tree diagram depicting various types of low and high temperature conventional electrolysis and CAWE systems, while Table 1 summarises further details of the cell materials used and operating conditions for these systems. The rest of this section describes the basic principles of the major types of electrolysers.

3.1.1. Acidic/alkaline solution and membrane based water electrolysis

Water electrolysis to produce hydrogen and oxygen was first discovered in acidic water solutions, but due to severe corrosion related issues that need relatively expensive materials, this method of electrolysis attracted less attention than alkaline based electrolysis. However, electrolysis based on a proton conducting membrane or proton exchange membrane (PEM), which is mildly acidic in nature and has similar electrode reactions, has gained remarkable popularity in recent times. In PEM based electrolysis process, water is circulated in the anode (positive electrode) chamber. On application of DC voltage to the electrodes, an oxygen evolution reaction (OER) occurs at the anode, generating protons and electrons. The protons are transported through the electrolyte membrane to the cathode, resulting in a hydrogen evolution reaction (HER) at the cathode (hydrogen electrode), which also involves the consumption of electrons. The associated electrode reactions and cell voltages (at 25 °C and 1 atm) for a PEM-based electrolysis process are given in Table 2.

In PEM-based system, a solid-state PEM such as Nafion® (Dupont™, perfluorosulfonic acid membrane) and sulfonated polyetheretherketone are commonly used as electrolytes. The catalysts used for the electrodes are noble metals such as Ir, Ru, IrO_2 and RuO_2 for the anode, and Pt black supported on carbon as the cathode. The typical operating temperature range for acidic water solution and PEM based systems is 20–80 °C. Fig. 4(a) shows the schematic of the electrochemical cell and the associated electrode reactions. This technology is at an advanced stage of development, with many companies selling commercial units now in the MW class capable of producing hydrogen in excess of 30 bar [6–8,44]. The costs of these units are still high but the lifetimes being quoted are in excess of 80,000 h. PEM electrolysis cells are typically operated at cell voltages of 1.8–2.2 V with current densities up to 1 A cm^{-2} and temperatures below 100 °C [44]. Further, these systems have advantage in terms of their operability with varying or intermittent load.

Alkaline solution based electrolysis offered the use of relatively cheaper materials for electrolysis cells and the plant compared with acidic solution based system, and was adopted early and at a large scale [7,44]. This technology is the most developed at commercial scale, with units available in the multi-MW class [6–8]. KOH solution with concentrations up to 30% is the preferred electrolyte used for these systems. The electrodes are separated by a diaphragm that keeps the gases evolved on the respective electrodes separate from each other, but allows exchange of hydroxyl ions and water between the electrodes. The advantage of alkaline based electrolysis is the lower cost of the electrode materials, due to the use of non-noble metal catalysts such as Ni based materials (Ni, Ni oxide, Co oxide and Ni alloys on the steel). However, these suffer from lower current densities, due to high electrolyte resistance, low capability to operate at high pressures and on

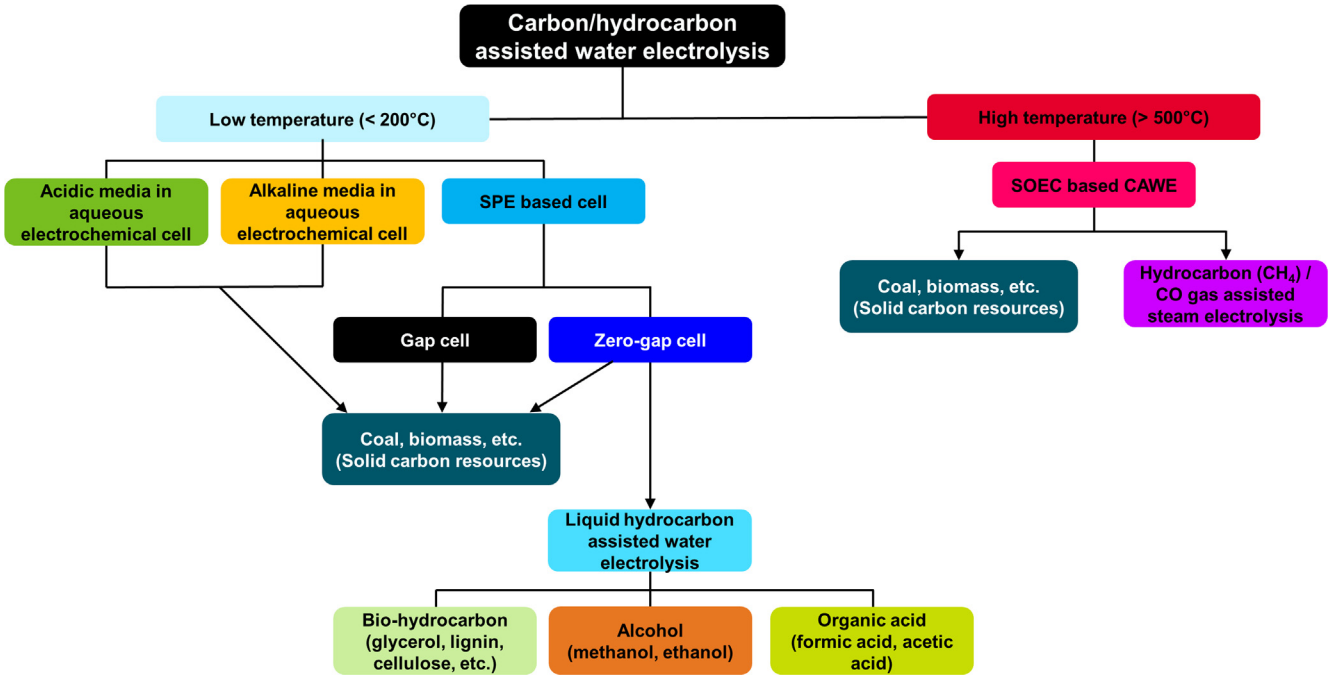

Fig. 3. Tree diagram depicting the various routes of carbon/hydrocarbon assisted water electrolysis.

Table 1
Operating parameters and cell materials used for different electrolysis technologies [1,6,7,20,44,105,175,176].

	Alkaline electrolysis	PEM electrolysis	SOEC electrolysis	CAWE in PEM	CAWE in SOEC
Operating temp./°C	< 100	< 100	500–1,000	< 100	700–1,000
Operating cell voltage/V	1.7–2.4	1.8–2.2	1.0–1.6	0.5–1.2	< 1.0
Current density/mA cm^{-2}	> 500	> 2,000	> 1,500	< 300	< 500
Anode	Mn, Fe, Co, Ni and its metal oxide	Ir, Ru, IrO_2 and RuO_2	LSM-YSZ, CGO, LSCF and BSCF	Pt, PtIr and PtRu	Pt, Ni, Ag and Sn
Cathode	Ni alloy and Pt	Pt/C and Pt	Ni-YSZ, SDC and LSM-YSZ	Pt/C and Pt	Pt, Ni and Ni-YSZ
Electrolyte	KOH, NaOH and NaCl solution	Nafion system (perfluorosulfonic acid membrane)	YSZ, ScSZ and doped-CeO_2 systems for O^{2-} conducting ceramics and doped-CeO_3, doped-ZrO_3 systems for H^+ conducting ceramics	Nafion system and porous fritted glass	Zirconia based solid oxide electrolyte (YSZ)

BSCF = Ba-doped strontium cobalt ferrite; CAWE = carbon/hydrocarbon-assisted water electrolysis; CGO = Gd-doped ceria; LSM = Sr-doped lanthanum manganite; LSCF = La-doped strontium cobalt ferrite; PEM = polymer electrolyte membrane; SDC = Sr-doped ceria; SOEC = solid oxide electrolysis cell; YSZ = yttria-stabilised zirconia.

varying load, and a greater chance of mixing of gases, resulting in lower Faradaic efficiencies (FE) and safety concerns. This has recently led to the development of anion-exchange membranes (AEM) for alkaline water electrolysis. There are already two commercial membranes available in the market: A201 membrane (Tokuyama Co., Japan) and Selemion AMV (Asahi Glass Co., Japan) – with several other groups developing different types. The basic principle of water electrolysis based on alkaline solutions and AEM is shown schematically in Fig. 4(b), and the associated electrolysis reactions and cell voltages (at 25 °C and 1 atm) are shown in Table 2. AEMs have lower ionic conductivities than PEM, and often electrolyte solutions are added to improve conductivity. For example, in the AEM based electrolysis cell, KOH is added to water for circulation in the anode chamber. Alkaline electrolysis cells are typically operated at cell voltages of 1.7–2.4 V with current densities up to 0.5 A cm^{-2} and temperatures below 100 °C.

3.1.2. Solid oxide electrolyte membrane based steam electrolysis

High temperature electrolysis (of steam) not only helps increase the reaction kinetics of the electrolysis reactions and reduce overvoltages, but also allows solar energy or waste heat from power plants and other industrial processes to be embedded into the process. One technology still at an early stage of development is based on the use of an oxygen ion conducting ceramic membrane, in which the electrolysis process occurs at high temperatures (> 500 °C) [6]. The steam supplied to the cathode in the electrolysis process is dissociated into hydrogen and oxygen ions (O^{2-}), leading to HER at the cathode. The oxygen ions are transported through the ceramic membrane to the anode, resulting in oxygen evolution and the generation of two electrons, as shown schematically in Fig. 4(c). The electrochemical cell used in this process is called a solid oxide electrolysis cell (SOEC). The electrochemical reactions and the associated cell voltages (at 827 °C and 1 atm) for the oxygen ion conducting ceramic electrolyte membrane based electrolysis are summarised in Table 2. In principle, the SOEC operation is the reverse process of solid oxide fuel cell (SOFC) operation. The reversible voltage for the overall reaction at 827 °C is around 0.97 V, and as expected is lower than that at 25 °C (1.23 V) mentioned for the PEM based system. This system can also use proton-conducting electrolytes, such as Sr or Ba-doped cerates and Zr-based materials [6,45]. The electrochemical reactions for the proton-conducting solid electrolyte membrane (PSEM) based electrolysis process are the same as for the PEM shown schematically in Fig. 4(d).

3.1.3. Low temperature carbon/liquid hydrocarbon assisted water electrolysis

The CAWE process involves feeding solid carbon particles or carbon powder dispersed in water (carbon slurries) to the anode. The carbon in the solution participates in the electrolysis reaction, producing CO_2 and/or CO as the gaseous product on the anode side rather than oxygen evolution reaction. The cathode reaction is the hydrogen evolution reaction. The overall principle for the CAWE process for acidic solution/PEM and alkaline solution/AEM is shown schematically in Fig. 4(e) and (f), respectively, and the associated reactions at the anode and cathode are described in Table 2 (at 25 °C and 1 atm). Note that the reversible voltages of the overall electrolysis reactions involving carbon are significantly lower (0.21 V for CO_2 and 0.52 V for CO) than in conventional electrolysis (1.23 V).

To date, most studies on carbon assisted electrolysis have been conducted in acidic solutions [33–37,46–54], with some in alkaline solutions [55–57] and some employing PEM as a separator or electrolyte [58–67]. None of the studies employed AEM. The operating conditions were mostly room temperature to below 100 °C and atmospheric pressure, with only few studies carried out at temperatures up to 160 °C and above atmospheric pressures (~10 bar) [67,68].

In the liquid hydrocarbon assisted water electrolysis, alcohols and liquid hydrocarbons such as methanol, ethanol, formic acid, glycerol and bio-hydrocarbons mixed with water provide part of the energy in the form of chemical energy for the electrolysis process. Fig. 4(g) shows a schematic of the basic principle of the electrolysis process for alcohols. Most of these studies have been conducted using PEM (some have used AEM) and at operating temperatures lower than 100 °C [22–24,69–88]. The catalysts used are similar to those used for PEM based direct liquid fuel cells. Table 3 provides the detailed electrochemical reactions that occur at the anode and cathode of the alcohol/bio-hydrocarbon/organic acid assisted co-electrolysis cells and the associated reversible voltages in each case (discussed in more detail in Section 5.1).

3.1.4. High temperature solid carbon and hydrocarbon/CO gas assisted steam electrolysis

In oxygen-ion conducting ceramic membrane (or SOEC) based CAWE (Fig. 4(h)), carbon and steam are supplied to the anode and cathode, respectively. In this configuration, one side of the cell acts as a direct carbon fuel cell (DCFC) and the other as a water electrolyser. The corresponding electrochemical reactions that occur at the anode and cathode are described in Table 2. Furthermore, in a PSEM based CAWE (Fig. 4(i)), carbon and steam are both fed to the anode, and hydrogen is produced at the cathode. In most of the studies on CAWE in a SOEC system, yttria-stabilised zirconia (YSZ) has been used as the electrolyte; Ni-YSZ, lanthanum strontium manganese oxides (LSM)-YSZ or Pt as the cathode; Ag, Sn, Pt or Ni-YSZ as the anode; and the operating temperature range has been 600–1000 °C [89–97].

In the hydrocarbon/CO gas assisted co-electrolysis, fuel gases such as NG or CO are used to assist high temperature steam electrolysis in SOECs. Steam is supplied to the cathode and fuel gas to the anode (Fig. 4(j)). YSZ was used as the electrolyte in these studies, which were conducted in the temperature range of 700–900 °C. The electrochemical reactions associated with this type of electrolysis are shown in Table 2 (at 827 °C). Limited studies have investigated fuel gas assisted water electrolysis [25–27].

Table 2
Summary of the electrochemical reactions and the thermodynamic cell voltages for different type of electrolysis.

Feed	Reaction	No. of electron	E°_{rev} / V	E°_{the} / V
Water in PEM	Anode $H_2O \rightarrow 2H^+ + 1/2O_2 + 2e^-$ Cathode $2H^+ + 2e^- \rightarrow H_2$ Overall $H_2O \rightarrow H_2 + 1/2O_2$	2	1.23 at 25°C	1.48 at 25°C
Water in alkaline	Anode $2OH^- \rightarrow 1/2O_2 + H_2O + 2e^-$ Cathode $H_2O + 2e^- \rightarrow H_2 + 2OH^-$ Overall $H_2O \rightarrow H_2 + 1/2O_2$	2	1.23 at 25°C	1.48 at 25°C
Water in O^{2-} conducting ceramic membrane	Anode $O^{2-} \rightarrow 1/2O_2 + 2e^-$ Cathode $H_2O + 2e^- \rightarrow O^{2-} + H_2$ Overall $H_2O \rightarrow H_2 + 1/2O_2$	2	0.97 at 827°C	1.29 at 827°C
Carbon/Coal in PEM	Anode $C + 2H_2O \rightarrow CO_2 + 4H^+ + 4e^-$ $C + H_2O \rightarrow CO + 2H^+ + 2e^-$ Cathode $4H^+ + 4e^- \rightarrow 2H_2$ $2H^+ + 2e^- \rightarrow H_2$ Overall $C + 2H_2O \rightarrow CO_2 + 2H_2$ $C + H_2O \rightarrow CO + H_2$	4 or 2	0.21 or 0.52 at 25°C	0.46 or 0.91 at 25°C
Carbon/Coal in O^{2-} conducting ceramic membrane	Anode $C + 2O^{2-} \rightarrow CO_2 + 4e^-$ Cathode $2H_2O + 4e^- \rightarrow 2O^{2-} + 2H_2$ Overall $C + 2H_2O \rightarrow CO_2 + 2H_2$	4	-0.06 at 827°C	0.26 at 827°C
Carbon/Coal in H^+ conducting ceramic membrane	Anode $C + 2H_2O \rightarrow CO_2 + 4H^+ + 4e^-$ Cathode $4H^+ + 4e^- \rightarrow 2H_2$ Overall $C + 2H_2O \rightarrow CO_2 + 2H_2$	4	-0.06 at 827°C	0.26 at 827°C
Methane in O^{2-} conducting ceramic membrane	Anode $CH_4 + 2O^{2-} \rightarrow CO_2 + 2H_2 + 4e^-$ $CH_4 + O^{2-} \rightarrow CO + 2H_2 + 2e^-$ Cathode $2H_2O + 4e^- \rightarrow 2O^{2-} + 2H_2$ $H_2O + 2e^- \rightarrow O^{2-} + H_2$ Overall $CH_4 + 2H_2O \rightarrow CO_2 + 4H_2$ $CH_4 + H_2O \rightarrow CO + 3H_2$	4 Or 2	0.08 or 0.17 at 800°C	-
Carbon monoxide in O^{2-} conducting ceramic membrane	Anode $CO + O^{2-} \rightarrow CO_2 + 2e^-$ Cathode $H_2O + 2e^- \rightarrow O^{2-} + H_2$ Overall $CO + H_2O \rightarrow CO_2 + H_2$	2	0.00 at 827°C	-

3.2. Thermodynamics and efficiency

3.2.1. Water electrolysis

The maximum energy obtainable as work from a chemical reaction is determined by the Gibbs free energy change (ΔG) of the reaction given by:

$$\Delta G = \Delta H - T\Delta S \quad (1)$$

where ΔH is enthalpy change and ΔS is entropy change. For the reaction to be spontaneous, ΔG must be negative for the reaction (negative thermodynamic potential).

As mentioned in the introduction, the common hydrogen production technology involves steam-methane reforming (SMR) followed by water gas shift (WGS) reaction. The chemical reactions associated with SMR and WGS reaction are as follows [1,2,98,99]:

$$CH_4 + H_2O \rightarrow CO + 3H_2 \quad \Delta H_{\text{at } 25^{\circ}C} = +206\ \text{kJ mol}^{-1} \quad (2)$$

$$CO + H_2O \rightarrow CO_2 + H_2 \quad \Delta H_{\text{at } 25^{\circ}C} = -41\ \text{kJ mol}^{-1} \quad (3)$$

The well-known steam–carbon reaction (one of the important reactions for coal gasification) produces H_2-rich syngas from a variety of carbon sources [34,35,100]:

$$C + H_2O \rightarrow CO + H_2 \quad \Delta H_{\text{at } 25^{\circ}C} = +31.14\ \text{kJ mol}^{-1} \quad (4)$$

The chemical Eqs. (2) and (4) are endothermic, as indicated by the enthalpy change values. To move the reaction forward for hydrogen production, additional heat energy is required (i.e. the process needs to

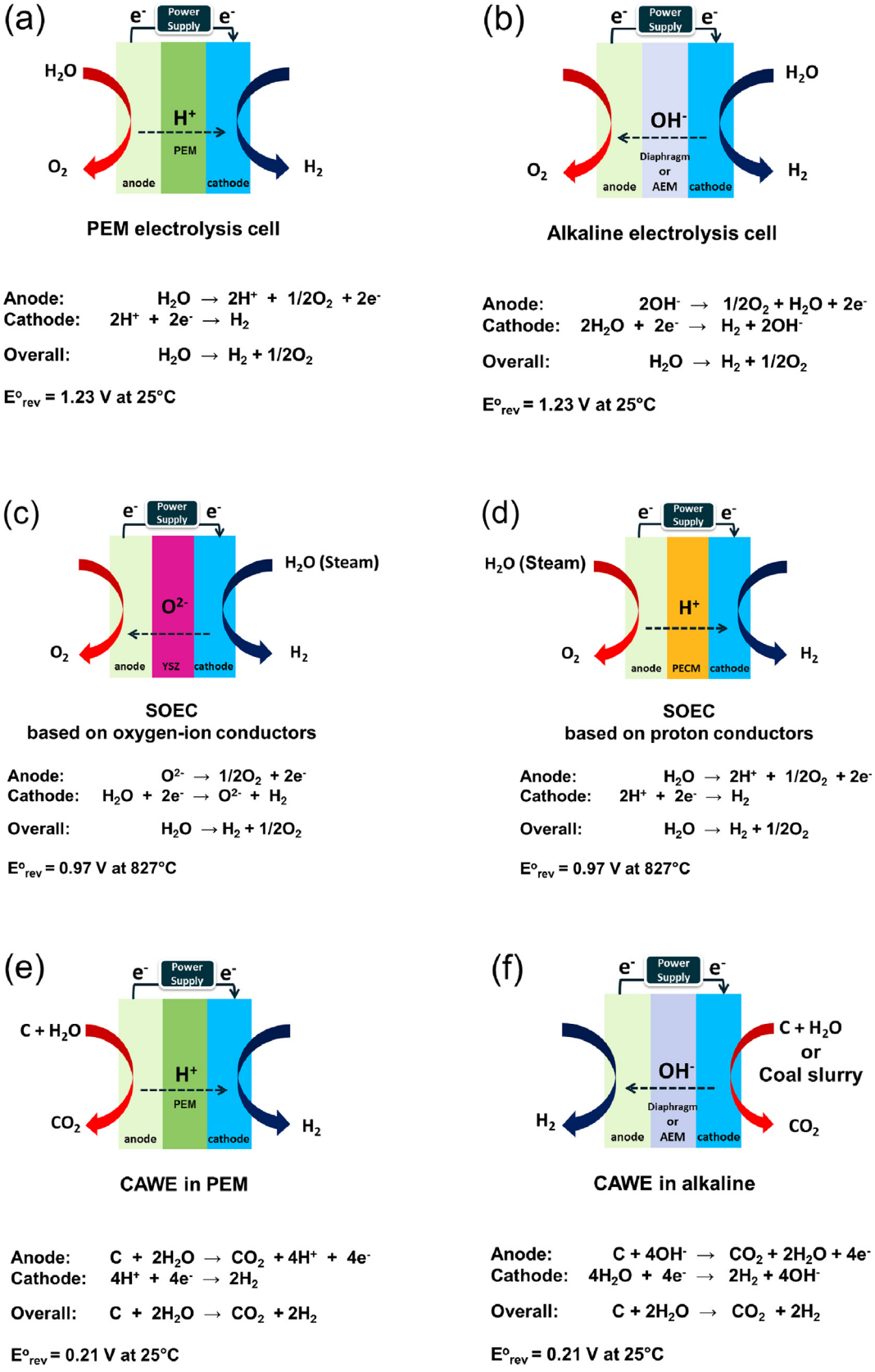

Fig. 4. Schematic configuration of the fundamental operating principles of different types of electrolysis. Low temperature (a) polymer electrolyte membrane (PEM) electrolysis cell; (b) alkaline electrolysis cell; high temperature solid oxide electrolysis cell (SOEC) based on (c) oxygen-ion and (d) proton conducting electrolytes; low temperature carbon/coal-assisted water electrolysis (CAWE) in (e) PEM-based and (f) alkaline based cell; (g) low temperature liquid hydrocarbon assisted water electrolysis; high temperature CAWE in SOEC based on (h) oxygen-ion and (i) proton conducting electrolytes; and (j) high temperature hydrocarbon/CO gas-assisted water electrolysis. AEM = anion-exchange membrane; PSEM = proton-conducting solid electrolyte membrane (Sr/Ba–ZrO_3/CeO_3-based materials).

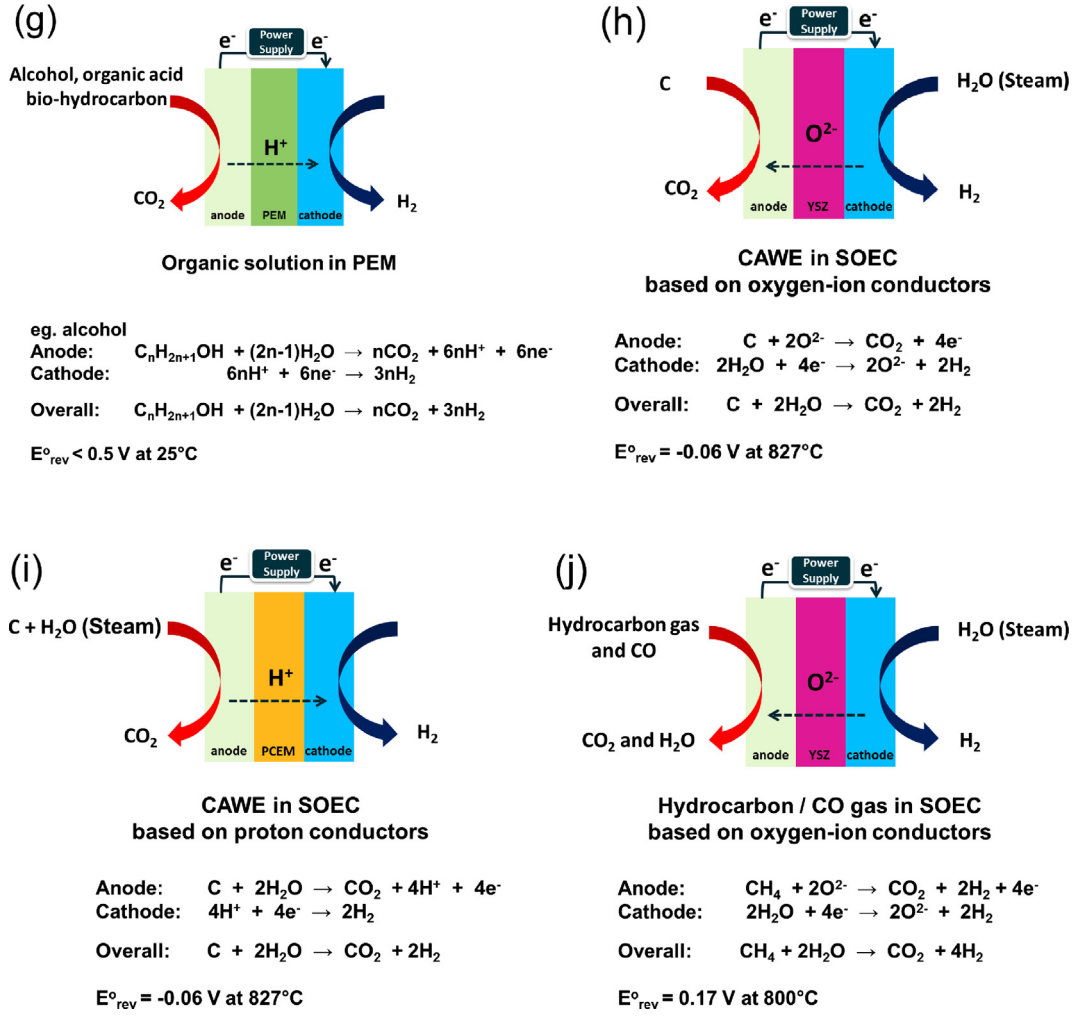

Fig. 4. (*continued*)

Table 3
Summary of the electrochemical reactions and the associated thermodynamic values for liquid hydrocarbon fuels assisted water electrolysis at 25 °C.

	Feed	Reaction	No. of electron	ΔG / kJ mol^{-1}	ΔH / kJ mol^{-1}	E^{o}_{rev} / V	E^{o}_{the} / V
Alcohol	Methanol	Anode $CH_3OH + H_2O \rightarrow CO_2 + 6H^+ + 6e^-$ Cathode $6H^+ + 6e^- \rightarrow 3H_2$ Overall $CH_3OH + H_2O \rightarrow CO_2 + 3H_2$	6	9.04	131.18	0.02	0.22
	Ethanol	Anode $C_2H_5OH + 3H_2O \rightarrow 2CO_2 + 12H^+ + 12e^-$ Cathode $12H^+ + 12e^- \rightarrow 6H_2$ Overall $C_2H_5OH + 3H_2O \rightarrow 2CO_2 + 6H_2$	12	97.46	298.16	0.08	0.26
Bio-hydrocarbon	Glycerol	Anode $C_3H_8O_3 + 3H_2O \rightarrow 3CO_2 + 14H^+ + 14e^-$ Cathode $14H^+ + 14e^- \rightarrow 7H_2$ Overall $C_3H_8O_3 + 3H_2O \rightarrow 3CO_2 + 7H_2$	14	3.9	324.8	0.24	0.003
	Ethylene glycerol	Anode $C_2H_6O_2 + 2H_2O \rightarrow 2CO_2 + 10H^+ + 10e^-$ Cathode $10H^+ + 10e^- \rightarrow 5H_2$ Overall $C_2H_6O_2 + 2H_2O \rightarrow 2CO_2 + 5H_2$	10	25.5	460.0	0.026	0.477
Organic acid	Formic acid	Anode $HCOOH \rightarrow CO_2 + 2H^+ + 2e^-$ Cathode $2H^+ + 2e^- \rightarrow H_2$ Overall $HCOOH \rightarrow CO_2 + H_2$	2	-33.02	31.21	-0.17	-0.02

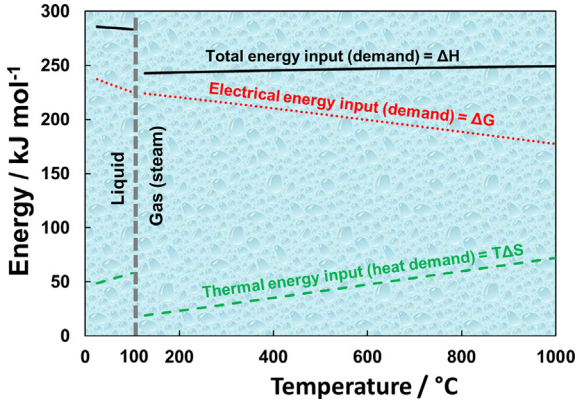

Fig. 5. Thermodynamic values of total energy (ΔH), electrical (ΔG) and thermal (TΔS) demands for water electrolysis as a function of temperature at atmospheric pressure. Thermodynamic values are taken from *CRC Handbook of Chemistry and Physics* [123].

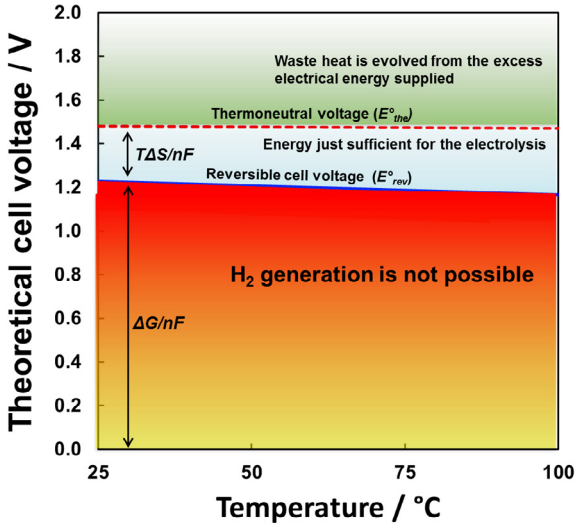

Fig. 6. Thermodynamic values of reversible cell voltage (E°_{rev}) and thermo-neutral voltage (E°_{the}) for water electrolysis as a function of temperature at atmospheric pressure. Thermodynamic values are taken from *CRC Handbook of Chemistry and Physics* [123].

be carried out at high temperatures, in excess of 700 °C).

The electrolysis of water ($H_2O \rightarrow H_2 + \frac{1}{2}O_2$) is an endothermic reaction with $\Delta H_{at\ 25\,^{\circ}C} = +285.83\,kJ\,mol^{-1}$ and $\Delta G_{at\ 25\,^{\circ}C} = +237.14\,kJ\,mol^{-1}$. Fig. 5 shows the variation in these values as a function of temperature. The figure also shows the entropy term (Eq. (1)) as a function of temperature. The figure reveals there is only a small change in the total energy demand (enthalpy change ΔH) for water electrolysis (< 100 °C) and steam electrolysis (> 100 °C) with temperature. However, the ΔG that represents the electrical energy input for the reaction decreases significantly with increasing temperature. A significant drop in enthalpy change at 100 °C represents the heat of water evaporation.

The entropy term (TΔS), which represents the thermal input required for the reaction, increases with temperature. This means that for an electrolysis process carried out at higher temperatures, for instance in the case of an oxygen-ion conducting ceramic electrolyte membrane (in SOEC system), the electrical input would be significantly reduced, as the thermal input will be also contributing to the required energy for the reaction. The thermal input for the reaction could come from a range of sources, including waste heat from nuclear power plants (future fast breeder reactors), thermal power plants, solar-thermal or industrial waste heat. Steam electrolysis at higher temperatures requires lower cell voltages (electric input), with part of the energy provided by thermal input, thus improving the overall electric efficiency of the process compared with low temperature (PEM or alkaline solution based) electrolysis processes that require most of the energy input as electric power [7,44,101].

When the electrochemical reaction occurs in the cell, the relationship between the standard Gibbs free energy change of the reaction ΔG and reversible voltage of the cell, E^{o}_{rev}, can be expressed as follows:

$$-\Delta G = nFE^{\circ}_{rev} \quad (5)$$

$$E^{\circ}_{rev} = -\Delta G/nF \quad (6)$$

The reversible voltage of the electrolysis cell is the theoretical minimum voltage required to provide the electrical input for the water electrolysis reaction. However, this is only possible if the thermal part of the energy (TΔS in Eq. (1)) is supplied from the surrounding environment, which leads to cooling of the cell, and eventually the electrolysis process ceases. Therefore, to continue electrolysis, the thermal part of the energy for the reaction has to be supplied, and hence a higher cell voltage than the reversible value is required. This cell voltage is called thermo-neutral voltage (E^{o}_{the}) and is determined from the enthalpy change (ΔH) of the electrolysis reaction as follows:

$$E^{\circ}_{the} = -\Delta H/nF \quad (7)$$

Note that at thermo-neutral voltage of the cell, no exchange of heat is required between the cell and the surroundings. Fig. 6 gives the reversible and thermo-neutral voltage values calculated respectively from standard ΔG and ΔH for conventional water electrolysis process, as a function of temperature. As discussed earlier, the figure shows that no hydrogen generation occurs in the region below the E^{o}_{rev}. Thermal energy is required in the region between the E^{o}_{rev} and E^{o}_{the} for the electrolysis process, i.e. a situation more favourable for electrolysis at a high temperature where thermal input is provided in addition to electric input. The process becomes feasible above the E^{o}_{the} (the minimum applied cell voltage is ~1.48 V at 25 °C), and the system, apart from the electrolysis process, generates heat above this voltage.

3.2.2. Carbon/coal-assisted water electrolysis

As mentioned in Section 3.1, the participation of carbon in the electrolysis reaction results in lower reversible cell voltages, and is a consequence of part of the electrical energy requirement being met by the chemical energy of carbon in the electrolysis process. However, the reversible voltage of such a process is dependent on whether the carbon oxidation occurs to form CO_2 (four-electron process) or CO (two-electron process), as summarised in Table 2. The reversible and thermo-neutral voltages for the electrolysis reactions (CAWE) given in Table 2 for four- and two-electron processes were calculated from their respective ΔG and ΔH values, and are plotted as a function of temperature in Fig. 7(a) (low temperature systems, such as PEM/AEM based electrolysis) and 7(b) (high temperature systems, such as SOEC).

Table 2 also shows that in terms of E°_{rev} for the overall reaction, the CAWE process ($E^{\circ}_{rev\ at\ 25^{\circ}C} = 0.21$ V, n = 4) requires one-sixth of the energy required for conventional water electrolysis ($E^{\circ}_{rev\ at\ 25^{\circ}C} = 1.23$ V, n = 2) at room temperature. In terms of E^{o}_{the}, the carbon participation in the electrolysis reaction decreases this value from 1.48 to 0.46 V (less than one-third). Thus, it is possible to operate the electrolyser at a much lower cell voltage (correspondingly lower energy consumption) by using carbon in the electrolysis process. However, due to overpotential losses in the electrochemical reactions at the respective electrodes and ohmic losses within the electrodes, electrolyte and current collectors the operating voltage for the electrolysis is expected to be significantly higher than the E^{o}_{the}. The thermo-neutral voltage is the actual voltage that must be supplied to the cells to start the electrolysis process. Therefore, even if the free energy requirement is satisfied by operating the cell at voltages between E°_{rev} and E°_{the} (endothermic

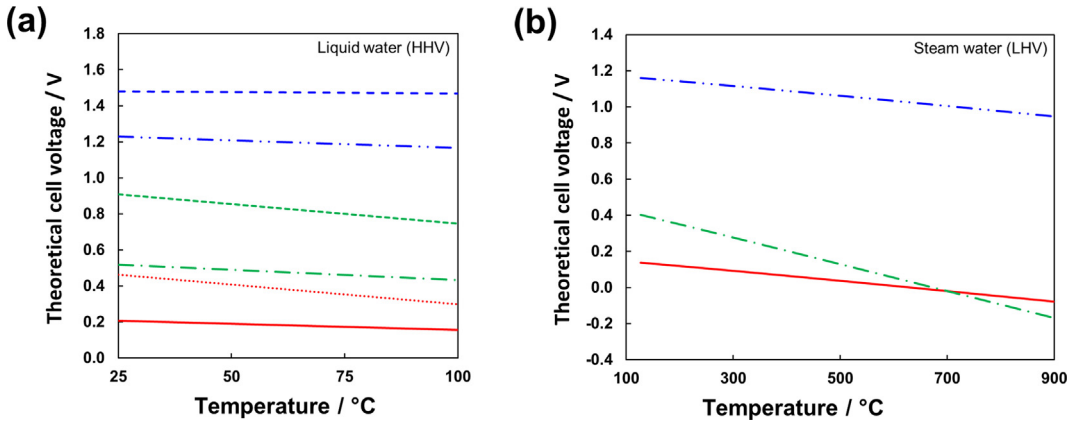

Fig. 7. Thermodynamic values of reversible cell voltage (E°_{rev}) and thermoneutral voltage (E°_{the}) for carbon/coal assisted water electrolysis (CAWE) as a function of temperature. (a) Comparison between water electrolysis and CAWE below 100 °C (HHV, liquid water); water electrolysis for E°_{rev} (blue dash-dot-dot) and E°_{the} (blue dash); CAWE 4-electron reactions for E°_{rev} (red solid) and E°_{the} (red dot); CAWE 2-electron reaction for E°_{rev} (green dash-dot-dash) and E°_{the} (green dash). (b) Comparison between steam electrolysis and CAWE from 100 to 900 °C (LHV, steam); Water electrolysis for E°_{rev} (blue); CAWE 4-electron reaction for E°_{rev} (red); CAWE 2-electron reaction for E°_{rev} (green). (For interpretation of the references to colour in this figure legend, the reader is referred to the web version of this article.)

reaction zone), the electrical energy supplied is not sufficient for splitting water, and external energy (heat source) would be essential [6,35,37]. In contrast to low temperature electrolysis processes, the operation of water splitting at higher temperatures is more favourable in terms of thermodynamics and reaction kinetics. For instance, an increase in temperature from 25 to 800 °C reduces not only the electrical energy input (ΔG) required (reduction in E°_{the} by ~ 50%), but also results in lower polarisation losses due to faster reaction kinetics. The total electric power requirement, therefore, can be reduced by using external waste heat from sources such as conventional coal, NG and nuclear power plants [6,45,102–104]. Another observation from Table 2 is the reduction in the thermo-neutral voltage at higher temperatures for both conventional electrolysis (1.48 V at 25 °C to 1.29 V at 827 °C) and CAWE (0.46 V at 25 °C to 0.26 V at 827 °C). This is due to the thermal energy input available at higher temperatures for the electrolysis process, as mentioned earlier.

In terms of electrochemical kinetics of the redox reactions, the high overpotential is necessary for desirable current density, due to the sluggish OER kinetics at the anode. This means that the anode reaction for OER or carbon–water oxidation reaction (COR) processes has a very low exchange current density (j_o), and the overall electrolysis process is governed by slow kinetics. For example, the j_o for OER ($j_{o,\ OER} = 10^{-6}$ to 10^{-12} mA cm^{-2}) is about three to six orders of magnitude lower than for HER ($j_{o,\ HER} = 10^{-3}$ mA cm^{-2}) [7]. Although both water and COR processes lead to a high anodic overpotential of electrolysis cells to achieve desirable hydrogen production rates (cell current density of > 1 A cm^{-2}) due to slow kinetics, the major advantage of the CAWE approach is that the anode overpotential can be dramatically reduced to below 0.8 V, as illustrated in Fig. 8. The $j-V$ curves representative of the Butler–Volmer kinetics law are presented for different types of electrolysis in acid medium at 25 °C and 1 atm. In particular, the reversible voltages (E°_{rev}) of the overall electrolysis reactions involving carbon/hydrocarbon are significantly lower ($E^{\circ}_{rev,\ carbon} = 0.21$ V) than the conventional electrolysis ($E^{\circ}_{rev,\ water} = 1.23$ V). However, the CAWE process can be expected to have similar issues with slower kinetics ($j_{o,\ methanol\ in\ electrolysis} > 1 \times 10^{-5}$ mA cm^{-2}) [72] and high overpotential losses, depending on its electrochemical reforming/decomposition reaction mechanism, molecular formula/weight and anode electrocatalysts.

3.2.3. Power consumption

The power consumption (electric energy consumption) in an electrolysis cell per 1 m^3 of hydrogen produced can be calculated from the cell voltage and the current passed through the cell for a fixed period of

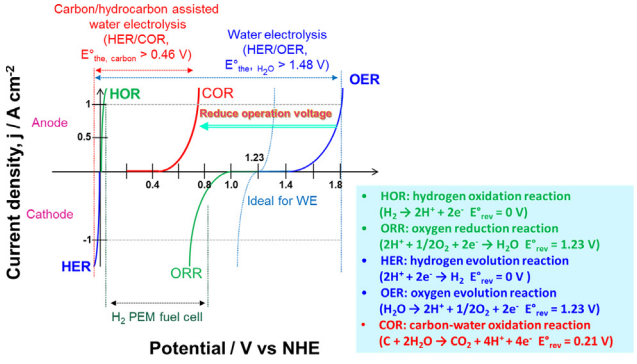

Fig.8. The electrolysis activity within the electrochemical potential windows for water electrolysis (WE) and carbon/hydrocarbon assisted electrolysis (CAWE) in acid medium at 25 °C and 1 atm. Conventional water electrolysis is represented by the hydrogen evolution and oxygen evolution reactions (HER/OER), while the CAWE process is represented by the carbon–water oxidation reaction (COR) and hydrogen evolution reaction (HER). A polymer electrolyte membrane (PEM) fuel cell can perform in a reversible mode by hydrogen oxidation and oxygen reduction reactions (HOR/ORR).

time. The current efficiency of hydrogen production is expected to be close to 100% if there is no short circuiting in the electrolysis cell, and all the current passed through the cell contributes to water dissociation to produce hydrogen. According to Faraday's law, the power consumption, P_i, for a water electrolysis process can be expressed as follows:

$$\text{Energy consumption, kWh m}^{-3} = V_{cell}\ x\ (nF/3600)\ x\ (1/24.47) = 2.19\ x\ V_{cell} \quad (8)$$

where one molar volume of an ideal gas at 25 °C and 1 atm is considered to be 24.47 L mol^{-1}, n is the number of electrons involved in the HER (n = 2) and F is Faraday constant of 96,485 C mol^{-1}. The minimum energy consumption in water electrolysis based on the thermo-neutral voltage value of 1.48 V is calculated to be 3.24 kWh m^{-3} (79.33 Wh mol^{-1}) H_2 at 25 °C and 2.83 kWh Nm^{-3} (69.15 Wh mol^{-1}) H_2 at 827 °C. However, as mentioned earlier, due to the other losses in the conventional electrolysis cell components, the cell operating voltage will be higher than the thermo-neutral voltage.

Typically, the electrical energy requirement in conventional electrolyser is 4.2–5.5 kWh m^{-3} H_2 for the stack and 6.7–7.6 kWh m^{-3} H_2 for a system [6,105]. Fig. 9 illustrates the theoretical electric energy

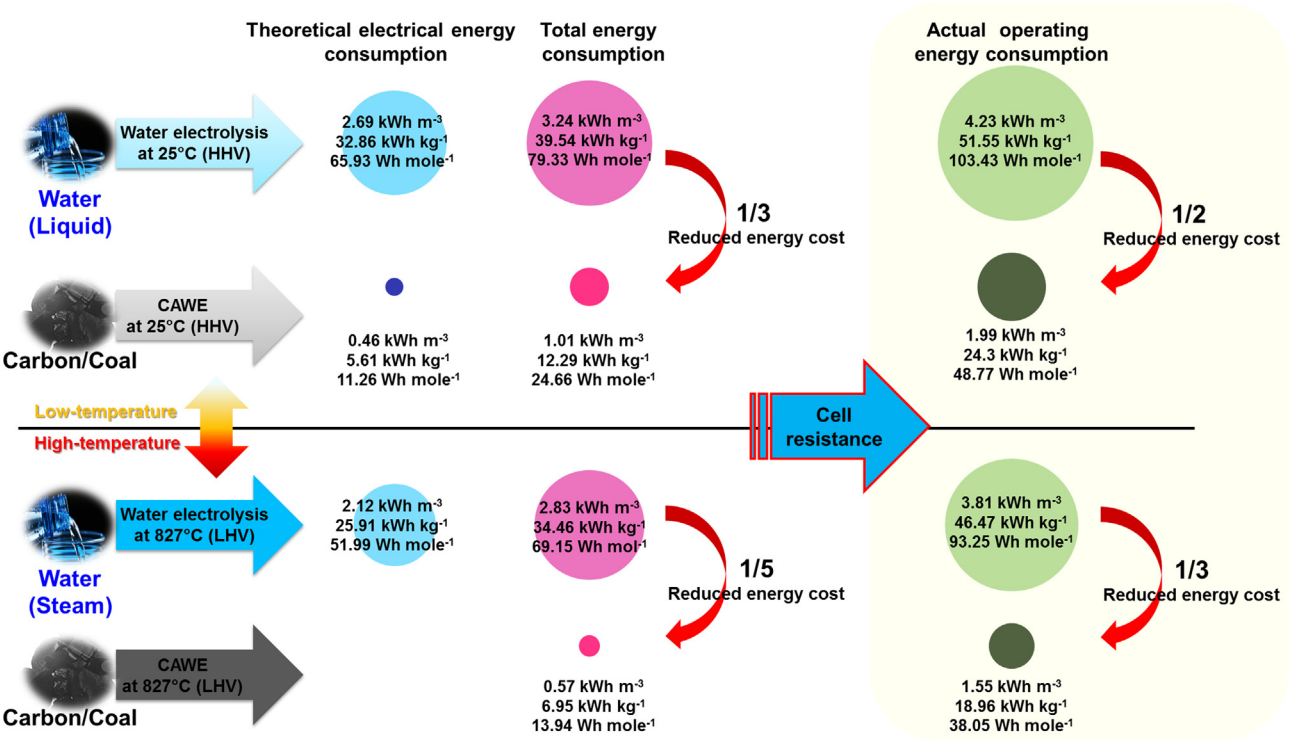

Fig. 9. Diagram of the energy consumption for water and carbon/hydrocarbon assisted electrolysis (CAWE) for hydrogen production at low temperature (25 °C) and high temperature (827 °C), calculated by Eq. (8): $V_{cell} \times 2.19\,kWh\,m^{-3}$. Electrical energy consumption is calculated from the reversible cell voltage (E°_{rev}) and total energy consumption from the thermo-neutral voltage (E°_{the}). The calculation for actual operation takes into account the cell resistance for both conventional water electrolysis and CAWE. The voltage loss is considered to be 0.45 V (0.45 Ω cm^2 at 1 A cm^{-2}). Other parameters used in the calculation are: H_2 molar volume 0.02447 $m^3\,mol^{-1}$ (25 °C and 1 atm) and density = 0.082 kg m^{-3}.

requirements to produce 1 m^3, 1 kg and 1 mol of hydrogen for conventional water electrolysis and CAWE at a low temperature (25 °C) and high temperature (827 °C) at 1 atm. The values given in the figure are electrical energy requirements based on ΔG and thermo-neutral voltage (ΔH). The actual power consumption for an electrolysis cell operating at reasonably high current densities (i.e. hydrogen generation rates) is also given assuming a typical cell area specific resistance of 0.25 Ω-cm^2. The figure shows that when using carbon in the anode reaction, the total electric energy consumption (based on thermo-neutral voltage) in the electrolysis process is 1.01 kWh m^{-3} (24.66 Wh $mole^{-1}$) H_2 at 25 °C (HHV), which is less than one-third of the energy required for conventional electrolysis. This means that based on the thermo-neutral voltage, a CAWE can be operated by using only about 30% of the electrical input required for conventional water electrolysis at near room temperature. The situation further improves by operating the carbon assisted electrolyser at a higher temperature, for example at 827 °C, where only 20% of the electrical input is required compared with the corresponding conventional electrolysis at 25 °C. Fig. 9 also reveals that at practical hydrogen generation rates, more than half of energy consumption in the CAWE process could come from the chemical energy of carbon, the anode reaction products being mainly pure CO_2 that can be easily sequestered. However, it is worth emphasising (i) the sluggish electrochemical and/or chemical oxidation kinetics of solid carbon, (ii) the mass-transport limitations due to the structure and complex composition of carbon/coal, and (iii) the surface functional groups, crystalline structure and impurities in coal, the effect of which is not yet clear [13,20,35].

4. Carbon/coal assisted water electrolysis via aqueous electrochemical cells

4.1. Acidic media based system

One of the earliest studies on coal assisted electrolysis employing aqueous electrolyte was by Coughlin and Farooque [33–37]. In a series of experimental investigations, coal, char and lignite were used in acidic medium (H_2SO_4 solution). The experiments were conducted in a simple beaker cell, with isolation between the anode and cathode provided by a porous fritted glass. This allowed the generation of pure hydrogen in a separate chamber and the prevention of inhibition reactions caused by impurities in the coal, such as sulfur, tar and ash. In most instances the cathode was a Pt mesh, and anode was Pt mesh, graphite rods or felt. The authors successfully demonstrated the onset potential of HER at mild temperatures (20–115 °C) and potentials of around 0.8 V (E°_{rev} at 25 °C = 0.21). However, the coal oxidation rate recorded was very low, as reflected by the current densities ($< 5\,mA\,cm^{-2}$) due to high ohmic resistance of the electrochemical cell employed. A simplified estimation of a scaled-up system, based on 0.36 g cm^{-3} concentration of the coal slurry at an operating potential of 1 V, revealed that a system volume of $1.8 \times 10^5\,m^3$ could produce 100 tons hr^{-1} hydrogen at 39 °C by applying current of 32.5 mA [33–36]. Gas production was also analysed using gas chromatography (GC). Almost pure hydrogen gas was detected at the cathode (hydrogen electrode) with close to 100% Faradaic efficiency (FE; coulombic or current efficiency), while a mixture of mainly CO_2 and CO (about 9:1 by

volume, respectively) was identified at the anode using Pt and graphite felt. It was suggested that a lower CO concentration was observed using Pt anode due to higher electrocatalytic activity that promoted further CO oxidation to CO_2 [36]. During the electrochemical oxidation of coal in these experiments, the coal oxidation and gas production rates decreased with time, thereby increasing the required oxidation potential. The authors revealed that the reactivity loss might be attributed to the formation of oxygen-containing functional groups, thereby preventing electron transfer. Carboxyl groups are suggested to be the predominant functional groups formed on the coal surface [34]. The carboxyl groups or carboxylated fragments can lead to formation of carbon oxide gases, aliphatic hydrocarbons and tar-like substances by a Kolbe-type reaction mechanism [33–35,106,107]:

$$RCOO^- + R'COO^- \rightarrow 2CO_2 + RR' + 2e^- \quad (9)$$

$$RCOO^- \rightarrow CO_2 + R' + e^- \quad (10)$$

where R' is alkyl free radicals, and R and R' are two different alkyl fractions. The activation energy measured for carbon (lignite) oxidation rate in the temperature range 25–110 °C was estimated to be 9–13 kcal mol^{-1} in the oxidation potential range of 0.8–1.3 V [34].

Coughlin and Farooque also investigated the effect of process variables on coal oxidation rates [33–35]. The oxidation rates increased to different extents with an increase in cell voltage (0.7–1.2 V), slurry concentration (12–300 g L^{-1}), temperature (25–90 °C) and coal particle surface area (40–200 μm size range). The type of coal and its source also had a significant effect on oxidation rates due mainly to the large variability between different coals in terms of organic chemistry and inorganic species and their chemical form. Another variable studied was the coal in contact with the anode and isolated from the anode; oxidation rates were an order of magnitude higher in the former case. Measurements of the gas volumes generated at cathode (H_2) and anode (CO_2 and CO mainly) revealed a high cathode to anode gas ratio of about 8 at the beginning that eventually decreased with time to about 4. This has been suggested to be initially due to the build-up of groups on the coal surface, such as −COOH, −CHO and $-CH_2OH$. Once a steady-state saturation of the coal surface was reached, further carbon oxide products were produced as gases, such as CO_2 and CO. This is reflected in the CO_2 production efficiency, which initially started at about 25%, but increased to around 50% with time [33,34].

Okada et al. [51] re-examined the studies carried out by Coughlin and Farooque [33,34] with anthracite and lignite coal slurries in H_2SO_4 solution. HER started at around 0.6 V and the limiting current density obtained was 5–10 mA cm^{-2} at 80 °C. A similar current density was obtained in the presence of Fe^{2+} ions, but without any coal in the solution. The potential regions for the electrolysis reaction (0.7–1.2 V), initial current densities and the cathode current efficiencies (close to 100%) were measured, and the results were similar to those reported by Coughlin and Farooque. However, in contrast to the HER (cathodic current) efficiency of near 100% observed by both studies, the measured CO_2 evolution efficiency was only 5–10%. The latter value is significantly lower than the 25–50% measured by Coughlin and Farooque. The authors also observed that the coal slurries prepared in H_2SO_4 after sufficient washing of coal produced a current density of only about 0.1 mA cm^{-2}. This may be due to the removal of significant inorganics (Na, K, Ca) that catalyse the oxidations reactions. The current density with pure carbon powder under the same conditions as for coal was also very low (ca. 0.1 mA cm^{-2}), but the FE of CO_2 reached 80% in this case. The higher CO_2 production current efficiency from carbon compared with coal has been explained to be due to the presence of carboxyl, nitrogen and sulfur-containing molecules on coal surface that result in other by-products rather than CO_2. The authors believe that coal oxidation at the anode involves two processes: (i) direct collisional reaction of slurry particles with electrode and (ii) dissolved impurity (Fe^{2+}/Fe^{3+} redox and desorbed material) undergoing oxidation.

Murphy and Bockris [108] studied the anodic oxidation of carbon by employing slurries of lignite, grass and household waste. The electrolytes used were H_2SO_4, H_3PO_4 and NaOH at 80–130 °C. The limiting current densities measured by cyclic voltammetry, with unwashed lignite at 1 V were around 10 mA cm^{-2}, and were confirmed to be due to the iron species leached out from coal. The steady-state current densities achieved for hydrogen evolution at 1 V were in the range of 1–5 mA cm^{-2}. Investigations using washed coal slurries revealed that the current density is three times greater when coal particles are allowed to make contact with the anode. This is explained on the basis of coal/electrode collisions resulting in an increased dissolution of organic compounds from coal by mechanical abrasion. The authors suggest that current densities can be increased to 200–400 mA cm^{-2} by forced stirring of the coal slurry, increasing temperature (up to 180 °C) and pressure (up to 10 bar), improving electrocatalysis and reducing pH.

Baldwin et al. [46] studied voltammetric and electrolysis behaviour of several coal mixtures (anthracite and bituminous) and coal-derived liquids in aqueous and organic solvents. The oxidation of aqueous coal slurry started at ca. 0.64 V, while higher overpotential was observed in dimethylsulfoxide (DMSO) and acetonitrile solvents. The oxidation current was attributed primarily to the oxidation of Fe^{2+} (produced by catalytic oxidation of coal by Fe^{3+} ions leached from pyrite (FeS_2) in the coal) to Fe^{3+}. Dhooge and Park [47–50] describe in more detail the mechanism of the electrocatalytic oxidation of coal slurry. They report a similar observation to Baldwin et al., that when acid-washed coal (with 3.6 M H_2SO_4 for ~100 h) was tested; near zero oxidation current was observed. This suggests that the coal slurry was catalytically oxidised by the existence of Fe^{3+} ions leached out from the coal into solution. In the presence of Fe^{3+} ions, the reaction mechanism proposed by several investigators [46,49] is as follows:

$$\text{in the solution: } C + 4Fe^{3+} + 2H_2O \rightarrow CO_2 + 4Fe^{2+} + 4H^+ \quad (11)$$

$$\text{at the anode: } Fe^{2+} \rightarrow Fe^{3+} + e^- \quad (12)$$

The Fe^{3+}/Fe^{2+} redox couple present in the coal slurry increases the carbon oxidation rate. The CAWE process can be described as follows: (i) in the first stage the formation of surface oxides with changing coal surface structure and the removal of the mineral impurities occur and (ii) in the second stage, the CO_2 evolution reaction predominantly occurs due to the dissolved carbonate species (HCO_3^-, CO_3^{2-}) present in the coal [47,50].

To investigate the role of dissolved iron species and the effect of desulfurisation during coal electrolysis, Lalvani et al. [32,109] conducted electrochemical tests using a three-electrode arrangement and a three-dimensional anode cell (made of heaped coal particles). Their preliminary experiments indicated that by coal electrolysis in acidic media, up to 40% of the total sulfur and a small quantity of nitrogen can be removed from the coal. This is simultaneously accompanied by leaching out of iron species in the acid electrolyte and the production of hydrogen with FE over 95%. They also suggest that the Fe^{2+}/Fe^{3+} redox couple acts as an electrocatalyst, as shown in the following reaction mechanism:

$$FeS_2 + Fe_2(SO_4)_3 + 4H_2O \rightarrow 6FeSO_4 + 4H_2SO_4 \quad (13)$$

$$2S + 6Fe_2(SO_4)_3 + 8H_2O \rightarrow 12FeSO_4 + 8H_2SO_4 \quad (14)$$

Kusunoki and co-workers [110–112] have been actively involved in the area of coal desulfurisation and electrolysis. To examine the feasibility of a large-scale cell in the CAWE, Kusakabe et al. demonstrated a hybrid process of chemical desulfurisation combined with water electrolysis using a flow-through packed-bed electrode cell [111]. They propose that chemical desulfurisation of coal can be achieved by leaching the pulverised coal in acidic solutions (HCl or H_2SO_4) containing Fe^{3+} ions (leached out from coal and/or added). This results in the formation of elemental sulfur and sulfates, followed by the electrolysis of coal filtrate in the flow-through cell. Fig. 10(a) and (b) shows

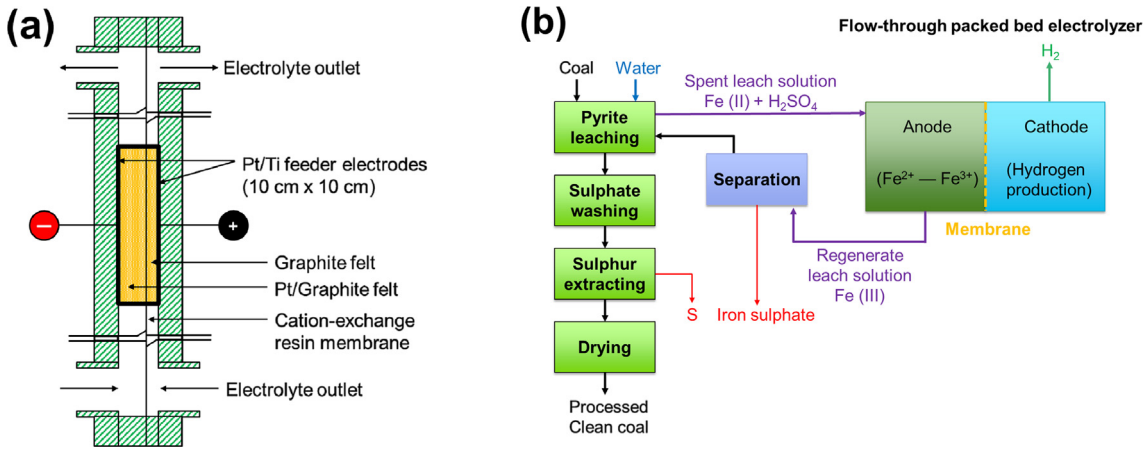

Fig. 10. Schematic drawings of (a) flow-through packed bed with Pt-plated Ti pellets with anolyte and catholyte circulated through each chamber, and (b) hybrid process of CAWE combined with coal desulfurisation. Figure redrawn from [110,111].

the block diagram of the hybrid process and schematic of the flow-through cell, respectively. The chemical and electrochemical reactions associated with the hybrid process are as follows.

Desulfurisation and coal oxidation:

$$FeS_2 + 2Fe^{3+} \rightarrow 3Fe^{2+} + 2S \quad (15)$$

$$FeS_2 + 14Fe^{3+} + 8H_2O \rightarrow 15Fe^{2+} + 12H^+ + 2H_2SO_4 \quad (16)$$

$$\text{Coal} + 4Fe^{3+} + 2H_2O \rightarrow CO_2 + 4Fe^{2+} + 4H^+ + \text{Others-oxidised/consumed coal} \quad (17)$$

Electrolysis reactions:

$$\text{at the anode: } Fe^{2+} \rightarrow Fe^{3+} + e^- \quad (12)$$

$$\text{at the cathode: } 2H^+ + 2e^- \rightarrow H_2 \quad (18)$$

The electrolysis cell used in Kusakabe et al.'s investigation consisted of Pt-deposited Ti plates as anode and cathode, separated by a cation-exchange membrane (Nafion 415) [111]. The space between each electrode and the membrane was packed with graphite felt to increase the electrode surface area. The graphite felt in the cathode chamber was electroplated with Pt to reduce hydrogen evolution overpotential losses. Pyritic sulfur was removed (chemical desulfurisation) in a solution of 1 M HCl and ca. 0.9 M Fe^{3+} at 90–110 °C in this flow-through packed-bed electrolysis system [111,112]. The coal filtrate used in the electrolysis process was prepared by treating pulverised coal in a solution of 4 M H_2SO_4 and 0.5 M Fe^{3+} at 110 °C for 2 h. The filtrate was circulated through the anode packed bed at 50 °C for the electrolysis experiments. The pyritic sulfur removal reported from these experiments for two types of coals was 87–100%. The current densities achieved with Illinois No.6 coal filtrate were significantly high (100 mA cm^{-2} at 1 V), due to the presence of graphite felt with no deactivation of felt after up to 20 h of electrolysis; the power consumption for hydrogen generation was half that of conventional electrolysis.

In another study by Kusunoki and co-workers [110], the anode chamber of the flow-through cell described above was packed with Pt-coated Ti pellets (5 mm long × 5 mm diameter pellets, instead of graphite felt) in contact with the Pt-coated Ti plate. This increased the surface area of anode and created more collisions between the coal particles in the coal slurry and the anode surface. The cathode chamber was left unfilled. The slurries of different coals and activated carbon in 4 M H_2SO_4 were circulated through anode chamber at 50 °C, with a superficial velocity of around 10 cm s^{-1}. The electrolysis investigations were carried out with 4 M H_2SO_4 alone, coal slurries made with different coals (Miike, Taiheiyo, Yallourn), washed Yallourn coal, activated carbon and purified graphite with added Fe^{3+}. The electrolysis process (H_2 evolution) started at 1.6 V for H_2SO_4 electrolyte alone, compared with 0.8 V in all other cases. The current densities measured with graphite slurry at 1.6 V were 10 times those measured by Okada et al. [68], thus demonstrating the effect of the collision of graphite particles with the anode surface in the flow-through cell in the present case. The current densities measured with coal slurry and filtrate were similar, but lower in the case of washed coal. Coal slurries with Fe^{3+} added to 20-fold of the amount initially present in the coal resulted in an order-of-magnitude increase in current densities compared with coal slurry in the absence of Fe^{3+}. On the basis of these studies, the authors postulate that anodic reactions in the coal slurry comprise the oxidation of Fe^{2+} ions dissolved from coal and the reduction of Fe^{3+} by chemical reactions with reducing compounds in coal. In addition, water-soluble organic compounds in coal can partially oxidise to produce CO_2 and CO. The study also highlighted the effect of collisions between the coal particles and anode electrode, which increased the rate of coal oxidation. Their suggested reaction mechanism is in reasonably good agreement with that of Lalvani et al. [32,109].

Unlike the above studies, Taylor et al. [113] argue that CO_2 evolution from leached macromolecules of well-washed coals arises only at high anode voltages (> 2.8 V) with very low FE of CO_2, with oxygen evolution as the main anodic reaction. However, this anodic potential is much higher than the OER potential. Thus it is expected that the electrochemical coal oxidation is most likely mainly replaced by water electrolysis to produce oxygen.

Carbon and carbonaceous materials (cellulose) assisted water electrolysis at a somewhat higher temperature (> 120 °C) and pressure (150 psi) than the previous studies was attempted by Clarke et al. [67] to investigate the effect of these test conditions on the process. The Fe^{2+}/Fe^{3+} redox couple was also used as a mediator. The limiting current densities achieved at 1 V with coal slurries (100 mesh, 0.33 g ml^{-1}) made with 2.5 M H_2SO_4 at 180 °C (150 psi) were 30 mA cm^{-2} with coal slurry alone, 150 mA cm^{-2} with added 0.13 M ferric ions and 200 mA cm^{-2} with added 0.25 M ferric ions. However, current density degraded after the initial period, due to sluggish decarboxylation of the thermally stable carboxylated surface of the coal particles. Clarke et al. concluded that two kinds of by-products were produced during the CAWE process: soluble, thermally stable, low-molecular-weight humic and fulvic acid substances, and heavily carboxylated carbon fines. The economics of the CAWE under high temperature and pressure as investigated by these authors will depend on the reduction in power input to the system for hydrogen generation, and the value of by-products formed in the process.

Thomas et al. [106,114] selected four different types of Alberta coals and studied the kinetics of the Fe^{3+} mediated electrochemical oxidation of coal in 1 M H_2SO_4 at 90 °C. They found that coal activity for oxidation increases as the fixed carbon content (rank of coal) of coal

increases. The kinetic analysis of the current vs time data revealed two rate constants corresponding to initial and later stages of coal oxidation; this was explained in relation to the different organic functional groups present on the coal surface. The authors suggested that the nature of the functional groups, such as hydroquinones, phenols, aromatic amines and organosulfur compounds, on the external surface of the coal would be a more dominant oxidation factor in short-term periods (< 10 h) of electrolysis, while the accessibility of Fe^{3+} ions in the internal pore surface and within the solid coal matrix would be more important for further oxidation of coal. This was also confirmed by measuring the CO_2 generation current efficiencies, initially observed to be around 40% after ca. 3 h of electrolysis (mainly due to oxidation of the coal surface) and 70–80% after ca. 22 h (mainly due to the oxidation of coal mediated by Fe^{3+} present in internal pore surfaces and within the solid coal matrix).

After a relatively short hiatus, the strategy of using carbon in water electrolysis was taken up again by researchers in 2005 due to the growing demand for hydrogen as a renewable source of energy and the increasing environmental consideration given to clean coal technology. Yin et al. [115] fabricated multilayer nanoporous Ti/TiO_2 films as a catalyst support using an electrochemical etching method and investigated the catalytic activity of Pt, Ru, RuO_2, IrO_2 and their alloys intercalated and deposited on the Ti/TiO_2 film pores. These multilayer structures showed the current density and amount of hydrogen production improved around twofold compared with those with pure Pt and Pt-coated Ti electrodes. The best performance was achieved with Pt–Ru supported on nanoporous Ti/TiO_2 films, producing a current density of about 4 mA cm^{-2} at 1 V from coal slurry (< 6 μm particles at 0.12 g L^{-1} concentration) prepared in 0.5 M H_2SO_4 at 85 °C. The FE achieved for H_2 and CO_2 gases were 98% and 10%, respectively. In another study of carbon assisted electrolysis by Yin et al. [116], electrodes were prepared by dip coating a Ti sheet with inks containing Pt, Ru or Ir individually or in combination followed by thermal decomposition. The Ti/IrO_2 electrode had the best performance of the electrodes tested.

To increase the coal electrolysis rate, Yin et al. [116] used various redox liquid catalysts such as Fe^{3+}, $K_3Fe(CN)_6$, KBr and V_2O_5. The better performance observed when using redox liquid catalysts was explained on the basis of these catalysts bridging the coal particles and the solid electrode surface. The best performance obtained was with Fe^{3+} due to Fe^{3+}/Fe^{2+} dynamic transformation. Researchers from the same institute (Yu et al. [117]) also studied the effect of different electrolytes (H_2SO_4 and HCl), and further investigated the effect of liquid catalyst K3Fe(CN)6 on the electro-oxidation of coal in HCl. The results showed that HCl was more suitable for coal oxidation than H_2SO_4, due to the Cl^- anion interacting more strongly with coal particles. When $K_3Fe(CN)_6$ liquid catalyst was added into the coal slurry with HCl as electrolyte, the current densities were three times greater (ca. 10 mA cm^{-2} at 1.3 V). This catalytic mechanism seems to be a two-step, indirect reaction. The dynamic transformation of $[Fe(CN)_6]^{3-}/[Fe(CN)_6]^{4-}$ redox proposed by the investigators is shown in Fig. 11 [117]:

$$\text{in the solution: } 4[Fe(CN)_6]^{3-} + H_2O + C \rightarrow 4[Fe(CN)_6]^{4-} + 4H^+ + \text{other coal intermediates} \quad (19)$$

$$\text{at the anode: } [Fe(CN)_6]^{4-} \rightarrow [Fe(CN)_6]^{3-} + e^- \quad (20)$$

Hesenov et al. [61,62] investigated the effects of various experimental conditions, such as geometric area of the membrane, electrolyte concentration, cell potential and coal type, as well as the relationship between anode and cathode gas evolution. They observed that the generation of CO_2 was independent of the HER in an H-cell with Nafion 117 membrane, because coal was indirectly oxidised in the electrolyte media (see Eqs. (9) and (10)) and may convert into other organic matter during the electrolysis. This was confirmed by analysing the total organic carbon (TOC) with a non-dispersive infrared detector and gas analysis by GC connected to a thermal conductivity detector. They

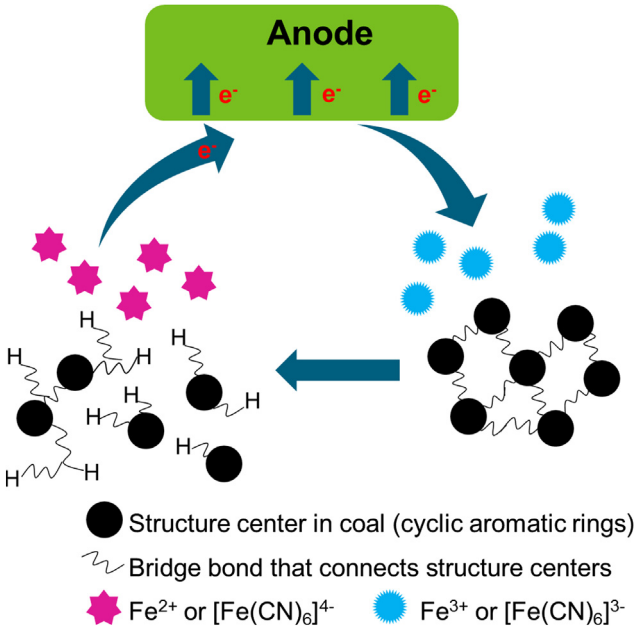

Fig. 11. Synergistic effect of $K_3Fe(CN)_6$ catalyst in HCl electrolyte for electrochemical oxidation of coal. Figure redrawn from [117].

assume that the efficiency of CAWE process could be measured by hydrogen generation as opposed to the CO_2 generation efficiency considered by some previous investigators. In the presence of Fe^{2+}/Fe^{3+} ions in coal slurries (0.12 g ml^{-1} concentration in 5 M H_2SO_4), current densities as high as 62.7 mA cm^{-2} (dropped to 30 mA cm^{-2} in 8 h) at 1 V and 163 mA cm^{-2} (dropped to 80 mA cm^{-2} in 8 h) at 2 V were achieved at 100 °C. However, there was no significant effect on cell voltage without Fe ions. In addition, Hesenov et al. observed that the organic compounds dissolved from coal into aqueous anolyte were strongly adsorbed on the Nafion membrane separator surface, and that this membrane fouling hindered further migration of protons to the cathode.

Seehra et al. [54] compared the HER rate for various carbon materials using an H-cell with anode and cathode chambers separated from each other by glass frit, and employing 3.4 M H_2SO_4 as the electrolyte (carbon slurries concentration ~0.08 g ml^{-1}) at room temperature. The carbon sources used were: carbon GX203, Black Pearl (BP2000), single and multi-carbon nanotubes, graphite and coal. Using nano-crystalline carbon (BP2000) with a high surface area (1500 $m^2 g^{-1}$) and high electrical conductivity, about a 10-fold increase in HER rate was observed compared with carbon GX203 (SA 1000 $m^2 g^{-1}$) at 1.12 V.

The physicochemical properties of carbon/coal have been also investigated by other researchers [33,34,37,51,112]. The effect of additive catalysts was also studied using $FeSO_4$ and $Ce(SO_4)_2$ in 3.7 M H_2SO_4 [54]. By adding Fe ions to the BP2000 slurry, the energy required for hydrogen generation at 0.72 V reduced to 30%. Gong et al. [59] studied the effect of different kinds of coal slurries (lignite, bituminous and anthracite coals, graphite) and catalyst additives in slurries ($FeSO_4$, $Fe_2(SP_4)_3$, $NiSO_4$, $CoSO_4$) on cell voltage as a function of time. They employed cyclic voltammetry in an electrolysis cell using 1.5 M H_2SO_4 as the electrolyte and Nafion N115 membrane as a separator between the cathode and anode chambers, as shown in Fig. 12(a). The overall cell voltage for CAWE fell with a decrease in the coal rank (lignite < bituminous < anthracite < graphite), which was explained as being related to the surface functional groups present on the coal surface. Further, the effect of presence of catalytic ionic species in coal slurry on the cell voltage was $Co^{2+} < Ni^{2+} < Fe^{2+} < Fe^{3+}$. In another study, Gong et al. [60] compared the cell voltages required for CAWE with raw and demineralised lignite coals. The electrolysis cell

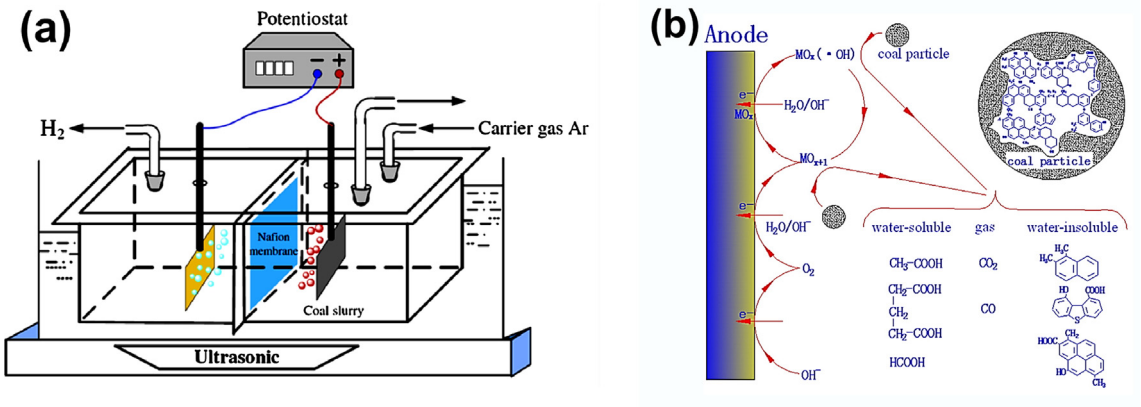

Fig. 12. Schematic drawings of (a) ultrasonic bath system for CAWE and (b) mechanism for formation of total organic carbon in CAWE. Figure reproduced with permission from [57,60].

used in this study was similar to the one in previous work [59]; however, the solution was kept stirred to improve mass-transfer with ultrasonic wave energy. The authors demonstrated that due to the catalytic effect of ionic species present on the coal surface, the required cell voltage was lower for raw lignite than for demineralised lignite coal. Moreover, in another study by Gong et al. [57], CAWE kinetics of three types of coals (raw coal, coal washed in HCl and coal washed in HF) in 1 M NaOH solution was investigated by monitoring the TOC in the electrolysis solutions. The effect of ultrasonic wave energy on the TOC was also investigated; ultrasonic waves are expected to affect TOC due to the breaking of the coal structures and facilitation of mass transfer in the solution. However, the activation energy values for CAWE were found to only slightly change from 28.37 to 27.61 kJ mol^{-1}. The TOC in the electrolyte solution after electrolysis decreased with the presence of mineral content in coal (raw coal > HCl-washed coal > HF-washed coal), and this effect was more pronounced when using ultrasonic wave energy. Fig. 12(b) shows the mechanism of formation of TOC by CAWE in NaOH media as described by the authors using an unreacted shrinking-core model. The main controlling step was thought to be the chemical-oxidation reaction occurring between coal particles and the oxidising media, such as metal ions (Fe^{2+}/Fe^{3+}) as electron transfer mediators and the physisorbed/chemisorbed active oxygen, but further investigation is required to confirm this view. Chen et al. [118] investigated coal desulfurisation using ionic liquid-assisted coal water electrolysis in KNO_3 by applying a constant current. However, their report mainly focused on desulfurisation of coal using methylimidazole-cation (Br^-, BF_4^-, and Cl^-) ionic liquids.

In summary, the most common approach for acid-based CAWE is to use carbon/coal slurry mixed with 0.5–5 M H_2SO_4 solution in the temperature range of 25–120 °C with Fe ions to facilitate solid carbon oxidation. The various additives investigated are: metal ion redox couples (Ce^{4+}/Ce^{3+}, V^{5+}/V^{2+}, Mn^{3+}/Mn^{2+}, I_3^-/I^-, and $Fe(CN)_6^{3-}/Fe(CN)_6^{4-}$) [49,54,109,116,117], metal halides (NaCl, NaBr, $CeCl_2$, and KBr) [32,109,116] and various anolytes (HCl, NaCl, HNO_3, H_3PO_4, $HClO_4$, and DMSO) [36,49,109]. Table 4 provides the details of the investigations carried out using different types of solid fuels and system configurations at low temperature in acid media, along with the best performance achieved in each investigation. As proposed in the studies reviewed above, the mechanism of CAWE – essentially, the electrochemical oxidation of coal or carbon with or without mediation by catalytic additives (i.e. metal ions) in acid media – can be described by a four or two-electron pathway (Table 2), as discussed below [32,47–49,51,52,59,59,61,111,112,119–122].

In the acid electrolyte solution, Fe^{3+} ions are leached from coal particles and coal/carbon can be also oxidised indirectly – see also Eqs. (11), (12), (15)–(17), (19) and (20). Complex coal structures could be broken down and surface functional groups changed; for example, pyritic sulfur in coal could be leached out as sulfate or elemental sulfur. These reactions can be summarised as follows.

In the solution:

$$FeS_2 + Fe_2(SO_4)_3 + 4H_2O \rightarrow 6FeSO_4 + 4H_2SO_4 \quad (13)$$

$$2S + 6Fe_2(SO_4)_3 + 8H_2O \rightarrow 12FeSO_4 + 8H_2SO_4 \quad (14)$$

$$C + 4Fe^{3+} + 2H_2O \rightarrow CO_2 + 4Fe^{2+} + 4H^+ + \text{oxidised/consumed coal/carbon} \quad (21)$$

$$C + 2Fe^{3+} + H_2O \rightarrow CO + 2Fe^{2+} + 2H^+ + \text{oxidised/consumed coal/carbon} \quad (22)$$

At the anode: $Fe^{2+} \rightarrow Fe^{3+} + e^-$ (12)

The standard equilibrium potential of the Fe^{3+}/Fe^{2+} redox reaction is 0.77 V, which is within the experimental onset potential range of 0.5–1.0 V for CAWE [32,47,123]. At actual operating voltage, Fe^{2+} could be spontaneously oxidised at the electrode/electrolyte interface to Fe^{3+}, and produce electrons, while the Fe^{3+} ions are reduced to Fe^{2+} again by carbon species in solution. The reactions (21), (22) and (12) can also occur simultaneously. For this reason, in previous studies, a sharp decline in the current density and hydrogen evolution rate have been observed at voltages > 1 V, probably due to the faster consumption of Fe^{2+} ions by reaction (12) compared with their regeneration by reactions (21) and (22). Thus, the kinetics of electrochemical oxidation of both coal and Fe species need to be further examined. The current efficiency of the process should be analysed by monitoring CO/CO_2 generation rates to relate these to coal oxidation [54,65,124,125]. However, it is still difficult to provide a distinct evidence that Fe^{3+} ions react with carbon to regenerate Fe^{2+} ions in the CAWE process.

The direct electrochemical conversion of solid coal/carbon at the anode interface is thought to be intrinsically sluggish, as demonstrated by the low rates of CO_2 generation. The main causes of this can be summarised as (i) the lack of physiochemical contact sites at the anode for the reaction, (ii) poor dispersion of coal/carbon particles in the bulk of slurries, (iii) continuous formation of passive oxide surface at the coal/carbon anode, and (iv) the sluggish reaction kinetics of coal oxidation compared with the oxidation of other coal impurities (e.g. other organic matter, minerals). Thus, CAWE in aqueous electrochemical cells can be mainly attributed to the indirect electrochemical oxidation pathway via the redox couple of the dissolved metal ions as an electrochemical mediator (see Table 4 for electrolyte additives). From the work reviewed above on acidic solution electrochemical cells, we conclude that to date, relatively low current density (around 50 mA cm^{-2}) values have been reported for systems operating at < 100 °C under atmospheric pressures. High temperatures and pressures seem to favour this process, with current densities reaching

Table 4
Summary of CAWE performance using different types of fuels and system configurations at low temperature in acid media.

Coal used	Anolyte (supporting electrolyte)	Additive	Anode	Anode area/cm^2	Separator	Cathode	Cell configuration	Onset potential/V	Cell temp./°C	Best performance (near 0.8 ~ 1.2 V)	Ref.
Coal, lignite, activated charcoal, and char	0.1–0.56 M H_2SO_4		Pt mesh	6.5and 96.5	PFG	Pt mesh	BC	0.8–1.2	40–80	1.55 mA cm^{-2} at 1.2 V	[34]
Coal, lignite, and char	3.7–5.6 M H_2SO_4		Pt mesh	6.5	PFG	Pt mesh	BC	0.78	23–114	1.4 mA cm^{-2} at 0.83 V, 23 °C	[33]
Coal, lignite, and char	3.7–5.6 M H_2SO_4		Pt mesh	6.5and 96.5	PFG	Pt mesh	BC	0.78	23–114	< 5 mA cm^{-2} at 0.9 V, 114 °C	[35]
Lignite	4.1–5.6 M H_2SO_4, H_3PO_4, and trifluoromethane sulphonic acid monohydrate		Graphite rods and felt, and Pt mesh	104	PFG	Pt mesh	BC	~0.85	40–114	< 5 mA cm^{-2} at 0.9 V, 114 °C with graphite felt	[36]
Coal, lignite, and peat	5.6 M H_2SO_4		Pt mesh	96.5	PFG	Pt mesh	BC	0.84	110–114	1.4 mA cm^{-2} at 1 V, 114 °C with 10–30% consumed fuels	[37]
Coal	Various conditions with HCl, H_2SO_4, NaOH, and HNO_3	$FeCl_3$, NaCl, $K_2Cr_2O_7$, and NaBr	Pt mesh, packed graphite particles, and graphite felt	5.5, 10, 96.5, and 385	PFG	Pt mesh	PB, and 3-D anode cell (3ES)	0.67	22–80	40 mA cm^{-2} at 1.64 V, 80 °C with graphite felt in 100 ml of 15% HCl + 5% H_2SO_4	[32]
Coal	Various conditions with HCl, NaCl, $CuCl_2$, $Ce_2(SO_4)_3$, and H_2SO_4		Pt mesh	4	PFG	Pt mesh	BC (3ES)		75	325 mA cm^{-2} at 1.64 V, 75 °C in 15% HCl + 5% H_2SO_4	[109]
Anthracite, lignite, pure carbon, and washed slurries	1 and 4.15 M H_2SO_4		Pt plate and foil	3.55 and 14	PFG	Pt gauze	BC and H-cell (3ES)	0.6	25–80	5–10 mA cm^{-2} at 0.8 V, 80 °C in 4.15 M H_2SO_4 (FE_{CO2} 10%) with coal	[51]
Coal and liquefied coal	0.1 M $LiClO_4$ in water, DMSO, and acetonitrile		Pt mesh	6	medium PFG	Pt mesh	H-cell (3ES)	0.64	At room temp.	1.3 mA cm^{-2} at 1.24 V	[46]
Coal and activated carbon	3.6 M H_2SO_4	Fe^{3+} and Ce^{4+}	Pt		K_2SO_4 SD		Separated two cells (3ES)	0.67		2 mA cm^{-2} at 1.04 V (FE_{CO2} 15–30%)	[47]
Coal	H_2SO_4, H_3PO_4, HCl, and $HClO_4$	$CeCl_3$, $Fe_2(SO_4)_3$, and $FeSO_4$	Pt foil	10	K_2SO_4 SD	Au-plated bronze screen	Separated two cells (3ES)		20–70	3 mA cm^{-2} at 1 V (vs. NHE), 70 °C in 1.0 M H_2SO_4 + 0.2 M Fe^{3+} (FE_{CO2} 100%)	[49]
Coal	0.1 M H_2SO_4	0.1 M $Fe_2(SO_4)_3$					BC (3ES)		85–95	3 mA/g at 0.7 V, 85 °C	[52]
Coal, activated carbon, and graphite	4 M H_2SO_4	Dissolved Fe	Pt/Ti plate		CEM	Pt plate	FPB with Pt/Ti pellets	0.8	30–50	~10 mA cm^{-2} at 1 V, 50 °C	[110]
Coal	4 M H_2SO_4	$Fe_2(SO_4)_3$, and $FeSO_4$	Pt/Ti plate	100	N415	Pt/Ti plate	FPB with graphite felt		50–110	100 mA cm^{-2} at 1 V, 50 °C (FE_{CO2} 100%)	[111]
Lignite, anthracite, carbon black, and bituminous coal	H_2SO_4		Pt mesh	60	PFG	Pt mesh	BC (3ES)	~0.5	60	6.6 mA cm^{-2} at 1 V with coal	[113]
Lignite, char, and graphite	5% H_3PO_4		Au or Pt sheet		Not used	Pt sheet	BC (3ES)	~0.5	25–165	20 mA at 0.8 V, 165 °C with lignite	[68]
Coal and petroleum coke	H_2SO_4	Fe	Ti		Nafion	SS	Fluidization and flow channel	~0.4	180 (150 psi)	200 mA cm^{-2} at 1 V with 0.25 M Fe in 2.5 M H_2SO_4	[67]
Bituminous and sub bituminous coal	1 M H_2SO_4	$FeSO_4{\cdot}7H_2O$	Pt foil		Glass frit	Pt gauze	BC (3ES)	~0.7	90	120 mA at 1 V, 90 °C with 15 mM $FeSO_4$	[106,114]
Coal	0.5 M H_2SO_4		Ti/TiO_2Pt–Ru, Ti/TiO_2Pt, Pt, and TiO_2		PFG	Pt foil	H-cell	~0.4	85	5 mA cm^{-2} at 1 V, 108 °C with Ti/TiO_2Pt–Ru (1:2) (FE_{H2} ~ 98%)	[115]

(*continued on next page*)

Table 4 (*continued*)

Coal used	Anolyte (supporting electrolyte)	Additive	Anode	Anode area/cm^2	Separator	Cathode	Cell configuration	Onset potential/V	Cell temp./°C	Best performance (near 0.8 ~ 1.2 V)	Ref.
Coal	1 M H_2SO_4	Fe^{3+}, $K_3Fe(CN)_6$, KBr, and V_2O_5	Ti/Pt, Ti/RuO_2, Ti/IrO_2 and Ti/IrO_2–RuO_2	4	PFG	Pt foil	H-cell (3ES and circulation)	~0.4	75	1.6 mA cm^{-2} at 1 V with Fe^{3+}	[116]
Coal	1 M HCl and 1 M H_2SO_4	$K_3Fe(CN)_6$	Ti/IrO_2	9	PFG	Pt	H-cell (circulation)	~0.6	80	5 mA cm^{-2} at 1 V	[117]
Activated carbon	3.7 M H_2SO_4		Pt plate	6.8	PFG	Pt coil	Double H-cell (3ES)	0.2	At room temp.	~1.5 mA cm^{-2} at 0.8 V	[53]
Activated carbon, CNT, graphite powder, and coal	3.7 M H_2SO_4	$FeSO_4$ and $Ce(SO_4)_2$	Pt plate	6.8	PFG	Pt coil	Double H-cell (3ES)	~0.4	At room temp.	~23.5 mA cm^{-2} at 1 V	[54]
Coal	1–5 M H_2SO_4	100 mM Fe^{2+} and 100 mM Fe^{3+}	Pt	1	N117	Pt	BC (3ES)		40–100	~60 mA cm^{-2} at 1 V, 80 °C with 5.0 M H_2SO_4	[61]
Coal	1 M H_2SO_4	100 mM Fe^{2+} and 100 mM Fe^{3+}	Pt	1 and 6	N117	Pt	BC (3ES) and H-cell		40	~20 mA cm^{-2} at 1 V	[62]
Lignite	H_2SO_4		PbAg	9	N115	Cu	Ultrasonic bath		30	~78 mA cm^{-2} at 3 V	[60]
Lignite, bituminous coal, anthracite, and high pure graphite	H_2SO_4	Fe^{2+}, Co^{2+}, and Ni^{2+}	PbAg	9	N115	Graphite	Water bath (3ES)	1.99		~56 mA cm^{-2} at 3.54 V	[59]
Coal and graphite	1 M H_2SO_4	Fe^{3+}/Fe^{2+}	Pt, Pt–Ru, Pt–Ir, and Pt–Rh foils	2.1, 3.78, 2.8 and 2.61	N117	Platinized Pt/Ti foil	BC and U-shaped cell	0.2	40	35 mA cm^{-2} at 0.8 V for coal with PtIr(4:1) and 100 mM Fe^{3+}/100 mM Fe^{2+}	[58]
Coal and graphite	1 M H_2SO_4	100 mM Fe^{2+} and 100 mM Fe^{3+}	Rh, Pt–Rh, Pt–Ir, and Pt–Ir–Rh (5 mg cm^{-2})/carbon fiber/Ti mesh		PM	Pt/carbon fiber/Ti mesh	Sandwich (circulation)	0.8	80	25 mA cm^{-2} at 1.2 V for coal–graphite slurry with PtIr (FE_{CO2} ~ 30%)	[63]
Coal	1.5 M H_2SO_4	100 mM Fe^{2+} and 100 mM Fe^{3+}	PtIrRh/carbon fiber/Ti mesh	4	N117	Pt/carbon fiber/Ti mesh	Sandwich (circulation)	0.85	40–80	50 mA cm^{-2} at 0.85 V, 80 °C (FE_{CO2} ~ 50%)	[64]
Coal	4 M H_2SO_4	100 mM Fe^{2+} and 100 mM Fe^{3+}	Pt (6 mg cm^{-2}) and PtIr (5.3 mg cm^{-2})/carbon fiber/Hastelloy mesh		PM	Pr and PtIr/carbon fiber/Hastelloy mesh	Sandwich (circulation)	0.8	80–108	32 mA cm^{-2} (0.1 A) at 0.8 V, 108 °C (FE_{CO2} ~ 57%)	[65]
Coal	4 M H_2SO_4	$FeSO_4{\cdot}7H_2O$ and $Fe_2(SO_4)_3{\cdot}7H_2O$	[65]	2	PM	[65]	Sandwich (circulation)	-0.2	100–108	50 mA cm^{-2} at 0.8 V, 108 °C (FE_{CO2} ~ 70%)	[66]
Carbon black	1 M H_2SO_4		IrPt-Ti-mesh	50	N115	Pt/C on carbon paper	Zero-gap cell (circulation)	~0.4	20–50	~15 mA cm^{-2} at 1.2 V, 50 °C	[28]
Carbon black	1 M H_2SO_4	100 mM Fe^{2+} and 100–500 mM Fe^{3+}	IrPt-Ti-mesh	9	N115	40 wt% Pt/C on Toray 120	Zero-gap cell (circulation)	0.55	70	52 mA cm^{-2} at 1 V, 70 with 100 mM Fe^{2+} ion	[125]

3ES = three electrode system; BC = beaker cell; CEM = cation exchange membrane; FE_{CO2} = Faradaic efficiency was calculated by CO_2; FE_{H2} = Faradaic efficiency of H_2; FPB = flow-through packed bed; N = Nafion; NHE = normal hydrogen electrode; PFG = porous fritted glass; PM = polyethylene membrane; SA = salt bridge; SS = stainless steel

250 mA cm^{-2}, but this raises serious material-related issues for acidic process conditions. The long-term stability of current density is also a major concern, due to factors such as passivity of coal particle surfaces, consumption of catalytic additives, and build-up of the soluble and insoluble organic by-products in electrolyte solutions. Other inherent issues with the aqueous system are the (i) long path of ion migration between the two electrodes contributing to the cell's high ohmic resistance, (ii) role of reaction interface at the anode being as yet unoptimised, and (iii) porous glass frit and polymer membrane acting only as a separator for gas evolution, which limits the proton diffusion between the two chambers.

4.2. Alkaline solution based system

Only a few studies have investigated CAWE using alkaline electrolytes, such as NaOH and KOH. The main advantage of alkaline solution-based CAWE is the easy formation and dissolution of the oxidation products from coal, such as humic, carbonic, acetic and several benzene carboxylic acids [50,55]. Wapner and Lalvani [55] reported that the generated OH^* radicals in the alkaline solution can play an important role in the electrochemical oxidation of coal, by attacking coal molecules via hydrogen abstraction and/or by addition to the aromatic rings. Table 5 summarises some results from alkaline solution-based CAWE reported in the literature [55–57,126]. The current densities achieved in these studies have been low, even at cell voltages as high as 1.4 V. Recently, Ge et al. [126] studied the mechanism of CAWE (coal, demineralised coal, graphite) using a well optimised electrolysis cell with H_2SO_4, NaOH and HCl electrolytes; the peak current density achieved was 150 mA cm^{-2} with NaOH electrolyte at 90 °C. They concluded that the rate of CAWE depends on the activity of carbon material. They also observed that the indirect oxidation of coal via the OH^* radical was dominant at a low concentration of coal slurry (0.1 mol L^{-1}). However, the formation of oxidising radicals from acid and alkaline electrolytes in the CAWE process and its indirect oxidation mechanism has not yet been confirmed. There is little information on the durability of the CAWE operation in alkaline media and the reaction mechanism of OH^* radical oxidation with carbon particles or coal surface impurities.

5. Carbon/coal assisted water electrolysis via solid electrolytic routes

5.1. Polymer electrolyte membrane based system

A wide variety of process conditions have been explored in aqueous based CAWE to improve the reaction kinetics of carbon oxidation. However, the primary limitations to using solid coal/carbon in liquid electrolyte-based systems are high electrolyte ohmic losses and poor ion transfer from one electrode to the other due to the large separation between the electrodes, as described in Section 4. One possible alternative to overcome this problem is to use a zero-gap cell configuration, which consists of gas-diffusion electrodes as the anode and cathode on both sides of a solid polymer electrolyte membrane (i.e. Nafion), known as a membrane electrode assembly (MEA). This strategy has proved very successful in reducing energy losses and increasing current efficiency in other electrochemical systems, such as fuel cells [127,128], water electrolysers [129,130] and electrocatalytic CO_2 conversion cells [131–133].

Botte and co-workers [58,63–66,134] recently studied the electrochemical oxidation of coal slurries using different noble metal catalysts in the presence of Fe^{2+}/Fe^{3+} redox couple. In these investigations, carbon fibre wrapped around a Hastelloy or Ti mesh was used as a substrate for the anode catalysts, as shown in Fig. 13(a). A number of noble metal catalysts (Pt, Pt–Ru, Pt–Ir, Pt–Rh) plated on the carbon fibre were evaluated in coal slurries (0.02 g ml^{-1}) in the temperature range of 40–108 °C. The Pt–Ir catalyst showed the best performance for

Table 5
Summary of CAWE performance using different types of fuels and system configurations at low temperature in alkaline media.

Coal used	Anolyte (supporting electrolyte)	Additive	Anode	Anode area/ cm^2	Separator	Cathode	Cell configuration	Onset potential/V	Cell temp./ °C	Best performance	Ref.
Coal	1 M NaOH		Pt gauze	12.74	Porous Teflon frit	Pt gauze	BC (3ES)		75	~56 mA cm^{-2} at 1.44 V (FE_{H2} ~ 98.6%)	[55]
Coal	1 M NaOH		Graphite rod	4	PFG	Pt mesh	BC (3ES)		25–90	~5 mA cm^{-2} at 1.44 V , 25 °C	[56]
Coal	NaOH		Fe	9	Nafion	Fe	Ultrasonic bath		50–90	Change of total organic carbon concentration	[57]
Bituminous coal, de-ashed bituminous coal and high purity graphite	1 M H2SO4, NaOH and HCl		Pt	4	n/a	Pt	BC (3ES)	~0.5	10–90	~150 mA cm^{-2} at 1 V , 90 °C with ultrasonic in 1 M NaOH	[126]

3ES = three electrode system; BC = beaker cell; FE_{CO2} = Faradaic efficiency was calculated by CO_2; FE_{H2} = Faradaic efficiency of H_2; PB = Pyrex beaker; PFG = porous fritted glass.

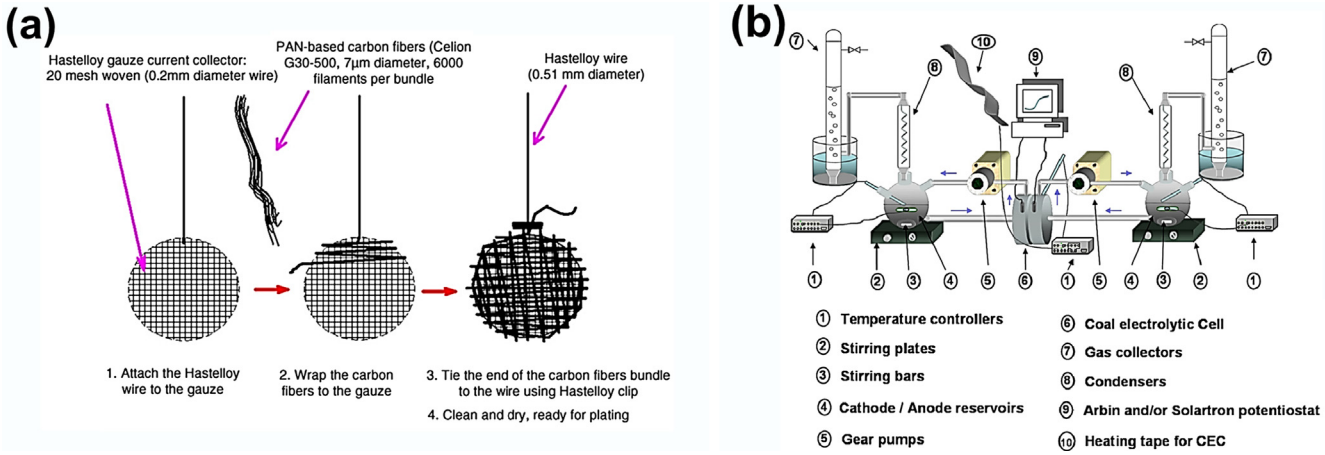

Fig. 13. Schematic configuration of (a) the procedure for the preparation of the catalyst/carbon fibre bundle/Hastelloy gauze and (b) the overall continuous CAWE assisted electrolysis testing system. Figure reproduced with permission from [65].

the conversion of coal–graphite slurry. The experiments were conducted in a sandwich configuration of the electrochemical cell, with a proprietary polyethylene membrane as a separator and by maintaining a regular flow pattern of the coal slurry over the electrode reaction surface, as illustrated in Fig. 13(b). In this gap cell configuration, the electrodes are merely touching and not bonded to the separator membrane (polyethylene or Nafion). The synergistic effect of the Fe ions in the coal slurry was demonstrated in terms of longer electrolysis time at stable cell voltages and under galvanostatic conditions. The authors also attempted to break down the intrinsic reaction barriers of solid carbon via increasing reaction temperature, which was explained on the basis of surface films having a greater tendency to dissolve at higher temperatures. The FE of CO_2 increased from 2.15 to 57.29% with an increase in temperature from 40 to 108 °C [65]; however, the coal conversion increased only from 0.2 to 3.2%. In these experiments, only a small fraction of coal was consumed, even above 100 °C. The coal FE of 91.15% was attributed mainly to coal oxidation due to the optimised concentration of Fe ionic species in the solution, which means ~8% of HER was attributed to the Fe^{2+} ions leaching out of the coal, as shown in Fig. 14(a). The energy consumption of the coal-assisted electrolysis process in the presence of Fe ionic species in the coal slurry was 22 Wh g^{-1} H_2 (1.98 kWh Nm^{-3}), corresponding to 32 mA cm^{-2} current density. This is 50% lower than the power required for conventional water electrolysis.

In a recent study, Jin et al. [66] from the same group systematically investigated the effect of the concentration of Fe ions in coal slurry on electrolysis operation at a constant current. The experiments were conducted with coal slurries consisting of 20 mg ml^{-1} coal in 4 M H_2SO_4 at 108 °C. Fig. 14(a) shows the effect of Fe ion concentration on cell voltage as a function of time, clearly revealing that electrolysis can be sustained for a longer time at cell voltages below 1 V with higher concentrations of Fe ions. The authors propose a possible reaction mechanism for electro-oxidation of coal in the presence of Fe^{2+}/Fe^{3+}, as shown in Fig. 14(b). Fe^{3+} ions seem to play the role of a catalytic mediator in this process. The following six steps of electrochemical oxidation mechanism were hypothesised, although the reaction mechanism has not been fully confirmed for the electro-oxidation interaction between anode surface, coal particles and anolyte in the presence of Fe^{2+}/Fe^{3+} ions:

Step I: In the liquid coal slurry, Fe^{3+} ions are adsorbed on the coal surface.

Step II: The adsorbed combination of coal-Fe^{3+} ads transports to the anode interface.

Step III: The electro-adsorbed Fe^{3+} ads on the coal surface acts as a

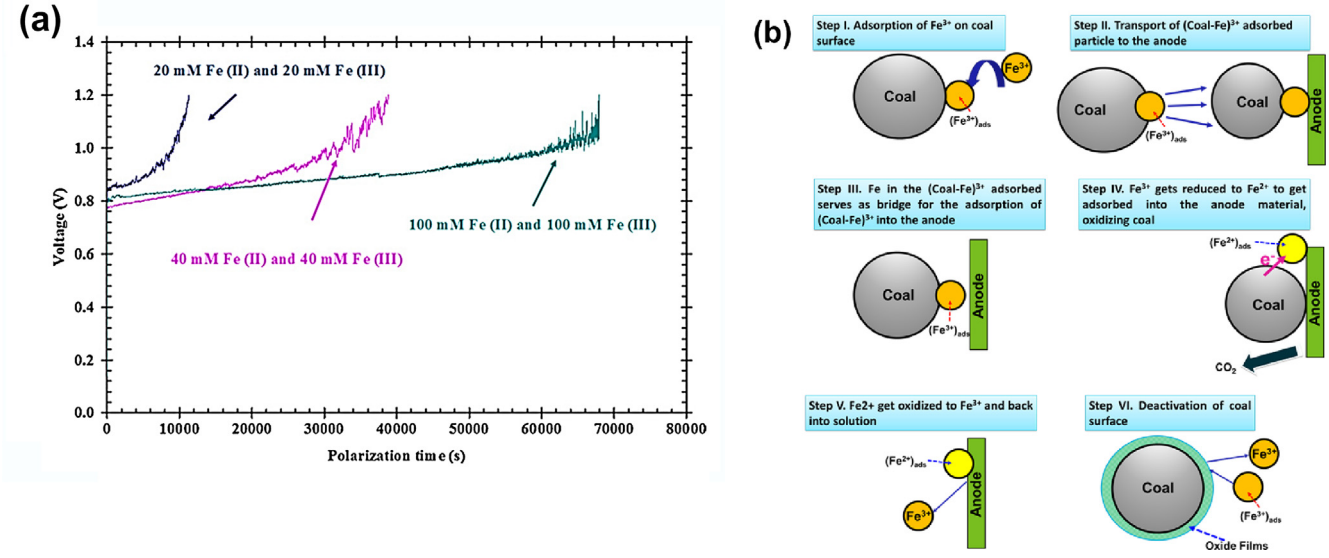

Fig. 14. (a) Performance curves of coal slurries with various concentrations of Fe ions at 100 mA at 108 °C and (b) schematic of the predicted mechanism for the coal electrochemical oxidation coupled with Fe^{2+}/Fe^{3+} redox system. Figure redrawn from [66].

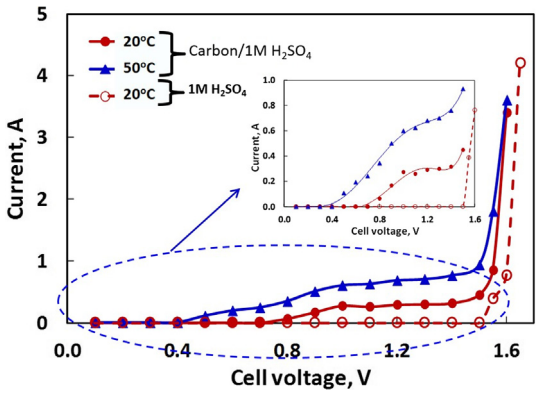

Fig. 15. CAWE performance using a polymer electrolyte membrane-based electrolysis cell operated with and without the presence of Vulcan XC-72 in 1 M H_2SO_4 solution. Figure reproduced with permission from [28].

bridge between the coal and the anode.

Step IV: Fe^{3+} ads is reduced to Fe^{2+} to become adsorbed on the anode surface, and simultaneously coal particles are oxidised to CO_2 and/or other intermediate species, such as CO or hydrocarbons [67].

Step V: The anode-Fe^{2+} ads ions are oxidised at the anode to release into the solution as a regenerating mediator to form Fe^{3+} ions.

Step VI: During this process, passive films may grow on the coal surface, preventing further oxidation by stopping the adsorption of Fe^{3+} ions and/or forming stable structures by combining with the adsorbed Fe^{3+} ions [63,64].

In another study, Giddey et al. [28] employed an MEA (electrodes bonded to the electrolyte membrane) to investigate the benefits of carbon assisted electrolysis. The MEA consisted of Ir black-coated, Pt-sputtered Ti mesh as the anode, Pt/C catalyst coated on carbon paper as the cathode, and a Nafion N 115 membrane as the electrolyte. The investigations used 1 M H_2SO_4 solution with Vulcan XC 72 carbon powder. The current densities achieved ranged between 12 and 15 mA cm^{-2} at 1.0–1.4 V at a cell temperature of 50 °C, as shown in Fig. 15. The authors suggested that this type of solid electrolyte system offers several advantages over aqueous electrolytes, such as the potential to stack cells, achieve higher current densities and produce pure CO_2 for sequestration (CO_2 and H_2 are produced in separate chambers).

Recently, Ju et al. [125] reported their findings on CAWE in a PEM-based (Nafion 115) zero-gap electrolysis cell with continuous circulation of carbon slurry in the anode chamber. Average current densities of about 55 mA cm^{-2} were achieved for up to 1 h at 70 °C and at a constant voltage of 1 V using 10 wt% carbon slurry (Vulcan XC-72 carbon black) with 100 mM Fe^{2+} ions added as an electrocatalytic mediator. The presence of Fe^{3+} (even up to 500 mM) as an additive species had a negligible effect on CAWE, possibly due to the poor activity of carbon and the absence of any involvement of Fe^{3+} ions in the electrolysis reactions. The main reason suggested for the performance degradation of the electrolysis cell over time was the physical blocking of the reaction interface by deposited carbon particles from the slurry.

5.2. Solid oxide electrolyte membrane-based system

The CAWE process is a potentially attractive, less energy-intensive alternative to current technologies for hydrogen production. Using the zero-gap cell system for CAWE at low temperatures seems to show some promise, with 50% of the electric energy required (2.19 kWh m^{-3}) compared with conventional electrolysis (> 4.1 kWh m^{-3}). However, breaking or decomposing complex physiochemical structures of coal and C—C bonds, and the formation of passive films on coal surface and other by-products with little value, are still major issues.

Hydrogen production by steam electrolysis using high temperature SOEC is currently under development due to the low electric energy requirements for the process at high temperatures [6]. Recently, there has been some interest in combining CAWE and SOEC for hydrogen production, to capture the advantage of lower cell voltages required due to the participation of carbon as well as higher operating temperatures. Gopalan and co-wokers [89–92] proposed liquid Ag and Sn as a consumable feed dispersed as a molten anode, with YSZ electrolyte and Ni-YSZ cathode. The carbon rod was inserted into the liquid metal anode (LMA) as a reductant and current collector, and the cathode side was provided with a gas mixture of H_2-H_2O (steam) or H_2, depending on the operation mode. This system could be operated in two different modes, like a reversible SOFC-SOEC: (i) in an electrolysis mode, to generate hydrogen from coal particles with steam; and (ii) in a power generation mode, to generate electricity from the hydrogen generated during the electrolysis cycles. This high temperature CAWE with LMA was operated at > 850 °C by feeding coal and hydrocarbon at the anode and steam into the cathode chamber. The oxygen ions (O^{2-}) transported from the cathode through the solid electrolyte membrane react with carbon at the electrolyte/anode interface or in the liquid metal phase as follows:

at cathode/YSZ interface: H_2O (steam) + $2e^- \rightarrow H_2 + O^{2-}$ (23)

at YSZ/LMA interface: $O^{2-} \rightarrow [O]_{LMA} + 2e^-$ (24)

at LMA/carbon interface: $[O]_{LMA} + R \rightarrow RO$ (CO or CO_2) (25)

overall: $H_2O + C \rightarrow H_2 + CO$ (26)

Gopalan et al. [92] suggested that the final product at the anode could be mostly CO rather than CO_2 at very high operating temperatures and the overall reaction (26) is spontaneous in this condition. The authors demonstrated the feasibility of this approach by feeding the electrolyser with waste materials, such as high-density polyethylene. By applying a potential of 1.5 V, they achieved a current density of 0.3 A cm^{-2}, producing 10 cc min^{-1} cm^{-2} (0.7–0.9 kWh Nm^{-3} of H2) of high-purity hydrogen at the cathode as well as syngas at anode (mixture of CO, CO_2 and H_2).

A steam-carbon fuel cell (SCFC) design has been proposed by Gür and co-workers [93–95,135,136] for the spontaneous and simultaneous production of hydrogen and electric energy with open-circuit voltage (OCV) achieved in the range 0.1–0.6 V based on the H_2/steam molar ratio in the inlet stream to the cathode chamber. This new approach was extended from their air–carbon fuel cell (ACFC) reactor, one of the categories of DCFC, which was operated by connecting a fluidised bed of coal gasifier with an anode-supported tubular SOFC [12,137]. In another study, they modelled a coupled steam-carbon-air fuel cell (SCAFC) that combines an ACFC and a SCFC with the carbon anode chamber shared between the two type of cells, and that also separates the two dense solid electrolyte membranes (YSZ) of each cell, as described in Fig. 16 [95]. The whole cell design of the SCAFC can be expressed as:

$O_{2(g)}$/Pt/YSZ/Pt/ $C_{(s)}$,CO,CO_2 /Pt/YSZ/Pt/$H_2O_{(g)}$,H_2 (27)

The ORR at the cathode/electrolyte (ACFC) and the HER (steam reduction) at the cathode/electrolyte (SCFC) can be written as:

ACFC: $O_{2,air} + 4e^- \rightarrow 2O^{2-}$ (28)

SCFC: $H_2O_{steam} + 2e^- \rightarrow H_2 + O^{2-}$ (29)

The anode reaction for the both ACFC and SCFC in the shared anode chamber would be the oxidation of CO produced by the Boudouard reaction as:

shared carbon chamber: $2CO + 2O^{2-} \rightarrow 2CO_2 + 4e^-$ (30)

Boudouard reaction: $C_{solid} + CO_2 \rightarrow 2CO$ (31)

The model based on the above design predicted high efficiencies of > 76% for both, producing electric power and hydrogen at the same

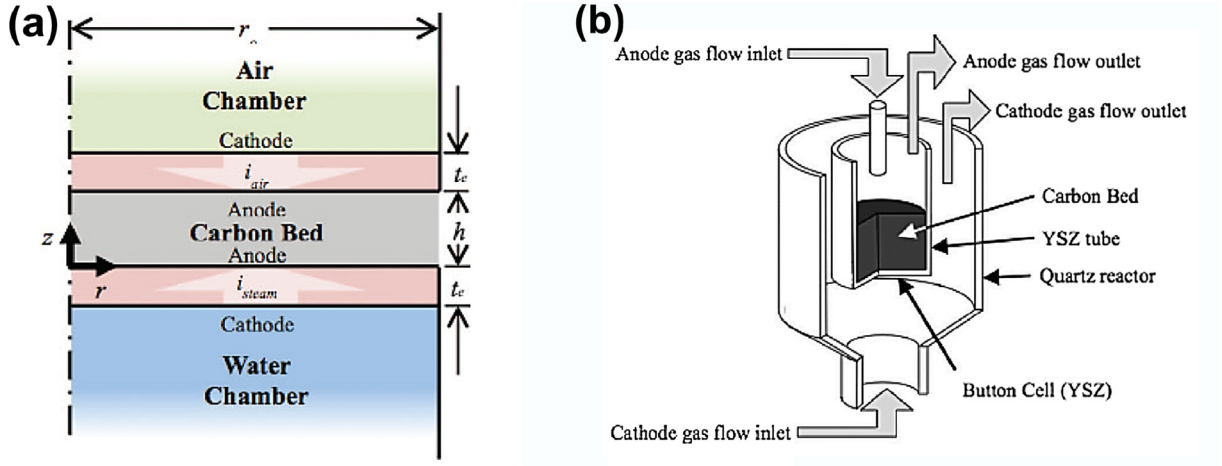

Fig. 16. Schematics of a steam–carbon–air fuel cell. (a) The air–carbon fuel cell is shown on top and the steam–carbon cell is shown at bottom; the cell configuration can be represented by O_2/LSM/YSZ/Ni/C, CO, CO_2/Ni/YSZ/Ni/H_2O. (b) Button cell configuration. Figure reproduced with permission from [95].

time. Two planar cells were fabricated, one for ACFC operation and the other for SCFC operation [95]. The electrolyte and anodes used for both cells were YSZ and Ni cermet, respectively. The cathodes used for the air and steam-side electrodes were LSM-YSZ and NiO-YSZ, respectively. Fig. 16(b) shows the schematic of the cell test arrangement. The two cells were connected in series or parallel and operated at 900 °C. With no power drawn from the coupled arrangement of cells, the voltage of the steam–carbon cell could be held at −0.2 V, producing a current density of 270 mA cm^{-2} for both cells. The modelling of this kind of arrangement revealed that if efficiency is the aim, a maximum cell efficiency of > 78% can be realised with a hydrogen production rate of 1.22 kg m^{-2} day^{-1} and electric power density of 45 mW cm^{-2}. This corresponds to a cell voltage of 0.8 V for ACFC and −0.5 V for SCFC. The results indicate that the coupled SCAFC can realise a sixfold increase in hydrogen production rates with only a twofold increase in active cell geometry.

Ewan et al. [96] report the comparison of three different high temperature electrochemical systems: DCFC, electrolysis cell (SOEC) and CAWE using a YSZ electrolyte-supported button cell. The electrodes used were bi-layers of Ni–YSZ/Ni–gadolinium-doped ceria (GDC) for anode, bi-layers of LSM/LSM–GDC for air cathode and Ni cermet for steam cathode. The fuel used was char from pyrolysed biomass. Fig. 17(a) shows the schematic of the cell test arrangement used by the investigators; Fig. 17(b) shows the voltage current characteristics for the electrolysis and carbon assisted electrolysis cells at 700–800 °C and the contribution of carbon to the water electrolysis as a reduction in voltage. The results indicate that CAWE can be realised at voltages around 0.7–1.0 V lower than those for steam electrolysis in the current density range of 0.2–0.3 A cm^{-2}. Based on this work, the authors expect that CAWE can occur with only 30% of the electric energy requirements of conventional water electrolysis, and that the remaining energy will be in the form of the carbon fuel's chemical energy and the thermal input.

Table 6 summarises the various investigations performed for carbon assisted electrolysis at high temperature, showing cell details, fuel used and the performance in terms of current density. A high temperature CAWE process based on SOEs is still at an early stage of development, with challenges including durability of anode catalyst, system configuration, degradation in performance and techno-economics of the process. The technology also seems to be dependent on enabling technologies, such as DCFCs and coal gasification with CO_2.

6. Hydrocarbon assisted water electrolysis

6.1. Low temperature liquid hydrocarbon assisted water electrolysis

The literature review above has highlighted a range of issues with carbon/coal-assisted electrolysis that still need to be resolved, and substantial effort and time may be needed to develop the technology to a commercial scale. With this in mind, another avenue of hydrogen generation is being explored, which is based on the use of alcohols as a source of hydrogen and energy to support the electrolysis process. The

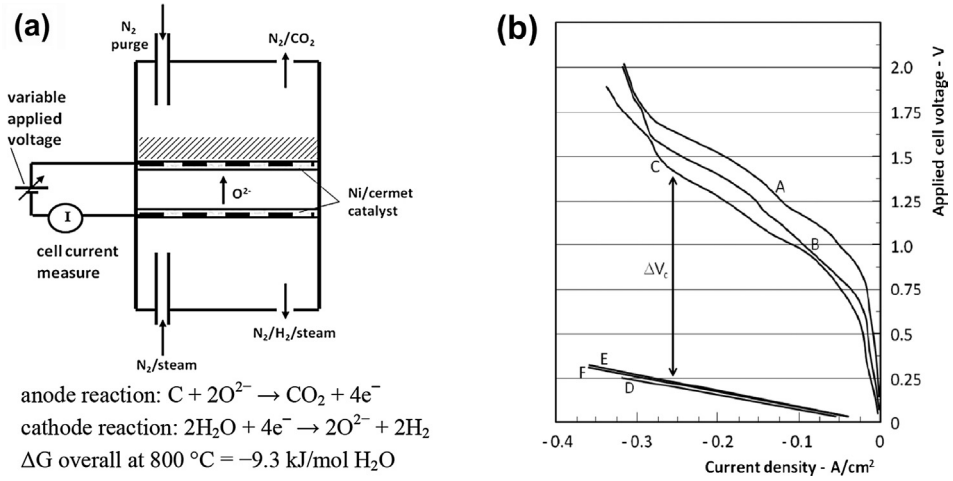

Fig. 17. (a) Schematic of CAWE cell and the associated reactions; (b) comparison of the electrochemical performance for electrolysis. Curves A, B and C are for a conventional solid oxide electrolysis cell system and D, E, and F are for a CAWE system at 700, 750, and 800 °C, respectively. Figure reproduced with permission from [96].

Table 6
Summary of CAWE performance using different types of fuels and system configurations at high temperature.

Carbon source used	Anode	Electrolyte	Cathode	Cell configuration	Open-circuit voltage/V	Cell temp./°C	Best performance	Ref.
Coal rods (consumable feed)	Ag	YSZ (t. 1 mm)	Ni-YSZ	Liquid anode SOFC (plate type)		1,000	$\eta_{th\text{-}H2}$: 83.7%	[89]
Coal rods (consumable feed)	Sn	6% YSZ (t. 2 mm)	Ni-YSZ	Liquid anode SOFC (plate type)	−0.2 (40% H_2O at cathode)	1,000	400 mA cm^{-2} at 3.1 V (40% H_2O at cathode)	[90]
Coal rods (consumable feed)	Sn	6% YSZ (t. 2 mm)	Ni-YSZ	Liquid anode SOFC (plate type)	−0.2 at 1,000 °C (40% H_2O at cathode)	900–1,000	400 mA cm^{-2} at 3.1 V, 1,000 °C (40% H_2O at cathode)	[91]
Coal rods (consumable feed)	Sn	6% YSZ	Ni-YSZ	Liquid anode SOFC (plate type)	-0.195		300 mA cm^{-2} at 1.5 V (50% H_2O-H_2 at cathode)	[97]
Activated carbon	Pt	YSZ (t. 0.3 mm)	Pt	Steam-carbon cell (fixed-bed) with button cell	0.1–0.6 (depend on H_2O/H_2)	800–900	25 mA cm^{-2} at -0.14 V, 900 °C with H_2O flow at cathode (generating both hydrogen and electricity)	[94]
Activated carbon	Pt	8% YSZ (t. 3 mm) and 10.5% YSZ (t. 1.3 mm)	Pt	Steam-carbon cell (fixed-bed) with button and tube cells	0.26	600–900	P_{max}: 8 mW cm^{-2} at 40.5 mA cm^{-2}, 900 °C with button cell (generating both hydrogen and electricity)	[93]
Activated carbon	Ni-YSZ	YSZ (t. 0.1 mm)	LSM-YSZ	SCAFC		700–1,000	270 mA cm^{-2} at -0.2 V, 900 °C (generating both hydrogen and electricity)	[95]
Biomass char	Ni/zirconia cermet	Stabilised zirconia (t. 150 μm)	Ni/zirconia cermet	Button cell		700–800	200 mA at 0.4 V, 900 °C	[96]

LSM = Sr-doped lanthanum manganite; $\eta_{th\text{-}H2}$ = theoretical hydrogen generation energy efficiency; SCAFC = coupled steam-carbon-air fuel cell (directly coupled to a Boudouard gasifier); SOFC = solid oxide fuel cell; t = thickness of solid electrolyte; YSZ = yttria-stabilised zirconia.

method is called organic solution assisted water electrolysis, or alcohol assisted water electrolysis. Scientists at NASA's Jet Propulsion Laboratory [22] employed an MEA consisting of PtRu catalyst deposited on a carbon paper as the anode, Pt or Pd catalyst deposited on carbon paper as the cathode, and Nafion membrane as the electrolyte. Methanol water solution was circulated on the anode side of the cell. Current densities as high as 800 mA cm^{-2} at a cell voltage of about 0.5 V were reported. The authors suggested that the cost of hydrogen production using methanol assisted water electrolysis (MAWE) may be about half that of conventional water electrolysis, even when including the cost of methanol.

Since then, there have been more attempts in this direction, with the use of methanol [69–78,138–147], ethanol/bio-alcohol [23,24,79,87,148–152], formic acid [81–83], glycerol [84,85,153–156], ethylene glycol [86] and biomass/high-molecular-weight hydrocarbon [157–160] in the co-electrolysis of water (also referred to as CAWE and electrochemical reforming). Table 3 summarises the electrochemical reactions associated with different organic solutions, and thermodynamic values (ΔG, ΔH, E°_{rev}, and E°_{the}) of the cell reactions. Among all the liquid hydrocarbons in the Table, the electrolysis reaction employing formic acid is the simplest, with only two electrons involved in the reaction. The free energy being negative and the reversible cell voltage (−0.17 V) being low for this reaction indicate the spontaneous nature of this reaction. However, in terms of cost effectiveness, high hydrogen-bonding organic compounds, such as cane sugar and bioethanol, are also suitable for clean production of hydrogen. Several investigations have been made into MAWE employing PEM as the electrolyte (mostly Nafion 117), to study the effect of methanol molar concentration (1–10 M), type of anode catalyst with various catalyst loadings (1–4 mg cm^{-2}) and cell temperature (room temperature to below 80 °C) on current densities and corresponding cell voltages.

Of the different liquid hydrocarbons investigated, methanol is a high-energy-density liquid fuel (6 kWh kg^{-1}, LHV) with 12.6 wt% hydrogen content and is an attractive energy-storage and energy-transport medium. The complete reaction of 5.34 kg of methanol can produce 1 kg hydrogen. Sasikumar et al. [71] carried out MAWE with an MEA consisting of 40 wt% PtRu/C as anode catalyst and 20 wt% Pt/C as cathode catalyst, with three different thicknesses of Nafion membrane to study the effect of methanol concentration, cell temperature, cell voltage and membrane thickness. The best cell performance obtained was a current density of 1.67 A cm^{-2} at 1.2 V using Nafion N112 membrane with 4 M methanol concentration at 80 °C. In a recent study, GIST and SK Innovation [73] report their findings on the optimisation of operating conditions for MAWE in terms of current efficiency and methanol loss. Pt and Pt–Ru black catalysts sprayed onto plain carbon paper (for better wettability) were used as the anode, and Pt black on Teflonised, micro-porous carbon paper (5% wet proofing for easy release of H_2 gas bubbles) was used as the cathode. Although the onset voltage for methanol electrolysis was lower for the Pt–Ru catalyst than for the Pt catalyst, the latter offered lower overvoltages at higher current densities. The current efficiency values were similar in both cases, with Pt catalyst having a value of 60–80% at current density of 0.3 A cm^{-2} at 0.67 V with 1 M methanol solution at 70 °C. This corresponds to an energy consumption of 17.8 kWh kg^{-1} (1.46 kWh m^{-3}) compared with 51.55 kWh kg^{-1} (4.23 kWh m^{-3}) for conventional electrolysis, thus showing a 65% saving on electric energy input. Pham et al. [74,75] investigated the effect of poly-tetrafluoroethylene (PTFE) treatment of the anode gas-diffusion layer (GDL) and the size of spherical metal particles in the porous, sintered, spherical-metal-powder flow field used for MAWE. Hydrogen production was improved by reducing the amount of PTFE treatment of the anode GDL, which was suggested to be due to better electrical conductivity and wettability of the GDL. The researchers concluded that more hydrophilic GDL may be favourable for methanol transport to the anode catalyst and membrane interface, leading to lower applied voltage and higher FE of methanol-assisted electrolysis to H_2. The smaller spherical particles (350–500 μm)

in the porous flow field on the anode side led to improved performance, due to better interfacial contact with the anode support.

Sethu et al. [78] investigated a Pt-catalysed membrane using the non-equilibrium impregnation reduction method for direct deposition of Pt on to the membrane for MAWE. The cell was assembled by putting carbon cloth with a special pore design (GDL) on both sides of the Pt-catalysed membrane. Graphite plates with parallel grooves were used as bipolar plates for reactant distribution and current collection. A five-cell methanol electrolyser stack with 50 cm^2 active area of each cell was assembled. At 50 A with a stack voltage of 3.95 V (at average single cell voltage of 0.79 V), the stack produced 102 L h^{-1} H_2 gas at 50 psi pressure (4 M methanol at 80 °C). This corresponds to an energy consumption of 1.89 kWh Nm^{-3} and shows about a 60% saving in electric energy input to the electrolyser. The stack was operated at 1 A cm^{-2} current density for 2500 h and showed a very stable performance, with negligible change in the stack voltage (3.95 V).

Recently, Ju et al. [147] investigated MAWE under different process conditions using a variety of Pt–based catalysts (Pt/C, Pt/C–SnO_2, Pt/C–CeO_2, PtRu/C, PtRu/C–SnO_2 and PtSn/C) using an optimised catalyst-spraying method in a PEM-based zero-gap electrolysis cell. The objective of this investigation was on-site/on-demand hydrogen generation with renewable energy to reduce the footprint of the latter, as shown in Fig. 18(a). The normalised current densities with respect to noble metal catalyst loading achieved at 0.8 V were in the order PtRu/C > Pt/C–SnO_2 > PtRu/C–SnO_2 > Pt/C > PtSn/C > Pt/C–CeO_2, as shown in Fig. 18(b). The authors suggest that the methanol oxidation reaction in MAWE occurs by an indirect electrochemical oxidation involving the adsorption of OH^- species on the secondary element (Ru or SnO_2) of the catalyst. The Pt catalyst enhances the electro-oxidation of CO_{ads} or intermediate molecules on the Pt surface via a bifunctional mechanism [76,138]. In the optimum conditions of MAWE, the investigators achieved > 600 mA cm^{-2} current density at less than 1 V at 60 °C with near 100% Faradic efficiency.

Of the different options for sources of hydrogen, ethanol or bioethanol are very attractive due to their well-established supply chain from various natural biomass sources (corn, crops, agricultural waste and wood waste), relatively high hydrogen to carbon ratio (six H atoms), and ease of storage and transportation safety [79,88,148]. Recently, Caravaca et al. reported the use of ethanol [23] and 23.1% w/w bioethanol (waste from the wine industry) [79] in an ethanol-assisted water electrolysis (EAWE) cell. The MEA used in this investigation consisted of a PtRu/C anode (3 mg cm^{-2}), a proton conducting membrane (Sterion) of 185 µm thickness, and 20 wt% Pt/C cathode (0.5 mg cm^{-2}). The optimum reaction conditions were found to be 4–6 M ethanol (or bioethanol) at 80 °C. Long-term tests on the electrolysis cell and subsequent regeneration tests confirmed that the deactivation behaviour of the cell could be attributed to a strong poisoning effect of reaction intermediate species (CO, acetaldehyde and

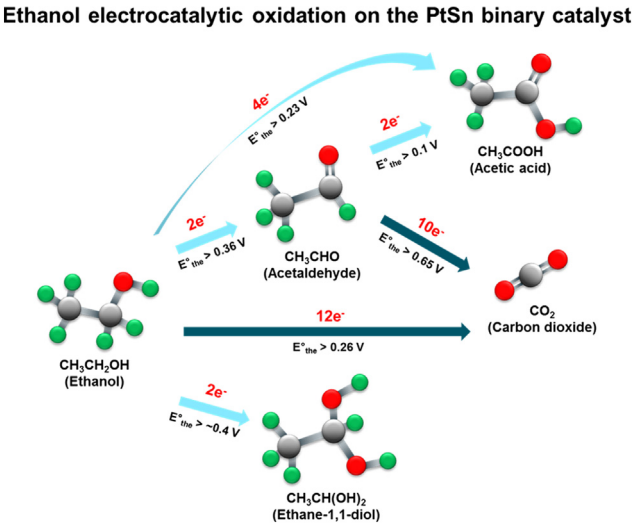

Fig. 19. Schematic diagram for potential mechanism of electrocatalytic oxidation of ethanol on PtSn binary catalyst in the ethanol-assisted water electrolysis process. Figure reproduced with permission from [148].

acetic acid) chemisorbed on the anode electrocatalyst active sites. The other possible sources of cell degradation, such as the swelling of the Nafion membrane or a crossover of the ethanol from the anode to the cathode, were ruled out. The peak current density obtained with ethanol was 0.25 A cm^{-2} at 1.1 V with 6 M ethanol at 80 °C [23]. This corresponds to an electric energy consumption of 2.62 kWh Nm^{-3}.

In another study on EAWE by Lamy et al. [24], three Pt–based anode catalysts (Pt/C, PtSn/C and PtSnRu/C) were investigated to reduce the anode overvoltage of ethanol oxidation. Significantly high reaction rates were observed at cell voltages under 0.9 V at room temperature (20 °C) with Sn and Ru-modified Pt catalysts, resulting in a current density of 100 mA cm^{-2}. This is equivalent to a 220 cm^3 h^{-1} hydrogen production rate while consuming less than 2.3 kWh Nm^{-3} electrical energy. Recently, Ju et al. [148] reported their investigation into an EAWE cell with Pt/C and PtSn/C as anode catalysts. Current densities of > 200 mA cm^{-2} were achieved at less than 0.75 V at 70 °C, clearly demonstrating the faster ethanol oxidation kinetics due to higher temperatures. The electric power input for the electrolysis was 1.62 kWh m^{-3}, a saving of > 50% electrical energy input compared with conventional water electrolysis cells. The authors propose a plausible ethanol electro-oxidation mechanism in EAWE, based on the Faradaic conversion of ethanol and mass balance of the by-products identified/quantified using ^1H nuclear magnetic resonance spectroscopy and gas analysis as illustrated in Fig. 19. The figure shows that the ethanol oxidation reaction leads to incomplete oxidation of ethanol

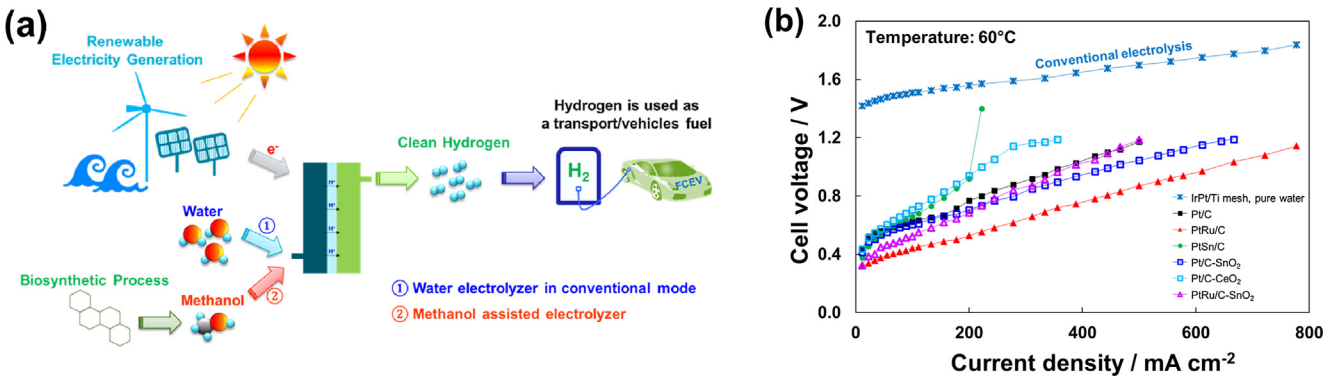

Fig. 18. (a) Schematic concept of methanol-assisted water electrolysis (MAWE) system integrated with renewable energy for clean hydrogen production. (b) MAWE performance with 2 M methanol at 60 °C using Pt/C, PtRu/C, PtSn/C, Pt/C–SnO_2, Pt/C–CeO_2 and PtRu/C–SnO_2 as anode catalysts. Water electrolysis performance using IrPt catalyst on Ti mesh at 70 °C is also given for comparison. Figure reproduced with permission from [147].

to produce acetaldehyde and acetic acid. These reactions are strongly dependent on the reaction potential and the properties of electrocatalysts, and the reaction pathway can lead to the formation of secondary intermediates in the presence of other metals (Sn, Pb, Bi and Ru) with Pt catalyst [161–166]. However, the complete oxidation of ethanol generating 12 electrons via a one-step reaction is significantly limited under low temperature electrolysis conditions (< 100 °C) due to poor catalytic activity to break the C—C bonds [23,166]. For these reasons, previous EAWE results show lower current densities, as well as lower FE of ethanol conversion to hydrogen as determined by CO_2 evolution. Further, the reaction intermediates lead to faster cell degradation in EAWE than in MAWE.

Similarly, Osa et al. [138] have performed various liquid hydrocarbon (methanol, ethanol and ethylene glycol)-assisted, PEM-based electrolysis studies with a bimetallic Pt_7Sn_3/C catalyst (1.5 mg cm^{-2}) at temperatures in the range of 60–90 °C. MAWE showed the highest performance among the alcohols, due to easier electrocatalytic oxidation of simple carbon molecule (C1). Thus, to meet hydrogen production cost targets (e.g. US Department of Energy cost of US$3–3.7 kg^{-1}), several factors must be addressed, such as lower ethanol/bioethanol production cost, a high-quality product, and significantly higher ethanol conversion efficiency with a durable catalyst (good CO tolerance and promote C–C bond scission) [79,138,148].

A few studies have investigated formic acid-assisted electrolysis by either employing PEM electrolyte-based cells [81,83] or aqueous electrolyte-based cells [82]; however, the operating current densities achieved so far are < 100 mA cm^{-2}. Formic acid-assisted electrolysis using an Ir oxide-coated titanium oxide anode was first performed by Kiliç et al. [81] using a cell that was operated at maximum current density of 50 mA cm^{-2} at 50 °C. Complete oxidation of formic acid to CO_2 and water was achieved, as measured by the chemical oxygen demand removal efficiency (95%) of the electrolysis process. In alkaline media (NaOH), Guo et al. [82] found a very low operating electrolysis voltage of 0.3 V using Pt foil electrodes, but the current densities seem to be relatively low (6 mA cm^{-2} at 0.7 V) and failed to produce any reasonable flow rates of hydrogen. Carbon-supported, Pd-based anode catalysts (Pd/C, PdAu/C and PdPt/C) were investigated in a PEM-based electrolysis cell by Lamy et al. to reduce overvoltages and improve the stability of the process [83]. They were able to achieve relatively low operating voltages of between 0.2 and 0.4 V at 100 mA cm^{-2} using Pd-based electrocatalysts. However, the performance stability of the electrolysis process was an issue, as shown by the increase in cell voltages with time. The proposed reason for this was the fast deactivation of Pd catalysts due to poisoning by the adsorbed species, such as formate, formic acid and CO [83,167].

Some researchers are also exploring the use of biomass-derived compounds, such as glycerol [84,85,153–156] and ethylene glycol [86], for electrochemical reforming using PEM-based electrolysis cells. The anode catalysts used for the glycerol electrolysis cells were Pt on Ru–Ir oxide [84] and Pt–Ru on carbon support [85]. The current densities achieved at voltages in the range 0.4–0.7 V were 5–10 mA cm^{-2} at 70–80 °C. These current densities indicate slow reaction kinetics for glycerol due to the 14 electrons involved in the complete oxidation to CO_2. Investigations into the stability of the electrolysis process over a period of 150 min resulted in 50% reduction in current densities at 1 V (80 °C), showing possible poisoning of the anode catalyst [85]. Although it was claimed that glycerol-assisted electrolysis can decrease the electric power input by 66% for hydrogen production, the operating current densities of around 10 mA cm^{-2} are too low for any practical significance. de Lucas-Consuegra et al. [86] studied ethylene glycol-assisted electrolysis with a Sterion based PEM, and Pt–Ru/C and Pt/C as the anode and cathode catalysts, respectively. The energy efficiency obtained from the electrolysis system was 57% at 80 mA cm^{-2} current density. This corresponds to an electric power consumption of 1.53 kWh Nm^{-3} hydrogen. The peak current densities achieved were around 250 mA cm^{-2} at 0.8 V with 6 M ethylene glycol at 90 °C. This performance looks encouraging, but the long-term stability of the cell was not studied.

Recently, Chen et al. [87] have reported their work on alcohol-assisted electrolysis by employing an anion-exchange polymer membrane (alkaline medium). Pd nanoparticles deposited on 3-D titania nanotube arrays were used as an anode and Pt/C deposited on carbon cloth as a cathode for the cell. The organic solutions tested were ethanol, ethylene glycol, glycerol and 1,2-propanediol at temperatures from 25 to 80 °C, and 2 M NaOH was used as the supporting electrolyte. The peak current density achieved with 2 M ethanol + 2 M NaOH at 80 °C was 1.95 A cm^{-2} at 0.9 V. All organic solutions tested at 80 °C produced 1 A cm^{-2} current density at around 0.7 V, which corresponds to electric power input to the cell in the range ~24 kWh kg^{-1} (~1.97 kWh m^{-3}) compared with 51.55 kWh kg^{-1} (4.23 kWh m^{-3}) for conventional electrolysis. However, the alkaline based electrolysis cell required around 10 kg of NaOH for the production of 1 kg of hydrogen [138].

Deng et al. [157,158] studied a PEM-based electrolysis cell with lignin to cogenerate valuable small organic molecules as well as hydrogen by using aqueous polyoxometalate solution as a catalyst and charge (electron–proton) carrier. They report that the electric energy consumption can be as low as 0.69 kWh Nm^{-3} H_2 at 0.2 A cm^{-2}, requiring only 16.7% of the energy consumption of water electrolysis. This is an interesting approach for using notable liquid hydrocarbons in a PEM-based electrolysis cell for the cogeneration of both hydrogen and conversion/reforming of high-molecular-weight chemical compounds (glycerol, sugar, pentose, glucose, cellulose, lignin, ethylene glycol) to value-added small organic molecules products for industrial platform applications (furfural, 5-hydroxymethylfurfural; HMF, sorbitol, 1,3-dihydroxyacetone; DHA, formic acid) [21,88,151–155,158–160,168,169]. For obtaining such value-added or industrially important chemicals, the selective or controlled oxidation of alcohols and C_4—C_6 polyols can be achieved without the need for the complete electrochemical oxidation into CO_2 or cleavage of the C—C bond [21,88,153,169].

Table 7 summarises the details of the cell materials, electrolysis onset potentials and best performance obtained by various investigators for alcohol assisted electrolysis with PEM-based electrolysis cells. Although this process shows significantly higher potential than carbon/coal-assisted electrolysis for hydrogen generation due to high current densities achieved by some investigators with lower electric power input per kg of hydrogen produced, several issues still need to be addressed. These include (i) high noble metal (i.e. Pt, Ir) catalyst loadings, (ii) degradation of membrane with organic solution crossover problems, (iii) poisoning of the anode catalyst by reaction intermediate species or impurities in the original organic solution, (vi) relatively sluggish kinetics of electrochemical oxidation of high molecular weight organic compounds at the anode, and (vii) the availability and cost of alcohol and organic solutions as feedstock compared with the value added to the hydrogen produced.

6.2. High temperature hydrocarbon/CO gas assisted steam electrolysis

An alternative approach being investigated for reducing the electric input to high temperature steam electrolysis for hydrogen production is by feeding steam to the cathode and a reducing gas (NG, CH_4 or CO) to the anode chamber of a high temperature (700–900 °C) electrolysis cell [25–27]. Lawrence Livermore National Laboratory (LLNL) [25] constructed a bench-scale SOE-based reactor to study the hydrocarbon/CO gas assisted co-electrolysis process in 2003, as shown in Fig. 20(a). Single YSZ electrolyte-based cells were investigated with a mixture of H_2/H_2O on cathode side and reducing gas on the anode side. They considered two different NG oxidation conditions in the anode chamber: (i) partial oxidation to CO and H_2 (hydrogen can be generated at both electrodes in the system), and (ii) total oxidation to produce CO_2 and steam. The complete oxidation of methane is expected to produce the lowest cell voltages during electrolysis. LLNL has focused

Table 7
Summary of low temperature, liquid hydrocarbon fuels assisted water electrolysis performance based on a polymer electrolyte membrane (proton and anion-exchange membranes) system.

Feed solution	Anode	Anodearea/cm^2	Anode electrode	Membrane	Cathode	Feed rate	Onset potential/V	Cell temp./ °C	Best performance (near 0.8 ~ 1.2 V)	Extended test	Ref
MeOH	Metal black or Me/C (1–4 mg cm^{-2})			Nafion			0.3	5–120	800 mA cm^{-2} at < 0.6 V		[22]
MeOH	60 wt% PtRu/C (2.5 mg cm^{-2})	6.25	Carbon paper (TGP-H-060)	N117	Pt-WC/C and Pt/C (1.5 mg cm^{-2})	12 sccm (cir.)	~0.25	30–90	200 mA cm^{-2} at 0.32 V, 90 °C with 2 M MeOH		[69]
MeOH	Pt	23		N117	Pt	5 sccm			350 mA cm^{-2} at 0.6 V with 17 M MeOH	60 min	[70]
MeOH	40 wt% PtRu/C (3 mg cm^{-2})	25	PI film/ platinized Ti mesh	N112, N115, N117	20 wt% Pt/C (0.5 mg cm^{-2})		0.4	30–80	500 mA cm^{-2} at 0.62 V, 80 °C with 4 M MeOH (N117)		[71]
MeOH	Pt–Ru/C (4 mg cm^{-2}), Pt/C (4 mg cm^{-2}), PtRu black (4 mg cm^{-2}), and Pt black (2 mg cm^{-2})	2		N117	Pt/C (2 mg cm^{-2})	Batch type		23–75	200 mA cm^{-2} at 1 V (vs. SHE), 75 °C with 16 M MeOH	500 min	[72]
MeOH	Pt black (3 mg cm^{-2}), and PtRu black (3 mg cm^{-2})	9	Carbon paper (SGL 25AA, no wet proof)	N115	Pt black (3 mg cm^{-2})		~0.3	30–70	300 mA cm^{-2} at 0.67 V, 70 °C with 2 M MeOH (Pt black)	600 min: < 0.8 V	[73]
MeOH	50 wt% PtRu/C (1 mg cm^{-2})	25	Carbon paper (TGP-H-90)	N117	50 wt% Pt/C (1 mg cm^{-2})	10 sccm	~0.35	30–60	200 mA cm^{-2} at 0.5 V, 60 °C with 2.6 M MeOH		[74]
MeOH	50 wt% PtRu/C (1 mg cm^{-2})	25	Carbon paper (TGP-H-90, no wet proof)	N117	50 wt% Pt/C (1 mg cm^{-2})	10 sccm	0.35	30	200 mA cm^{-2} at 0.65 V with 8.5 wt% MeOH		[75]
MeOH	PtRu/C (Pt:Ru = 2:1) (0.5 mg cm^{-2})	7.29		FAA-2	60 wt% Pt/C (0.5 mg cm^{-2})		~0.3	30–70	50 mA cm^{-2} at 1 V, 70 °C with 1 M MeOH		[76]
MeOH	80% Pt:Ru/C Pt-Ce Fe-Cu-Cr-Ce-Pt	4	Carbon paper	N212 and polyethersulfone	40% Pt/C	12 M KOH		60	10 mA cm^{-2} at 1 V with 12 M MeOH		[77]
MeOH	Pt	50	Graphite plate	N117	Pt		~0.3	80	1,000 mA cm^{-2} at 0.79 V with 50 psi	2,500 h CC 1 A cm^{-2}: < 0.8 V	[78]
MeOH	PtRu/C (Pt:Ru = 1:1) (4 mg cm^{-2})	5		N117	Pt/C (2 mg cm^{-2})	2 sccm (cir.)	~0.25 (at 85 °C)	25–85	100 mA cm^{-2} at 0.963 V at 70 °C	20 min: < 0.8 V	[139,140]
MeOH	PtPd (Pt:Pd = 7:3) (2 mg cm^{-2})	10	Graphite plate	N117	40% Pt/C (1 mg cm^{-2})				1.9 A cm^{-2} at 1 V at 80 °C with 4 M MeOH		[141]
MeOH	40%Pt-20%Ru/C (3 mg cm^{-2})	30	TNT powder in ePTFE substrate	N117, ePTFE-Nafion-TNT (t. 30 μm)	20% Pt/C (0.5 mg cm^{-2})	cir.	~0.3	60	400 mA cm^{-2} at 1 V at 60 °C with 2–3 M MeOH	120 min CC 100 mA cm^{-2}: < 0.6 V	[143]
MeOH	40%PtRu/C (3 mg cm^{-2})	5	Carbon cloth	SPES	20% Pt/C (0.5 mg cm^{-2})	cir.	~0.4	30–80	550 mA cm^{-2} at 1 V at 80 °C	35 h CC 0.5 A cm^{-2} : < 1 V	[145]
MeOH	PtRu/C (3 mg cm^{-2})	30	Carbon cloth	N117	Pd nanoparticles or 20% Pt/C (0.5 mg cm^{-2})	50 sccm cir.	~0.35	35–60	400 mA cm^{-2} at 1 V at 60 °C with 2 M MeOH	26 h CC 150 mA cm^{-2}: < 0.65 V	[146]
MeOH	40 wt% Pt/C, 40 wt% PtRu/C, 20 wt% PtSn/C, 40 wt% Pt/C-SnO_2 (Pt:SnO2 = 3:1), 40 wt% Pt/C-CeO_2 (Pt:SnO_2 = 3:1), and 40 wt% PtRu/C-SnO_2 (Pt:Ru:SnO_2 = 1.5:1.5:1) (2 mg cm^{-2})	9	Carbon paper (SGL 25AA, no wet proof)	N115	40 wt% Pt/C (0.5 mg cm^{-2})	200 sccm cir.	~0.4	30–60	440 mA cm^{-2} at 0.8 V at 60 °C with 2 M MeOH using PtRu/C	4 h CC 150 mA cm^{-2}: < 0.6 V	[147]
EtOH	PtRu/C (Pt:Ru = 2:1) (3 mg cm^{-2})	6.25	Carbon paper	Sterion	20 wt% Pt/C (0.5 mg cm^{-2})	330 ml h^{-1}	~0.4	40–80	~100 mA cm^{-2} at 0.8 V, 80 °C with 6 M EtOH		[23]

(*continued on next page*)

Table 7 (*continued*)

Feed solution	Anode	Anodearea/cm^2	Anode electrode	Membrane	Cathode	Feed rate	Onset potential/V	Cell temp./ °C	Best performance (near 0.8 ~ 1.2 V)	Extended test	Ref
										1 h CV 0.9–1.1 V: 30–200 mA cm^{-2}	
Bio-EtOH	PtRu/C (Pt:Ru = 2:1) (3 mg cm^{-2})	6.25	Carbon paper	Sterion	20 wt% Pt/C (0.5 mg cm^{-2})	330 ml h^{-1}	~0.3	60–80	33.6 mA cm^{-2} at 0.8 V, 80 °C with 4 M EtOH	6 h CV 0.8 V: 30–80 mA cm^{-2}	[79]
EtOH	30 wt% Pt/C, 30 wt% PtSn/C, 30wt% PtSnRu/C (2 mg cm^{-2})	5	Carbon cloth	N 117	30 wt% Pt/C (0.5 mg cm^{-2})			20	100 mA cm^{-2} at 0.8–0.9 V with 2 M EtOH	30 min CC 100 mA cm^{-2}: < 1 V	[24,80]
MeOH, EtOH, EG	20 wt% Pt_7Sn_3/C (1.5 mg cm^{-2})	6.25	Carbon paper	Sterion	20 wt% Pt/C (0.5 mg cm^{-2})	60 ml h^{-1}	~0.4	60–90	400 mA cm^{-2} at 1 V with 6 M MeOH	10 h CC 0.5 A cm^{-2}: < 1 V	[138]
EtOH, EG, G, 1,2-P	Pd nanoparticles (1.7 mg cm^{-2})	25	3D TiO_2 nanoute arrays	A201	40 wt% Pt/C (0.3 mg cm^{-2})	4 sccm with 2 M NaOH	~0.3	25–80	2,000 mA cm^{-2} at 0.92 V, 80 °C with 2 M EtOH + 2 M NaOH		[87]
EtOH	40 wt% Pt/C 20 wt% PtSn/C (Pt:Sn = 3:1) (2 mg cm^{-2})	9	Carbon paper (SGL 25AA, no wet proof)	N115	40 wt% Pt/C (0.5 mg cm^{-2})	200 sccm cir.	< 0.2	60–70	275 mA cm^{-2} at 0.1 V, 70 °C with 2 M EtOH	125 h CV 0.9 V: 50–145 mA cm^{-2}	[148]
EtOH	Pd mesh (1.93 mg cm^{-2})	6.25		A901	20 wt% Pt/C (0.5 mg cm^{-2})	100 sccm with KOH or NaOH	> 0.4	70–90	700 mA cm^{-2} at 1.3 V with 2 M EtOH + 1 M KOH	150 h (5 cycles) CC 160 mA cm^{-2}: < 1.1 V	[150]
EtOH, EG, G, 1,2-P, etc.	AuPd/C (0.75 mg cm^{-2})	4	Ni foam	A201	Pt/C (0.4 mg cm^{-2})	with 2 M KOH	~0.4	60	400–535 mA cm^{-2} at 1 V with EtOH, EG, G		[151]
EtOH, EG, G, 1,2-P	Rh/C (1 mg cm^{-2})	5	Ni foam	A201	40 t% Pt/C (0.4 mg cm^{-2})	30 sccm with 2 M KOH	> 0.3	60	492 mA cm^{-2} at 0.7 V with EtOH	40 min CC 125 mA cm^{-2}: < 0.65 V	[152]
FA	TiO_2/IrO_2 mesh	16		N 111 and 117	Pt	150 sccm with Na_2SO_4		25–50	50 mA cm^{-2}	2.5 h CC 50 mA cm^{-2}	[81]
FA	Pt foil	1			Pt foil	NaOH + FA, cir.	~0.3		6 mA cm^{-2} at 0.7 V with 2 M FA	60 min CC 8 mA cm^{-2}	[82]
FA	40 wt% PdAu/C, 40wt% Pt/C (2 mg cm^{-2})	5	Carbon cloth	N 117	40 wt% Pt/C (2 mg cm^{-2})	cir.	~0.2	25	100 mA cm^{-2} at 0.2–0.4 V with 5 M FA	30 min	[83]
Glycerol	20 wt% Pt/Ru-Ir oxide (3 mg cm^{-2})	3.14	Au plated porous Ti sinters	N 212	20 wt% Pt/C (3 mg cm^{-2})	4.2 L h^{-1} cir.	> 0.4	70	10 mA cm^{-2} at 0.65V with 2 M	30 min CC 5 mA cm^{-2}: < 0.8 V with 8.5 M	[84]
Glycerol	45.6 wt% Pt/C 53.3 wt% PtRu/C (Pt:Ru = 3:2)			N 117		6 sccm	~0.2	60–100	6 mA cm^{-2} at 0.6 V, 80°C with 15%	150 min CV 1 V: < 15 mA cm^{-2}	[85]
Ethylene glycol	60 wt% PtRu/C (Pt:Ru = 2:1, 3 mg cm^{-2})	3.14		Sterion	20 wt% Pt/C (3 mg cm^{-2})	1–5 sccm	~0.3	90	~250 mA cm^{-2} at 0.8 V, 90 °C with 6 M EG		[86]
Alcohols, cellulose, lignin, biomass	Polyoxometalates (POMs) solution	1	Graphite felt	N 115	Pt black (4 mg cm^{-2})	30 sccm	> 0.5	80 or light irradiation	500 mA cm^{-2} at 0.6–1.2 V	4000 s CV 0.5 V: 50 mA cm^{-2}	[157]

A201 (t. 28 μm), A901 (t. 10 μm) = anion exchange membrane from Tokuyama; CC = constant current density; cir. = circulation; CV = constant voltage; EG = ethylene glycol; EtOH = ethanol; FA = formic acid; FAA–2 = anion exchange membrane from FuMa-Tech; MeOH = methanol; N = Nafion (N115: t. 127 μm, N117: t. 175 μm, N212: t. 51 μm); P = –propandiol; PI = polyimide; PTFE = poly-tetrafluoroethylene; SPES = sulfonation polyethersulfone; sccm = cm^3 min^{-1} (ml min^{-1}); Sterion = 180 μm; TNT = titanate nanotubes

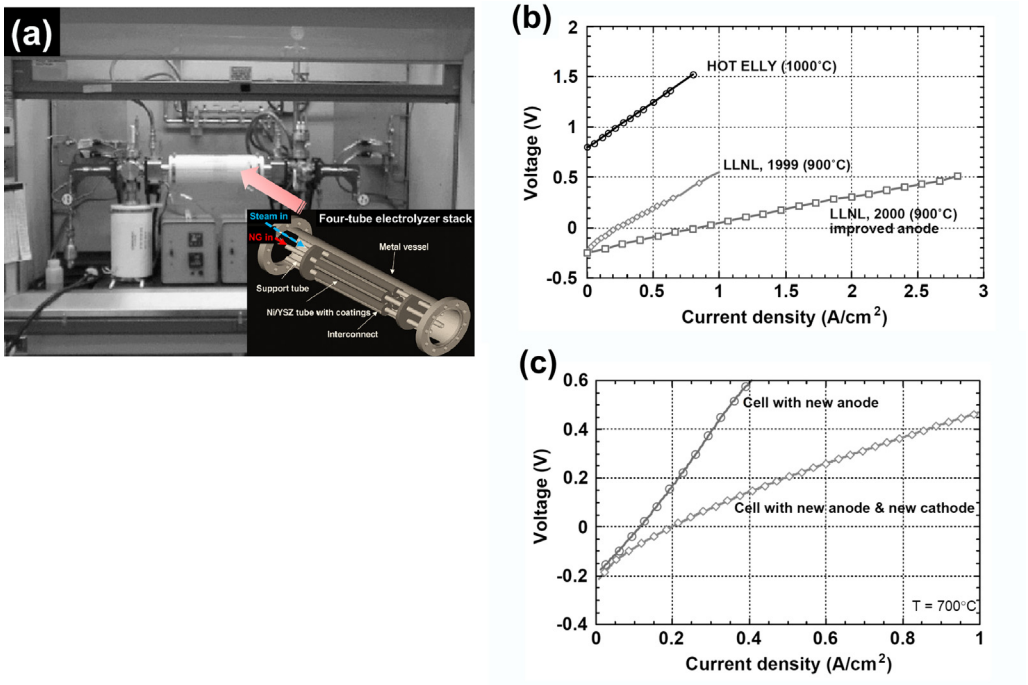

Fig. 20. (a) Lawrence Livermore National Laboratory (LLNL)'s bench-scale reactor for a 100-W electrolyser stack and (b) comparison of polarisation curves of HOT ELLY steam electrolyser and LLNL's natural gas assisted steam electrolyser. Fig. (a) redrawn based on [25] and (b) and (c) reproduced with permission from [25].

their work on the total oxidation reaction mode at 700 °C, as no additional water shift reaction and CO clean-up would be required. Fig. 20(b) compares the performance of the NG-assisted steam electrolysis (LLNL at 900 °C) with conventional steam electrolysis ('HOT ELLY' system at 1000 °C) [25]. The cell consisted of a NiO/YSZ anode-supported tube with a coated YSZ electrolyte thin film. The electrolysis current density achieved at 0.5 V was 2.8 A cm^{-2} at 900 °C and 1 A cm^{-2} at 700 °C (see Fig. 20(c)). An analysis of the energy flow with a heat exchanger revealed a system efficiency of up to 70% based on primary energy input. The operating temperatures of 900 °C produced higher current densities, but led to carbon deposition on the anode. This situation can be partly avoided by feeding a higher proportion of steam, but leads to lowering of the temperature due to the endothermic nature of steam reforming. Therefore, the authors suggested operating the cells at temperatures near 700 °C.

Wang et al. [26,27] evaluated ceria based porous composite electrodes (Cu–CeO_2–YSZ, Cu–Co–CeO_2–YSZ, Pd–CeO_2–YSZ) with 8 mol% YSZ (50 μm thick YSZ disc layered between 50 and 300 μm thick porous YSZ layers). The reducing gases used in the anode chamber of the cell were CO and CH_4. The cell with Pd–CeO_2–C–YSZ (anode)/YSZ/Co–-CeO_2–YSZ (cathode) using humidified CH_4 at 0.5 V was found to produce the highest catalytic activity and current densities of 0.45 A cm^{-2} at 700 °C [27]. The cell OCV values obtained were 21 mV for CH_4 and −74 mV for CO at 700 °C. The cathode (Co–CeO_2–YSZ) gas supplied in this case was a mixture of 20% H_2O/80% H_2. In another study with the above cell, Wang et al. [26] investigated the extent of CH_4 conversion using simulated gas compositions of gas mixture (CH_4, CO_2 and H_2O). The methane conversion in this case was considered to be an indication of the extent of methane reforming in the anode chamber. It was reported that the OCV and corresponding current densities obtained with conversions between 10 and 80% of methane were 0.22 V (0.25 A cm^{-2}) and 0.07 V (0.05 A cm^{-2}) at 700 °C, respectively. These results demonstrate the feasibility of CO gas assisted co-electrolysis, and the possibility of obtaining high hydrogen production rates without the need for applying external potential to the cell. It is worth mentioning that the advantage of this route of hydrogen production compared to conventional steam reforming is that CO_2 is generated in a separate chamber, and would be easy to sequester. Table 8 Summarises the high temperature, hydrocarbon/CO gas assisted steam electrolysis performance achieved by various investigators based on a solid oxide electrolysis cell system.

7. Technology status, challenges and opportunities

Hydrogen production from a carbon source, such as coal, alcohol, methane (NG) and biomass, using aqueous electrolytes or solid polymer electrolyte membranes at low temperatures and solid oxide electrolyte membranes at high temperatures could be a promising, practical technology for the world's transition to a low-emission economy. Current progress in system efficiency and plant capacity for different hydrogen production technologies is illustrated in Fig. 21. However, the practical applications of these technologies would demand proven reliability and long-term sustainability.

Table 8
Summary of high temperature, hydrocarbon/CO gas assisted steam electrolysis performance based on a solid oxide electrolysis cell system.

Feed	Anode	Membrane	Cathode/feed	Onset potential/V	Cell temp./°C	Best performance	Ref.
Natural gas (NG)	Ni-YSZ	YSZ	Ni-YSZ/steam/H_2	−0.2 −0.2	900 700	2.8 A cm^{-2} at 0.5 V 1.0 A cm^{-2} at 0.5 V	[22]
Methane	Pd-CeO_2-YSZ	YSZ	Co-CeO_2-YSZ/steam/H_2		700	OCV 0.22 V, Current: 0.32 A cm^{-2}	[69]
Methane/CO	Pd-CeO_2-YSZ	YSZ	Co-CeO_2-YSZ/steam/H_2		700	OCV 21 mV (CH_4) OCV −74 mV (CO)	[70]

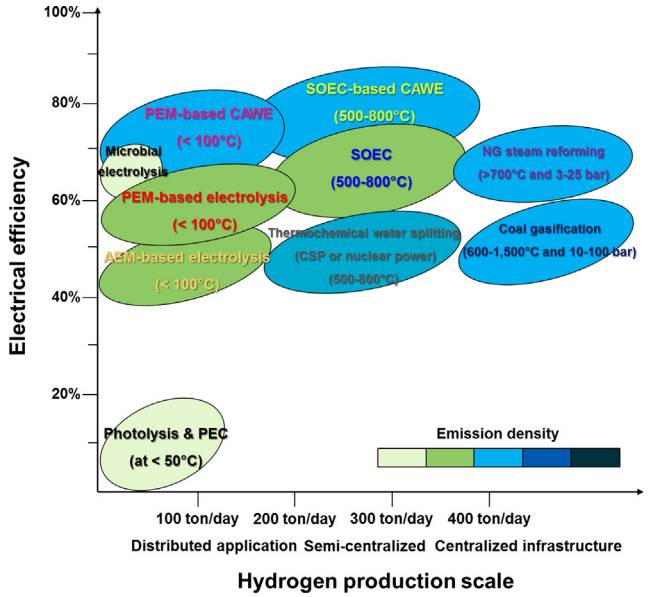

Fig. 21. Efficiency comparison of various hydrogen production technologies as a function of scale of hydrogen production. Information collected from references [1–8,172–174]. AEM = anion-exchange membrane; CAWE = carbon/hydrocarbon assisted electrolysis; CSP = concentrating solar power; NG = natural gas; PEC = photoelectrochemical cell; PEM = polymer electrolyte membrane; SOEC = solid oxide electrolysis cell.

7.1. Challenges for electrolysis

Various fundamental and engineering challenges need to be further studied and optimised to progress towards commercialisation of CAWE technology for hydrogen generation. These are summarised below for different categories of CAWE.

Solid carbon assisted water electrolysis

- System configuration and operating conditions, such as reaction interface design between electrode and membrane, pre-mixing of the carbon source, coal slurry feeding rates and design for continuous coal slurry feeding to the reactor.
- Methods of improving current density and long-term performance, and minimising the cell component degradation that increases the required cell voltages to maintain certain current densities.
- Effect of physicochemical properties of coal and biomass – particle size, porosity and crystallinity, impurities, surface functional groups and passive layers formed on the surface of coal particles due to electro-oxidation.
- Properties of carbon slurry fed to the electrolysis cell, such as particle dispersion, slurry viscosity and wettability.
- Suitability of anode and electrocatalyst materials for the type of coal used for the electrolysis, and development of electrocatalysts tolerant to impurities in coal that also assist in the electro-oxidation of coal.
- Role of additives, such as redox couples, to improve reactivity and reaction kinetics to achieve high current densities as well as improve coal electro-oxidation.
- Significance of coal desulfurisation and other by-products formed in the coal slurry electrolysis.

Liquid hydrocarbon assisted water electrolysis

- Various alcohols and liquid hydrocarbons can be considered as fuel for certain applications, and their use to produce hydrogen will need to be further justified from energy as well as economic point of view
- Cell stability has been shown in literature to some extent, but new anode catalysts would have to be developed to avoid or minimise poisoning due to intermediate compounds formed in the oxidation process
- Apart from methanol and formic acid, the breaking of C–C bond in other alcohols/polyols is still a challenge; thus the complete conversion of these fuels into CO_2 would be an issue unless either new catalysts are developed for complete conversion, or the intermediate products formed have an added value/application
- Crossover of the alcohols from cathode to anode chamber in the polymer membrane cell results in loss of alcohol, so new membrane materials less prone to alcohol crossover would need to be developed
- All alcohols are potentially toxic and their by-products might also cause other hazardous problems; they could be potentially harmful to the environment, corrosive to cell materials, and flammable due to low vapour pressure [170,171], requiring materials, strategies and regulations to overcome these issues

Hydrocarbon/CO gas assisted steam electrolysis

- High temperature operation increases the kinetics of the electrolysis process and will require only non-noble metal catalysts, but can cause various material-related issues that will require development/improvement of cell materials
- Methane supply to the anode may cause carbon deposition based on the anode catalyst, temperature and methane-to-steam ratio
- Methane oxidation to CO_2 is the preferred reaction in the anode chamber, rather than reforming, to realise the full benefit of reduction in electrochemical potential of the cell (thus power input for electrolysis); this may require a detailed study on optimisation of anode catalysts and other process variables

7.2. Opportunities and potential for carbon sources in electrolysis

Despite the challenges facing the development and commercialisation of this technology, there is enormous potential for various carbon sources to make electrolysis less energy intensive for hydrogen generation. This has been demonstrated by many investigators. For example:

- Current densities in the range of 100–200 mA cm^{-2} at cell voltages around 1 V have been achieved for coal slurry-assisted electrolysis in aqueous electrolyte cells with mediator redox couples, such as iron species, as additives [67,111] (see Tables 4 and 5)
- Activated carbon and biomass char assisted steam electrolysis employing SOEC reduces cell voltages to less than 0.4 V to achieve current densities in the range of 200–300 mA cm^{-2} at temperatures 700–900 °C [81,96], as shown in Table 6
- Liquid hydrocarbon assisted water electrolysis can produce current densities close to or above 1 A cm^{-2} at cell voltages < 1 V (MAWE and EAWE) [22,78,87,147], as shown in Table 7
- A five-cell methanol assisted electrolysis stack has produced 1 A cm^{-2} current density for 2500 h with negligible change in the stack voltage (3.95 V) [78]
- Methane (NG) assisted steam electrolysis using SOEC has produced current densities of 1 A cm^{-2} and 2.8 A cm^{-2} at 700 and 900 °C, respectively [25], as shown in Table 8.

The high current densities achieved for various carbon/hydrocarbon assisted water electrolysis processes at lower cell voltages compared with conventional electrolysis for hydrogen generation has also demonstrated electric energy input savings in excess of 50%.

8. Conclusion

Carbon/hydrocarbon assisted electrolysis has the potential to offer a

less energy intensive, cleaner method of using chemical energy in various sources of carbon, such as low-rank and high sulfur coals, biomass, alcohols and methane (Natural Gas), where pure CO_2 produced can be easily sequestered without the need for separation. In this paper, we have comprehensively reviewed the research work in this area employing aqueous electrolytes, polymer electrolyte membrane and solid oxide electrolytes. We have covered various types of carbon sources (coal, biomass, methanol, ethanol, glycerol, ethylene glycol, methane and CO); the electrochemical reactions involved; thermodynamic properties, such as free energy and enthalpy change of reactions and theoretical cell voltages required; and energy input required for electrolysis under different process conditions. The results obtained by various investigators in terms of cell designs, materials used, current densities obtained at given voltages and electric energy savings have also been discussed and summarised in the accompanying tables.

Coal is the cheapest source of carbon of the sources reviewed. The reasonable values of current densities (100–200 mA cm^{-2} at around 1 V) achieved in aqueous systems are only possible through redox ion additives in the coal slurries acting as mediators for the electrocatalytic oxidation of coal. Furthermore, the process is not stable, as current densities drop significantly over time due to formation of passive carboxylic compounds on the coal surface. The by-products of coal electrooxidation dissolved in the aqueous electrolyte may be useful, but this needs to be established. Similar current densities have been achieved at lower cell voltages (< 0.4 V) for carbon assisted steam electrolysis by employing solid oxide electrolyte systems above 700 °C, but materials degradation at high temperatures may be of concern for long-term performance.

Of the alcohols, methanol-assisted electrolysis has shown promise, as demonstrated by a study operating a five-cell methanol-assisted electrolysis stack at 1 A cm^{-2} for 2500 h without any increase in stack voltage (3.95 V). Methane used as a reductant on the anode side of a high temperature steam electrolysis cell to reduce electrochemical potential has been reported to show current densities of up to 1 A cm^{-2} (at 0.5 V) at 700 °C; however, the long-term performance of such a cell would need to be further assessed. A significantly high electric energy saving of $> 50\%$ for carbon/hydrocarbon assisted electrolysis has been demonstrated by various investigators.

The carbon assisted water electrolysis technology has been progressed to different levels for different carbon sources, and therefore a varying degree of effort would be required for commercialisation of this technology. Further, the advantages offered are also different by each source of carbon. For example coal is the cheapest source of carbon, but this technology is least advanced, and on the other hand methanol is an expensive source, but allows complete utilisation of the fuel in addition to its easy transport for distributed hydrogen production. This technology can also be explored for other sources of carbon such as waste water sludge and waste from food industry. Further, the advancements in the conventional electrolyser technology and its integration to renewable sources of energy can enable the development of this technology faster.

Acknowledgements

The authors would like to thank Dr Daniel Roberts (CSIRO) for reviewing this manuscript.

References

[1] Holladay JD, Hu J, King DL, Wang Y. An overview of hydrogen production technologies. Catal Today 2009;139:244–60. https://doi.org/10.1016/j.cattod.2008.08.039.
[2] Levin DB, Chahine R. Challenges for renewable hydrogen production from biomass. Int J Hydrog Energy 2010;35:4962–9. https://doi.org/10.1016/j.ijhydene.2009.08.067.
[3] Acar C, Dincer I. Comparative assessment of hydrogen production methods from renewable and non-renewable sources. Int J Hydrog Energy 2014;39:1–12. https://doi.org/10.1016/j.ijhydene.2013.10.060.
[4] Mueller-Langer F, Tzimas E, Kaltschmitt M, Peteves S. Techno-economic assessment of hydrogen production processes for the hydrogen economy for the short and medium term. Int J Hydrog Energy 2007;32:3797–810. https://doi.org/10.1016/j.ijhydene.2007.05.027.
[5] Stiegel GJ, Ramezan M. Hydrogen from coal gasification: An economical pathway to a sustainable energy future. Int J Coal Geol 2006;65:173–90. https://doi.org/10.1016/j.coal.2005.05.002.
[6] Badwal SPS, Giddey S, Munnings C. Hydrogen production via solid electrolytic routes: Hydrogen production. Wiley Interdiscip Rev Energy Environ 2013;2:473–87. https://doi.org/10.1002/wene.50.
[7] Carmo M, Fritz DL, Mergel J, Stolten D. A comprehensive review on PEM water electrolysis. Int J Hydrog Energy 2013;38:4901–34. https://doi.org/10.1016/j.ijhydene.2013.01.151.
[8] Badwal SPS, Giddey S, Munnings C. Emerging technologies, markets and commercialization of solid-electrolytic hydrogen production. e286 Wiley Interdiscip Rev Energy Environ2018. https://doi.org/10.1002/wene.286.
[9] BP Energy Outlook, Energy economics, BP Global. http://www.bp.com/en/global/corporate/energy-economics/energy-outlook.html [accessed June 26, 2017].
[10] Giddey S, Badwal SPS, Kulkarni A, Munnings C. A comprehensive review of direct carbon fuel cell technology. Prog Energy Combust Sci 2012;38:360–99. https://doi.org/10.1016/j.pecs.2012.01.003.
[11] Rady AC, Giddey S, Badwal SPS, Ladewig BP, Bhattacharya S. Review of fuels for direct carbon fuel cells. Energy Fuels 2012;26:1471–88. https://doi.org/10.1021/ef201694y.
[12] Gür TM. Critical review of carbon conversion in “carbon fuel cells”. Chem Rev 2013;113:6179–206. https://doi.org/10.1021/cr400072b.
[13] Ju H, Eom J, Lee JK, Choi H, Lim T-H, Song R-H, et al. Durable power performance of a direct ash-free coal fuel cell. Electrochim Acta 2014;115:511–7. https://doi.org/10.1016/j.electacta.2013.10.124.
[14] Jiang C, Ma J, Corre G, Jain SL, Irvine JTS. Challenges in developing direct carbon fuel cells. Chem Soc Rev 2017. https://doi.org/10.1039/C6CS00784H.
[15] Cao T, Huang K, Shi Y, Cai N. Recent advances in high-temperature carbon–air fuel cells. Energy Environ Sci 2017;10:460–90. https://doi.org/10.1039/C6EE03462D.
[16] Badwal SPS, Ju H, Giddey S, Kulkarni A. Direct carbon fuel cells. Ref. Module Earth Syst. Environ. Sci., Elsevier; 2016.
[17] Badwal SPS, Giddey SS, Munnings C, Bhatt AI, Hollenkamp AF. Emerging electrochemical energy conversion and storage technologies. Front Chem 2014:2. https://doi.org/10.3389/fchem.2014.00079.
[18] Bambagioni V, Bevilacqua M, Bianchini C, Filippi J, Lavacchi A, Marchionni A, et al. Self-sustainable production of hydrogen, chemicals, and energy from renewable alcohols by electrocatalysis. ChemSusChem 2010;3:851–5. https://doi.org/10.1002/cssc.201000103.
[19] Gutiérrez-Guerra N, Jiménez-Vázquez M, Serrano-Ruiz JC, Valverde JL, de Lucas-Consuegra A. Electrochemical reforming vs. catalytic reforming of ethanol: A process energy analysis for hydrogen production. Chem Eng Process Process Intensif 2015;95:9–16. https://doi.org/10.1016/j.cep.2015.05.008.
[20] Wang M, Wang Z, Gong X, Guo Z. The intensification technologies to water electrolysis for hydrogen production – A review. Renew Sustain Energy Rev 2014;29:573–88. https://doi.org/10.1016/j.rser.2013.08.090.
[21] Coutanceau C, Baranton S. Electrochemical conversion of alcohols for hydrogen production: a short overview: Electrochemical conversion of alcohols for hydrogen production. n/a-n/a Wiley Interdiscip Rev Energy Environ2016. https://doi.org/10.1002/wene.193.
[22] Nakamura BJ, Narayanan SR, Valdez TI, Chun W. Making hydrogen by electrolysis of methanol. JPL NTR Inventor’s Report 2002.
[23] Caravaca A, Sapountzi FM, de Lucas-Consuegra A, Molina-Mora C, Dorado F, Valverde JL. Electrochemical reforming of ethanol–water solutions for pure H_2 production in a PEM electrolysis cell. Int J Hydrog Energy 2012;37:9504–13. https://doi.org/10.1016/j.ijhydene.2012.03.062.
[24] Lamy C, Jaubert T, Baranton S, Coutanceau C. Clean hydrogen generation through the electrocatalytic oxidation of ethanol in a proton exchange membrane electrolysis cell (PEMEC): Effect of the nature and structure of the catalytic anode. J Power Sources 2014;245:927–36. https://doi.org/10.1016/j.jpowsour.2013.07.028.
[25] Martinez-Frias J, Pham A-Q, Aceves MS. A natural gas-assisted steam electrolyzer for high-efficiency production of hydrogen. Int J Hydrog Energy 2003;28:483–90. https://doi.org/10.1016/S0360-3199(02)00135-0.
[26] Wang W, Gorte RJ, Vohs JM. Analysis of the performance of the electrodes in a natural gas assisted steam electrolysis cell. Chem Eng Sci 2008;63:765–9. https://doi.org/10.1016/j.ces.2007.10.026.
[27] Wang W, Vohs JM, Gorte RJ. Hydrogen production via CH_4 and CO assisted steam electrolysis. Top Catal 2007;46:380–5. https://doi.org/10.1007/s11244-007-9005-8.
[28] Giddey S, Kulkarni A, Badwal SPS. Low emission hydrogen generation through carbon assisted electrolysis. Int J Hydrog Energy 2015;40:70–4. https://doi.org/10.1016/j.ijhydene.2014.11.033.
[29] Narkiewicz MR, Mathews JP. Visual representation of carbon dioxide adsorption in a low-volatile bituminous coal molecular model. Energy Fuels 2009;23:5236–46. https://doi.org/10.1021/ef900314j.
[30] Mochizuki Y, Sugawara K. Selective adsorption of organic sulfur in coal extract by using metal-loaded carbon. Fuel 2011;90:2974–80. https://doi.org/10.1016/j.fuel.2011.04.002.
[31] Calkins WH. The chemical forms of sulfur in coal: a review. Fuel 1994;73:475–84. https://doi.org/10.1016/0016-2361(94)90028-0.
[32] Lalvani S, Pata M, Coughlin RW. Sulphur removal from coal by electrolysis. Fuel

1983;62:427–37. https://doi.org/10.1016/0016-2361(83)90006-6.
[33] Coughlin RW, Farooque M. Hydrogen production from coal, water and electrons. Nature 1979;279:301–3. https://doi.org/10.1038/279301a0.
[34] Farooque M, Coughlin RW. Electrochemical gasification of coal (investigation of operating conditions and variables). Fuel 1979;58:705–12. https://doi.org/10.1016/0016-2361(79)90066-8.
[35] Coughlin RW, Farooque M. Electrochemical gasification of coal-simultaneous production of hydrogen and carbon dioxide by a single reaction involving coal, water, and electrons. Ind Eng Chem Process Des Dev 1980;19:211–9. https://doi.org/10.1021/i260074a002.
[36] Coughlin RW, Farooque M. Consideration of electrodes and electrolytes for electrochemical gasification of coal by anodic oxidation. J Appl Electrochem 1980;10:729–40. https://doi.org/10.1007/BF00611276.
[37] Coughlin RW, Farooque M. Thermodynamic, kinetic, and mass balance aspects of coal-depolarized water electrolysis. Ind Eng Chem Process Des Dev 1982;21:559–64. https://doi.org/10.1021/i200019a004.
[38] Wigmans T. Industrial aspects of production and use of activated carbons. Carbon 1989;27:13–22. https://doi.org/10.1016/0008-6223(89)90152-8.
[39] Ioannidou O, Zabaniotou A. Agricultural residues as precursors for activated carbon production—A review. Renew Sustain Energy Rev 2007;11:1966–2005. https://doi.org/10.1016/j.rser.2006.03.013.
[40] Badwal SPS, Giddey S, Kulkarni A, Goel J, Basu S. Direct ethanol fuel cells for transport and stationary applications – A comprehensive review. Appl Energy 2015;145:80–103. https://doi.org/10.1016/j.apenergy.2015.02.002.
[41] Methanol Institute. http://www.methanol.org/ [accessed September 18, 2018].
[42] Riaz A, Zahedi G, Klemeš JJ. A review of cleaner production methods for the manufacture of methanol. J Clean Prod 2013;57:19–37. https://doi.org/10.1016/j.jclepro.2013.06.017.
[43] Giddey S, Badwal SPS, Fini D. A novel design of bipolar interconnect plate for self-air breathing micro fuel cells and degradation issues. Int J Hydrog Energy 2012;37:11431–47. https://doi.org/10.1016/j.ijhydene.2012.04.103.
[44] Badwal SPS, Kulkarni AP, Ju H, Giddey S. Solar fuels. Uosaki K, editor. Electrochem Sci Sustain Soc Springer International Publishing; 2017. p. 223–59. https://doi.org/10.1007/978-3-319-57310-6_10.
[45] Bi L, Boulfrad S, Traversa E. Steam electrolysis by solid oxide electrolysis cells (SOECs) with proton-conducting oxides. Chem Soc Rev 2014. https://doi.org/10.1039/C4CS00194J.
[46] Baldwin RP, Jones KF, Joseph JT, Wong JL. Voltammetry and electrolysis of coal slurries and H-coal liquids. Fuel 1981;60:739–43. https://doi.org/10.1016/0016-2361(81)90229-5.
[47] Dhooge PM, Stilwell DE, Park S-M. Electrochemical studies of coal slurry oxidation mechanisms. J Electrochem Soc 1982;129:1719–24. https://doi.org/10.1149/1.2124257.
[48] Dhooge PM, Park S-M. Electrochemistry of coal slurries III. FTIR studies of electrolysis of coal. J Electrochem Soc 1983;130:1539–42. https://doi.org/10.1149/1.2120028.
[49] Dhooge PM, Park S-M. Electrochemistry of coal slurries II. Studies on various experimental parameters affecting oxidation of coal slurries. J Electrochem Soc 1983;130:1029–36. https://doi.org/10.1149/1.2119879.
[50] Park S-M. Electrochemistry of carbonaceous materials and coal. J Electrochem Soc 1984;131:363C–73C. https://doi.org/10.1149/1.2116055.
[51] Okada G, Guruswamy V, Bockris JO. On the electrolysis of coal slurries. J Electrochem Soc 1981;128:2097–102. https://doi.org/10.1149/1.2127197.
[52] Anthony KE, Linge HG. Oxidation of coal slurries in acidified ferric sulfate. J Electrochem Soc 1983;130:2217–9. https://doi.org/10.1149/1.2119555.
[53] Seehra MS, Ranganathan S, Manivannan A. Carbon-assisted water electrolysis: An energy-efficient process to produce pure H_2 at room temperature. 044104 Appl Phys Lett 2007;90. https://doi.org/10.1063/1.2432241.
[54] Seehra MS, Bollineni S. Nanocarbon boosts energy-efficient hydrogen production in carbon-assisted water electrolysis. Int J Hydrog Energy 2009;34:6078–84. https://doi.org/10.1016/j.ijhydene.2009.06.023.
[55] Wapner PG, Lalvani SB, Awad G. Organic sulfur removal from coal by electrolysis in alkaline media. Fuel Process Technol 1988;18:25–36. https://doi.org/10.1016/0378-3820(88)90071-9.
[56] Lalvani S, Pata M, Coughlin RW. Electrochemical oxidation of lignite in basic media. Fuel 1986;65:122–8. https://doi.org/10.1016/0016-2361(86)90152-3.
[57] Gong X, Wu Y, Wang Z, Wang M, Guo Z. Changes of total organic carbon and kinetics of ultrasonic-assisted coal water slurry electrolysis in NaOH system. Fuel Process Technol 2014;119:166–72. https://doi.org/10.1016/j.fuproc.2013.10.029.
[58] Patil P, De Abreu Y, Botte GG. Electrooxidation of coal slurries on different electrode materials. J Power Sources 2006;158:368–77. https://doi.org/10.1016/j.jpowsour.2005.09.033.
[59] Gong X, Wang M, Liu Y, Wang Z, Guo Z. Variation with time of cell voltage for coal slurry electrolysis in sulfuric acid. Energy 2014;65:233–9. https://doi.org/10.1016/j.energy.2013.11.083.
[60] Gong X, Wang M, Wang Z, Guo Z. Roles of inherent mineral matters for lignite water slurry electrolysis in H_2SO_4 system. Energy Convers Manag 2013;75:431–7. https://doi.org/10.1016/j.enconman.2013.07.004.
[61] Hesenov A, Kinik H, Puli Gökçen, Gözmen B, Irmak S, Erbatur O. Electrolysis of coal slurries to produce hydrogen gas: Relationship between CO_2 and H_2 formation. Int J Hydrog Energy 2011;36:5361–8. https://doi.org/10.1016/j.ijhydene.2011.02.017.
[62] Hesenov A, Meryemoğlu B, Içten O. Electrolysis of coal slurries to produce hydrogen gas: Effects of different factors on hydrogen yield. Int J Hydrog Energy 2011;36:12249–58. https://doi.org/10.1016/j.ijhydene.2011.06.134.
[63] Sathe N, Botte GG. Assessment of coal and graphite electrolysis on carbon fiber electrodes. J Power Sources 2006;161:513–23. https://doi.org/10.1016/j.jpowsour.2006.03.075.
[64] De Abreu Y, Patil P, Marquez AI, Botte GG. Characterization of electrooxidized Pittsburgh No. 8 Coal. Fuel 2007;86:573–84. https://doi.org/10.1016/j.fuel.2006.08.021.
[65] Jin X, Botte GG. Feasibility of hydrogen production from coal electrolysis at intermediate temperatures. J Power Sources 2007;171:826–34. https://doi.org/10.1016/j.jpowsour.2007.06.209.
[66] Jin X, Botte GG. Understanding the kinetics of coal electrolysis at intermediate temperatures. J Power Sources 2010;195:4935–42. https://doi.org/10.1016/j.jpowsour.2010.02.007.
[67] Clarke RL, Foller PC, Wasson AR. The electrochemical production of hydrogen using a carbonaceous fuel as an anode depolarizer. J Appl Electrochem 1988;18:546–54. https://doi.org/10.1007/BF01022249.
[68] Johnson KE, Verdet L. Electrochemical gasification of lignite in phosphoric acid. Can J Chem 1986;64:419–23. https://doi.org/10.1139/v86-066.
[69] Hu Z, Wu M, Wei Z, Song S, Shen PK. Pt-WC/C as a cathode electrocatalyst for hydrogen production by methanol electrolysis. J Power Sources 2007;166:458–61. https://doi.org/10.1016/j.jpowsour.2007.01.083.
[70] Take T, Tsurutani K, Umeda M. Hydrogen production by methanol–water solution electrolysis. J Power Sources 2007;164:9–16. https://doi.org/10.1016/j.jpowsour.2006.10.011.
[71] Sasikumar G, Muthumeenal A, Pethaiah SS, Nachiappan N, Balaji R. Aqueous methanol electrolysis using proton conducting membrane for hydrogen production. Int J Hydrog Energy 2008;33:5905–10. https://doi.org/10.1016/j.ijhydene.2008.07.013.
[72] Cloutier CR, Wilkinson DP. Electrolytic production of hydrogen from aqueous acidic methanol solutions. Int J Hydrog Energy 2010;35:3967–84. https://doi.org/10.1016/j.ijhydene.2010.02.005.
[73] Uhm S, Jeon H, Kim TJ, Lee J. Clean hydrogen production from methanol–water solutions via power-saved electrolytic reforming process. J Power Sources 2012;198:218–22. https://doi.org/10.1016/j.jpowsour.2011.09.083.
[74] Pham AT, Baba T, Sugiyama T, Shudo T. Efficient hydrogen production from aqueous methanol in a PEM electrolyzer with porous metal flow field: Influence of PTFE treatment of the anode gas diffusion layer. Int J Hydrog Energy 2013;38:73–81. https://doi.org/10.1016/j.ijhydene.2012.10.036.
[75] Pham AT, Baba T, Shudo T. Efficient hydrogen production from aqueous methanol in a PEM electrolyzer with porous metal flow field: Influence of change in grain diameter and material of porous metal flow field. Int J Hydrog Energy 2013;38:9945–53. https://doi.org/10.1016/j.ijhydene.2013.05.171.
[76] Tuomi S, Santasalo-Aarnio A, Kanninen P, Kallio T. Hydrogen production by methanol–water solution electrolysis with an alkaline membrane cell. J Power Sources 2013;229:32–5. https://doi.org/10.1016/j.jpowsour.2012.11.131.
[77] Ulusoy I, Uzunoglu A, Ata A, Ozturk O, Ider M. Hydrogen generation from alkaline solutions of methanol and ethanol by electrolysis. ECS Trans 2009;19:77–94. https://doi.org/10.1149/1.3237110.
[78] Sethu SP, Gangadharan S, Chan SH, Stimming U. Development of a novel cost effective methanol electrolyzer stack with Pt-catalyzed membrane. J Power Sources 2014;254:161–7. https://doi.org/10.1016/j.jpowsour.2013.12.103.
[79] Caravaca A, de Lucas-Consuegra A, Calcerrada AB, Lobato J, Valverde JL, Dorado F. From biomass to pure hydrogen: Electrochemical reforming of bio-ethanol in a PEM electrolyser. Appl Catal B Environ 2013;134–135:302–9. https://doi.org/10.1016/j.apcatb.2013.01.033.
[80] Lamy C, Baranton S, Coutanceau C. The electrocatalytic oxidation of ethanol in a proton exchange membrane electrolysis cell (PEMEC): A way to produce clean hydrogen for PEFC. ECS Trans 2013;58:1907–21. https://doi.org/10.1149/05801.1907ecst.
[81] Kiliç EÖ, Koparal AS, Öğütveren ÜB. Hydrogen production by electrochemical decomposition of formic acid via solid polymer electrolyte. Fuel Process Technol 2009;90:158–63. https://doi.org/10.1016/j.fuproc.2008.08.011.
[82] Guo WL, Li L, Li LL, Tian S, Liu SL, Wu YP. Hydrogen production via electrolysis of aqueous formic acid solutions. Int J Hydrog Energy 2011;36:9415–9. https://doi.org/10.1016/j.ijhydene.2011.04.127.
[83] Lamy C, Devadas A, Simoes M, Coutanceau C. Clean hydrogen generation through the electrocatalytic oxidation of formic acid in a proton exchange membrane electrolysis cell (PEMEC). Electrochim Acta 2012;60:112–20. https://doi.org/10.1016/j.electacta.2011.11.006.
[84] Marshall AT, Haverkamp RG. Production of hydrogen by the electrochemical reforming of glycerol–water solutions in a PEM electrolysis cell. Int J Hydrog Energy 2008;33:4649–54. https://doi.org/10.1016/j.ijhydene.2008.05.029.
[85] Yahiro H, Matsunaga Y, Asamoto M, Yamaji T. Low potential electrolysis of aqueous glycerin using polymer electrolyte membrane. ECS Trans 2009;25:1943–9. https://doi.org/10.1149/1.3210750.
[86] de Lucas-Consuegra A, Calcerrada AB, de la Osa AR, Valverde JL. Electrochemical reforming of ethylene glycol. Influence of the operation parameters, simulation and its optimization. Fuel Process Technol 2014;127:13–9. https://doi.org/10.1016/j.fuproc.2014.06.010.
[87] Chen YX, Lavacchi A, Miller HA, Bevilacqua M, Filippi J, Innocenti M, et al. Nanotechnology makes biomass electrolysis more energy efficient than water electrolysis. Nat Commun 2014:5. https://doi.org/10.1038/ncomms5036.
[88] Miller HA, Vizza F, Fornasiero P. Coproduction of hydrogen and chemicals by electrochemical reforming of biomass-derived alcohols. In: Voorde Van de, Sels B, editors. Nanotechnology in catalysis: applications in the chemical industry, energy development, and environment protection, 1. Wiley-VCH Verlag GmbH & Co. KGaA; 2017. p. 961–78. https://doi.org/10.1002/9783527699827.ch36.

[89] Gopalan S, Ye G, Pal UB. Regenerative, coal-based solid oxide fuel cell-electrolyzers. J Power Sources 2006;162:74–80. https://doi.org/10.1016/j.jpowsour.2006.07.001.

[90] Pati S, Yoon KJ, Chin J, Gopalan S, Pal U. Solid Oxide membrane electrolyzer utilizing the energy value in solid and gaseous reductant for hydrogen production. ECS Trans 2009;19:1–8. https://doi.org/10.1149/1.3237103.

[91] Pati S, Yoon KJ, Gopalan S, Pal UB. Hydrogen production using solid oxide membrane electrolyzer with solid carbon reductant in liquid metal anode. J Electrochem Soc 2009;156:B1067–77. https://doi.org/10.1149/1.3158746.

[92] Pal UB, Pati S, Yoong KJ, Gopalan S. (Invited) Electrolyzer for waste to energy conversion. ECS Trans 2012;41:93–101. https://doi.org/10.1149/1.3697432.

[93] Alexander BR, Mitchell RE, Gür TM. Steam-carbon fuel cell concept for cogeneration of hydrogen and electrical power. J Electrochem Soc 2011;158:B505–13. https://doi.org/10.1149/1.3560475.

[94] Lee AC, Mitchell RE, Gür TM. Feasibility of hydrogen production in a steam-carbon electrochemical cell. Solid State Ion 2011;192:607–10. https://doi.org/10.1016/j.ssi.2010.05.034.

[95] Alexander BR, Mitchell RE, Gür TM. Viability of coupled steam-carbon-air fuel cell concept for spontaneous co-production of hydrogen and electrical power. J Electrochem Soc 2012;159:F810–8. https://doi.org/10.1149/2.032212jes.

[96] Ewan BCR, Adeniyi OD. A demonstration of carbon-assisted water electrolysis. Energies 2013;6:1657–68. https://doi.org/10.3390/en6031657.

[97] Cinti G, Bidini G, Hemmes K. An experimental investigation of fuel assisted electrolysis as a function of fuel and reactant utilization. Int J Hydrog Energy 2016;28:11857–67. https://doi.org/10.1016/j.ijhydene.2016.05.205.

[98] Simpson AP, Lutz AE. Exergy analysis of hydrogen production via steam methane reforming. Int J Hydrog Energy 2007;32:4811–20. https://doi.org/10.1016/j.ijhydene.2007.08.025.

[99] Ding Y, Alpay E. Adsorption-enhanced steam–methane reforming. Chem Eng Sci 2000;55:3929–40. https://doi.org/10.1016/S0009-2509(99)00597-7.

[100] Klei HE, Sahagian J, Sundstrom DW. Kinetics of the activated carbon-steam reaction. Ind Eng Chem Process Des Dev 1975;14:470–3. https://doi.org/10.1021/i260056a020.

[101] Sapountzi FM, Gracia JM, Weststrate CJ (Kees-J, Fredriksson HOA, Niemantsverdriet JW (Hans). Electrocatalysts for the generation of hydrogen, oxygen and synthesis gas. Prog Energy Combust Sci 2017;58:1–35. doi:10.1016/j.pecs.2016.09.001.

[102] Laguna-Bercero MA. Recent advances in high temperature electrolysis using solid oxide fuel cells: A review. J Power Sources 2012;203:4–16. https://doi.org/10.1016/j.jpowsour.2011.12.019.

[103] Fujiwara S, Kasai S, Yamauchi H, Yamada K, Makino S, Matsunaga K, et al. Hydrogen production by high temperature electrolysis with nuclear reactor. Prog Nucl Energy 2008;50:422–6. https://doi.org/10.1016/j.pnucene.2007.11.025.

[104] O'Brien JE, McKellar MG, Harvego EA, Stoots CM. High-temperature electrolysis for large-scale hydrogen and syngas production from nuclear energy – summary of system simulation and economic analyses. Int J Hydrog Energy 2010;35:4808–19. https://doi.org/10.1016/j.ijhydene.2009.09.009.

[105] Zeng K, Zhang D. Recent progress in alkaline water electrolysis for hydrogen production and applications. Prog Energy Combust Sci 2010;36:307–26. https://doi.org/10.1016/j.pecs.2009.11.002.

[106] Thomas G, Chettiar M, Birss VI. Electrochemical oxidation of acidic Alberta coal slurries. J Appl Electrochem 1990;20:941–50. https://doi.org/10.1007/BF01019569.

[107] Rifi MR, Covitz FH. Introduction to organic electrochemistry. New York: Marcel Dekker; 1974.

[108] Murphy OJ, Bockris JO, Later DW. Products found in the anodic oxidation of coal. Int J Hydrog Energy 1985;10:453–74. https://doi.org/10.1016/0360-3199(85)90074-6.

[109] Lalvani SB, Nand S, Coughlin RW. Electrolytic pretreatment of Illinois No. 6 coal. Fuel Process Technol 1985;11:25–36. https://doi.org/10.1016/0378-3820(85)90013-X.

[110] Morooka S, Murakami A, Kusakabe K, Kato Y, Kusunoki K. Anodic oxidation of coal slurries in flow-through packed bed electrodes. Fuel 1984;63:947–51. https://doi.org/10.1016/0016-2361(84)90316-8.

[111] Kusakabe K, Nishida H, Morooka S, Kato Y, Kawakami K, Kusunoki K. Kinetic investigations for hybrid process of water electrolysis and chemical coal desulphurization. Fuel 1987;66:271–5. https://doi.org/10.1016/0016-2361(87)90254-7.

[112] Kawakami K, Fujio K, Kusunoki K, Kusakabe K, Morooka S. Kinetic study of coal slurry electrolysis-oxidation and desulfurization of Illinois No. 6 coal by aqueous ferric chloride. Fuel Process Technol 1988;19:15–29. https://doi.org/10.1016/0378-3820(88)90083-5.

[113] Taylor N, Gibson C, Bartle KD, Mills DG, Richards DG. Electrochemical oxidation of coals: Voltammetry and mass spectrometry. Fuel 1985;64:415–9. https://doi.org/10.1016/0016-2361(85)90435-1.

[114] Thomas G, Whitcombe S, Farebrother MD, Birss VI. A kinetic study of the electrochemical oxidation of alberta coal slurries. J Electrochem Soc 1990;137:3104–8. https://doi.org/10.1149/1.2086167.

[115] Yin R, Ji X, Zhang L, Lu S, Cao W, Fan Q. Multilayer nano Ti / TiO_2 – Pt electrode for coal-hydrogen production. J Electrochem Soc 2007;154:D637–41. https://doi.org/10.1149/1.2783778.

[116] Yin R, Zhao Y, Lu S, Wang H, Cao W, Fan Q. Electrocatalytic oxidation of coal on Ti-supported metal oxides coupled with liquid catalysts for H_2 production. Electrochim Acta 2009;55:46–51. https://doi.org/10.1016/j.electacta.2009.07.090.

[117] Yu T, Lv S, Zhou W, Cao W, Fan CQ, Yin R. Catalytic effect of $K_3Fe(CN)_6$ on hydrogen production from coal electro-oxidation. Electrochim Acta 2012;83:485–9. https://doi.org/10.1016/j.electacta.2012.08.010.

[118] Chen Z, Gong X, Wang Z, Wang Y, Zhang S, Xu D. Sulfur removal from ionic liquid-assisted coal water slurry electrolysis in KNO_3 system. J Fuel Chem Technol 2013;41:928–36. https://doi.org/10.1016/S1872-5813(13)60040-7.

[119] Kreysa G, Kochanek W. Kinetic investigations of the primary step of electrochemical coal oxidation. J Electrochem Soc 1985;132:2084–9. https://doi.org/10.1149/1.2114296.

[120] Yu J, Tian F-J, Chow MC, McKenzie LJ, Li C-Z. Effect of iron on the gasification of Victorian brown coal with steam: Enhancement of hydrogen production. Fuel 2006;85:127–33. https://doi.org/10.1016/j.fuel.2005.05.026.

[121] Kawakami K, Okumura T, Kusunoki K, Kusakabe K, Morooka S, Kato Y. An empirical kinetic model and simulation for anodic oxidation of coal slurry. J Chem Eng Jpn 1986;19:134–6. https://doi.org/10.1252/jcej.19.134.

[122] Aboushabana M, de Tacconi NR, Rajeshwar K. Chemical pre-treatment of coal and carbon black: implications for electrolytic hydrogen generation and electrochemical/thermal reactivity. J Electrochem Soc 2012;159:B695–701. https://doi.org/10.1149/2.034206jes.

[123] Lide DR. CRC handbook of chemistry and physics. 84th Edition CRC Press; 2003.

[124] Jin X. Coal electrolysis to produce hydrogen at intermediate temperatures. Ohio University; 2009.

[125] Ju H, Giddey S, Badwal SPS. Role of iron species as mediator in a PEM based carbon-water coelectrolysis for cost-effective hydrogen production. Int J Hydrog Energy 2018;43(19):9144–52. https://doi.org/10.1016/j.ijhydene.2018.03.195.

[126] Ge L, Gong X, Wang Z, Zhao L, Wang Y, Wang M. Insight of anode reaction for CWS (coal water slurry) electrolysis for hydrogen production. Energy 2016;96:372–82. https://doi.org/10.1016/j.energy.2015.12.077.

[127] Giddey S, Ciacchi FT, Badwal SPS, Zelizko V, Edwards JH, Duffy GJ. A versatile polymer electrolyte membrane fuel cell (3 kWe) facility. Solid State Ion 2002;152–153:363–71. https://doi.org/10.1016/S0167-2738(02)00342-9.

[128] Giddey S, Ciacchi FT, Badwal SPS. Design, assembly and operation of polymer electrolyte membrane fuel cell stacks to 1 kWe capacity. J Power Sources 2004;125:155–65. https://doi.org/10.1016/j.jpowsour.2003.08.026.

[129] Clarke RE, Giddey S, Badwal SPS. Stand-alone PEM water electrolysis system for fail safe operation with a renewable energy source. Int J Hydrog Energy 2010;35:928–35. https://doi.org/10.1016/j.ijhydene.2009.11.100.

[130] Giddey S, Ciacchi FT, Badwal SPS. High purity oxygen production with a polymer electrolyte membrane electrolyser. J Membr Sci 2010;346:227–32. https://doi.org/10.1016/j.memsci.2009.09.042.

[131] Lee J, Kwon Y, Machunda RL, Lee HJ. Electrocatalytic recycling of CO2 and small organic molecules. Chem – Asian J 2009;4:1516–23. https://doi.org/10.1002/asia.200900055.

[132] Machunda RL, Ju H, Lee J. Electrocatalytic reduction of CO_2 gas at Sn based gas diffusion electrode. Curr Appl Phys 2011;11:986–8. https://doi.org/10.1016/j.cap.2011.01.003.

[133] Lee S, Ju H, Machunda RL, Uhm S, Lee JK, Lee HJ, et al. Sustainable production of HCOOH via an electrolytic reduction of gas-phase $12CO_2$. J Mater Chem A 2014. https://doi.org/10.1039/C4TA03893B.

[134] Yu P, Botte GG. Bimetallic platinum–iron electrocatalyst supported on carbon fibers for coal electrolysis. J Power Sources 2015;274:165–9. https://doi.org/10.1016/j.jpowsour.2014.10.054.

[135] Alexander BR, Lee A, Mitchell R, Gür T. Carbon-free hydrogen production in a steam-carbon electrochemical cell. ECS Trans 2010;28:67–76. https://doi.org/10.1149/1.3501096.

[136] Alexander BR, Mitchell RE, Gür TM. Hydrogen and electricity from carbon in a coupled steam-carbon-air fuel cell. ECS Trans 2012;41:69–80. https://doi.org/10.1149/1.3697430.

[137] Gür TM, Homel M, Virkar AV. High performance solid oxide fuel cell operating on dry gasified coal. J Power Sources 2010;195:1085–90. https://doi.org/10.1016/j.jpowsour.2009.08.098.

[138] de la Osa AR, Calcerrada AB, Valverde JL, Baranova EA, de Lucas-Consuegra A. Electrochemical reforming of alcohols on nanostructured platinum-tin catalyst-electrodes. Appl Catal B Environ 2015;179:276–84. https://doi.org/10.1016/j.apcatb.2015.05.026.

[139] Guenot B, Cretin M, Lamy C. Clean hydrogen generation from the electrocatalytic oxidation of methanol inside a proton exchange membrane electrolysis cell (PEMEC): effect of methanol concentration and working temperature. J Appl Electrochem 2015. https://doi.org/10.1007/s10800-015-0867-3.

[140] Lamy C, Guenot B, Cretin M, Pourcelly G. Kinetics analysis of the electrocatalytic oxidation of methanol inside a DMFC working as a PEM electrolysis cell (PEMEC) to generate clean hydrogen. Electrochim Acta 2015;177:352–8. https://doi.org/10.1016/j.electacta.2015.02.069.

[141] Sethu SP, Ramalinga Viswanathan M, Mani U, Chan SH. Evaluation of impregnated nanocomposite membranes for aqueous methanol electrochemical reforming. Solid State Ion 2015;283:16–20. https://doi.org/10.1016/j.ssi.2015.11.006.

[142] Halme A, Selkäinaho J, Noponen T, Kohonen A. An alternative concept for DMFC – Combined electrolyzer and H_2 PEMFC. Int J Hydrog Energy 2016;41:2154–64. https://doi.org/10.1016/j.ijhydene.2015.12.007.

[143] Manjula N, Balaji R, Ramya K, Dhathathreyan KS, Ramachandraiah A. Studies on development of titania nanotube (TNT) based ePTFE-Nafion®-composite membrane for electrochemical methanol reformation. Int J Hydrog Energy 2016;41:8777–84. https://doi.org/10.1016/j.ijhydene.2016.02.123.

[144] Menia S, Tebibel H, Lassouane F, Khellaf A, Nouicer I. Hydrogen production by methanol aqueous electrolysis using photovoltaic energy: Algerian potential. Int J Hydrog Energy 2016. https://doi.org/10.1016/j.ijhydene.2016.11.178.

[145] Muthumeenal A, Pethaiah SS, Nagendran A. Investigation of SPES as PEM for hydrogen production through electrochemical reforming of aqueous methanol. Renew Energy 2016;91:75–82. https://doi.org/10.1016/j.renene.2016.01.042.
[146] Naga Mahesh K, Balaji R, Dhathathreyan KS. Palladium nanoparticles as hydrogen evolution reaction (HER) electrocatalyst in electrochemical methanol reformer. Int J Hydrog Energy 2016;41:46–51. https://doi.org/10.1016/j.ijhydene.2015.09.110.
[147] Ju H, Giddey S, Badwal SPS. The role of nanosized SnO_2 in Pt-based electrocatalysts for hydrogen production in methanol assisted water electrolysis. Electrochim Acta 2017;229:39–47. https://doi.org/10.1016/j.electacta.2017.01.106.
[148] Ju H, Giddey S, Badwal SPS, Mulder RJ. Electro-catalytic conversion of ethanol in solid electrolyte cells for distributed hydrogen generation. Electrochim Acta 2016;212:744–57. https://doi.org/10.1016/j.electacta.2016.07.062.
[149] Ehteshami SMM, Vignesh S, Rasheed RKA, Chan SH. Numerical investigations on ethanol electrolysis for production of pure hydrogen from renewable sources. Appl Energy 2016;170:388–93. https://doi.org/10.1016/j.apenergy.2016.03.001.
[150] de Lucas-Consuegra A, de la Osa AR, Calcerrada AB, Linares JJ, Horwat D. A novel sputtered Pd mesh architecture as an advanced electrocatalyst for highly efficient hydrogen production. J Power Sources 2016;321:248–56. https://doi.org/10.1016/j.jpowsour.2016.05.004.
[151] Miller HA, Bellini M, Vizza F, Hasenöhrl C, Tilley RD. Carbon supported Au–Pd core–shell nanoparticles for hydrogen production by alcohol electroreforming. Catal Sci Technol 2016;6:6870–8. https://doi.org/10.1039/C6CY00720A.
[152] Pagliaro MV, Bellini M, Bevilacqua M, Filippi J, Folliero MG, Marchionni A, et al. Carbon supported Rh nanoparticles for the production of hydrogen and chemicals by the electroreforming of biomass-derived alcohols. RSC Adv 2017;7:13971–8. https://doi.org/10.1039/C7RA00044H.
[153] Simões M, Baranton S, Coutanceau C. Electrochemical valorisation of glycerol. ChemSusChem 2012;5:2106–24. https://doi.org/10.1002/cssc.201200335.
[154] de Paula J, Nascimento D, Linares JJ. Influence of the anolyte feed conditions on the performance of an alkaline glycerol electroreforming reactor. J Appl Electrochem 2015;45:689–700. https://doi.org/10.1007/s10800-015-0848-6.
[155] Kim HJ, Lee J, Green SK, Huber GW, Kim WB. Selective glycerol oxidation by electrocatalytic dehydrogenation. ChemSusChem 2014;7:1051–6. https://doi.org/10.1002/cssc.201301218.
[156] Lee S, Ju Kim H, Ja Lim E, Kim Y, Noh Y, W. Huber G, et al. Highly selective transformation of glycerol to dihydroxyacetone without using oxidants by a PtSb/C-catalyzed electrooxidation process. Green Chem 2016;18:2877–87. doi:10.1039/C5GC02865E.
[157] Liu W, Cui Y, Du X, Zhang Z, Chao Z, Deng Y. High efficiency hydrogen evolution from native biomass electrolysis. Energy Env Sci 2016;9:467–72. https://doi.org/10.1039/C5EE03019F.
[158] Du X, Liu W, Zhang Z, Mulyadi A, Brittain A, Gong J, et al. Low-energy catalytic electrolysis for simultaneous hydrogen evolution and lignin depolymerization. ChemSusChem 2017;10:847–54. https://doi.org/10.1002/cssc.201601685.
[159] Kwon Y, Birdja YY, Raoufmoghaddam S, Koper MTM. Electrocatalytic hydrogenation of 5-hydroxymethylfurfural in acidic solution. ChemSusChem 2015;8:1745–51. https://doi.org/10.1002/cssc.201500176.
[160] Kwon Y, Schouten KJP, van der Waal JC, de Jong E, Koper MTM. Electrocatalytic conversion of furanic compounds. ACS Catal 2016;6:6704–17. https://doi.org/10.1021/acscatal.6b01861.
[161] Watanabe M, Motoo S. Electrocatalysis by ad-atoms: Part III. Enhancement of the oxidation of carbon monoxide on platinum by ruthenium ad-atoms. J Electroanal Chem Interfacial Electrochem 1975;60:275–83. https://doi.org/10.1016/S0022-0728(75)80262-2.
[162] Li H, Sun G, Cao L, Jiang L, Xin Q. Comparison of different promotion effect of PtRu/C and PtSn/C electrocatalysts for ethanol electro-oxidation. Electrochim Acta 2007;52:6622–9. https://doi.org/10.1016/j.electacta.2007.04.056.
[163] Kwon Y, Birdja Y, Spanos I, Rodriguez P, Koper MTM. Highly selective electro-oxidation of glycerol to dihydroxyacetone on platinum in the presence of bismuth. ACS Catal 2012;2:759–64. https://doi.org/10.1021/cs200599g.
[164] Kwon Y, Koper MTM. Electrocatalytic hydrogenation and deoxygenation of glucose on solid metal electrodes. ChemSusChem 2013;6:455–62. https://doi.org/10.1002/cssc.201200722.
[165] Lamy C, Rousseau S, Belgsir EM, Coutanceau C, Léger J-M. Recent progress in the direct ethanol fuel cell: development of new platinum–tin electrocatalysts. Electrochim Acta 2004;49:3901–8. https://doi.org/10.1016/j.electacta.2004.01.078.
[166] Antoniassi RM, Oliveira Neto A, Linardi M, Spinacé EV. The effect of acetaldehyde and acetic acid on the direct ethanol fuel cell performance using $PtSnO_2$/C electrocatalysts. Int J Hydrog Energy 2013;38:12069–77. https://doi.org/10.1016/j.ijhydene.2013.06.139.
[167] Jeon H, Uhm S, Jeong B, Lee J. On the origin of reactive Pd catalysts for an electrooxidation of formic acid. Phys Chem Chem Phys 2011;13:6192–6. https://doi.org/10.1039/C0CP02863K.
[168] Green S K, Lee J, Ju Kim H, Tompsett G A, Bae Kim W, Huber G W. The electrocatalytic hydrogenation of furanic compounds in a continuous electrocatalytic membrane reactor. Green Chem 2013;15:1869–79. https://doi.org/10.1039/C3GC00090G.
[169] Kwon Y, de Jong E, van der Waal JK, Koper MTM. Selective electrocatalytic oxidation of sorbitol to fructose and sorbose. ChemSusChem 2015;8:970–3. https://doi.org/10.1002/cssc.201402880.
[170] Demirci UB. Direct liquid-feed fuel cells: Thermodynamic and environmental concerns. J Power Sources 2007;169:239–46. https://doi.org/10.1016/j.jpowsour.2007.03.050.
[171] Miesse CM, Jung WS, Jeong K-J, Lee JK, Lee J, Han J, et al. Direct formic acid fuel cell portable power system for the operation of a laptop computer. J Power Sources 2006;162:532–40. https://doi.org/10.1016/j.jpowsour.2006.07.013.
[172] US Department of Energy, Fuel Cell Technologies Office, Hydrogen Production, http://energy.gov/eere/fuelcells/hydrogen-production.
[173] García Cortés C, Tzimas E, Peteves SD. Technologies for coal based hydrogen and electricity co-production power plants with CO2 capture, European Commission, Joint Research Centre, Institute for Energy; 2009.
[174] IEA, 2007, IEA energy technology essentials: hydrogen production and distribution. International Energy Agency.
[175] Ursua A, Gandia LM, Sanchis P. Hydrogen production from water electrolysis: current status and future trends. Proc IEEE 2012;100:410–26. https://doi.org/10.1109/JPROC.2011.2156750.
[176] Ni M, Leung MKH, Leung DYC. Technological development of hydrogen production by solid oxide electrolyzer cell (SOEC). Int J Hydrog Energy 2008;33:2337–54. https://doi.org/10.1016/j.ijhydene.2008.02.048.